

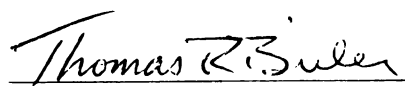


This is to certify that the
thesis entitled
An Analysis of Global and Localized Creep Strains and Creep
Properties of Non-Composite and Composite Lead-Free
Solders at Room and Elevated Temperatures
presented by

Jeffrey Lee McDougall

has been accepted towards fulfillment
of the requirements for

Master's degree in Materials Science


Major professor

Date December 16, 1998

PLACE IN RETURN BOX to remove this checkout from your record.
TO AVOID FINES return on or before date due.
MAY BE RECALLED with earlier due date if requested.

DATE DUE	DATE DUE	DATE DUE
<hr/>	<hr/>	<hr/>
<hr/>	<hr/>	<hr/>
<hr/>	<hr/>	<hr/>
<hr/>	<hr/>	<hr/>
<hr/>	<hr/>	<hr/>

**AN ANALYSIS OF GLOBAL AND LOCALIZED CREEP STRAINS AND CREEP
PROPERTIES OF NON-COMPOSITE AND COMPOSITE LEAD-FREE
SOLDERS AT ROOM AND ELEVATED TEMPERATURES**

By

Jeffrey Lee McDougall

A THESIS

**Submitted to
Michigan State University
in partial fulfillment of the requirements
for the degree of**

MASTER OF SCIENCE

Department of Materials Science and Mechanics

1998

ABSTRACT

AN ANALYSIS OF GLOBAL AND LOCALIZED CREEP STRAINS AND CREEP PROPERTIES OF NON-COMPOSITE AND COMPOSITE LEAD-FREE SOLDERS AT ROOM AND ELEVATED TEMPERATURES

By

Jeffrey Lee McDougall

Due to the adoption of “green” manufacturing practices in Europe, as well as the need for solders with better creep resistance at higher temperatures, there has been new interest in developing lead-free solders. Understanding and quantification of the effects of creep deformation is essential for lifetime prediction of electronic systems. Miniature single shear-lap creep specimens, similar in size to actual solder joints used in electronic packaging, have been developed to examine the effect of in-situ composite microstructures on the creep resistance and damage accumulation in lead-free solder joints. Average and localized strain measurements have been made optically, by monitoring the displacement of a scratch across the thickness of the solder joint. By analysis of the local strains, criteria for damage initiation are expressed in terms of the onset of tertiary creep, which starts sooner in some regions of the microstructure than others, leading to heterogeneous strain in the joint. The in-situ composite solders result in a more homogeneous strain evolution, which causes an improved creep resistance at lower temperatures, and much greater uniform strain at higher strain-rates before a critical damage level is reached.

This work is dedicated with love and gratitude to mom, Wendy, dad., and of course to grandma.

Also, I would like to dedicate this to the memory of Gramma and Grampa and my great grandmother, Gram, my departed and current best friends, Casey and Drexyl, the Glennie Chapter of the MacDougall Clan for providing me with Scottish blood, Rico for being Rico, Tommy - who has shown me that one man's ego can never be too large, Curtis for introducing me to Atlanta and showing me that space and time are meaningless in the realm of friendship, Joel - for his Scotch and song, Don - my eternal Glennie Buddy, Wade - for helping me realize a computer's true purpose, Cousin Ed and all the boys up at Alcona Park, and Edna & Jeff Felmlee for making this all possible.

Finally, I dedicate this to Sylvann for mending my broken faith and heart.

ACKNOWLEDGEMENTS

I would like to express sincere gratitude to Dr. Thomas R. Bieler for his guidance, support, friendship, and belief in my capabilities. Sincere thanks is also directed towards Dr. Lucas and Dr. Subramanian. I would also like to thank Dr. Case for placing in me the desire to become a better student. Finally, I want to express sincere appreciation for my colleagues and friends Sunghak Choi and Alan Gibson for their contributions, both academic and cultural.

I would also like to acknowledge the Composite Materials and Structure Center for their financial contributions which made this research possible, Dong Yi Seo for the use of his Macintosh computer, Kurt Neimeyer for his contributions to the miniature creep frame, and my family and friends for their financial support and encouragement throughout my academic career.

TABLE OF CONTENTS

LIST OF TABLES	viii
LIST OF FIGURES.....	ix
CHAPTER 1: INTRODUCTION.....	1
CHAPTER 2: REVIEW OF RELATED LITERATURE.....	3
2.1 SOLDER OVERVIEW	3
2.1.1 The History of Soldering.....	3
2.1.2 Solders and Soldering	5
2.2 CURRENT SOLDERING ISSUES	7
2.3 MICROSTRUCTURE TAILORING.....	11
2.4 CREEP OVERVIEW	13
2.4.1 History of Creep.....	13
2.4.2 Stress and Strain.....	14
2.4.3 Homologous Temperature.....	15
2.4.4 Creep Testing	16
2.4.5 The Creep Curve	17
2.4.5.1 Secondary Creep-Rate.....	20
2.4.5.2 Scattering of Data.....	22
2.4.6 Creep on an Atomic Scale.....	22
2.4.7 The Role of Dislocations in Deformation.....	23
2.4.8 Steady-State Creep-Rate	24
2.4.9 Secondary Creep-Rate Normalization.....	26
2.5 CREEP MECHANISMS	27
2.5.1 Dislocation Controlled Creep Mechanisms	27
2.5.2 Diffusion-Controlled Creep Mechanisms	28
2.6 CREEP-FATIGUE INTERACTIONS.....	30
2.6.1 Stress Relaxation.....	32
2.6.2 Fatigue.....	33
2.6.3 Fatigue of Solder Joints	35
2.7 CREEP IN SOLDER JOINTS	40
CHAPTER 3: EXPERIMENTAL PROCEDURE.....	41
3.1 SAMPLE PREPARATION	41
3.1.1 Joint Fabrication.....	41
3.1.2 Solder Microstructures.....	43
3.1.3 Polishing	43
3.2 CREEP TESTING	47

3.2.1 Miniature Creep Frame	47
3.2.2 Miniature Electrical Resistance Furnace.....	47
3.2.3 Deformation of Solder Joints.....	49
3.3 DATA EXTRACTION TECHNIQUE	54
3.3.1 Image Enhancement.....	54
3.3.2 Data Extraction	55
3.3.3 Reproducibility of Data Extraction	58
3.4 DATA PROCESSING	59
3.4.1 Global Creep Strain Measurement.....	59
3.4.2 Localized Creep Strain Measurement.....	61
3.4.3 Strain-Rate, Position, and Time.....	63
3.5 SEM OBSERVATIONS	65
3.5.1 Determination of Stress.....	65
3.5.2 Initiation of Fracture	65
3.5.3 Location of Fracture.....	66
CHAPTER 4: RESULTS	67
4.1 COMPARISON OF EXPERIMENTAL CREEP DATA TO DATA FOUND IN THE LITERATURE	67
4.1.1 Room Temperature Composite Data	69
4.1.2 Room Temperature Non-Composite Data	69
4.1.3 85°C Data	70
4.1.4 125°C Data	70
4.2 GLOBAL VS. LOCALIZED CREEP STRAIN	71
4.2.1 Room Temperature Composite Creep Data.....	71
4.2.2 Room Temperature Non-Composite Creep Data.....	73
4.2.3 85°C Composite Creep Data.....	75
4.2.4 85°C Non-Composite Creep Data.....	75
4.2.5 125°C Composite Creep Data.....	78
4.2.6 125°C Non-Composite Creep Data.....	80
4.3 POSITION OF MAXIMUM LOCALIZED CREEP STRAIN	82
4.4 FRACTURE SURFACES	83
4.5 RESULTS OF LOCATION OF FRACTURE EXAMINATION.....	86
4.6 RESULTS OF CRACK INITIATION TESTS	87
CHAPTER 5: DISCUSSION	90
5.1 CREEP BEHAVIOR.....	90
5.2 HOMOGENEITY OF DEFORMATION	91
CHAPTER 6: CONCLUSIONS	96
APPENDIX A: CREEP MECHANISMS.....	98
APPENDIX B: DATA REDUCTION	100

APPENDIX C: DISPLACEMENT, STRAIN, AND STRAIN-RATE HISTORIES	105
APPENDIX D: GLOBAL SECONDARY STRAIN-RATE DATA	125
APPENDIX E: FRACTURE SURFACES AND PROFILES	136
APPENDIX F: SOLDER JOINT CREEP DATA	154
REFERENCES	157

LIST OF TABLES

Table 1. Creep Mechanisms.....	99
Table 2. Scratch Displacement Data.....	102
Table 3. Normalized Position and Modified Scratch Displacement Data..	104
Table 4. Solder Joint Creep Data.....	155

LIST OF FIGURES

Figure 1. The Model Shape of a Typical Creep Curve.	19
Figure 2. The Process of Stress Relaxation.....	36
Figure 3. The Process of Thermo-Mechanical Fatigue	38
Figure 4. Differences Between Normal (a) and Accelerated (b) Thermo-Mechanical Fatigue Testing Adapted From Darveaux <i>et al.</i>	39
Figure 5a. Assembly of the Solder Joint.	42
Figure 5b. Finished Solder Joint with Magnified View of Joint Area.	42
Figure 6a. Eutectic 96.5Sn-3.5Ag Non-Composite Solder Micrograph.	44
Figure 6b. Eutectic 96.5Sn-3.5Ag Composite Solder Micrograph.	44
Figure 7. Specimen Grip and Polishing Bar.	45
Figure 8. Development of the Miniature Creep Frame.	48
Figure 9. Miniature Electrical Resistance Furnace.	50
Figure 10. Creep Frame Set Up for Elevated Temperature Testing.....	51
Figure 11. Displacement of Scratch Due to Creep Shown as: (a) Raw Captured Image in Negative Format. (b) Enhanced Image for use in <i>Datathief</i>	53 53
Figure 12. Normalized Position Across the Thickness of a Solder Joint.....	56
Figure 13. Screen Capture of Data Extraction Using <i>Datathief</i>	56
Figure 14. Scratch Displacement History.	60
Figure 15. Difference Between Global and Localized Deformation.....	60
Figure 16. Cubic Polynomial Curve Fit.	62

Figure 17. Localized and Global Creep Strain.....	62
Figure 18a. Variation of Strain-Rate to Time and Normalized Position for a Composite Solder Creep Tested at 25°C.....	64
Figure 18b. Variation of Strain-Rate to Time and Normalized Position for a Non-Composite Solder Creep Tested at 85°C.	64
Figure 19. Comparison of Secondary Creep-Rate Data.....	68
Figure 20. Displacement (a), Localized Creep Strain (b), and Strain-Rate (c) Histories for Composite Solder at 25°C.....	72
Figure 21. Displacement (a), Creep Strain (b), and Strain-Rate (c) Histories for Non-Composite Solder at 25°C.....	74
Figure 22. Displacement (a), Creep Strain (b), and Strain-Rate (c) Histories for Composite Solder at 85°C.....	76
Figure 23. Displacement (a), Creep Strain (b), and Strain-Rate (c) Histories for Non-Composite Solder at 85°C.....	77
Figure 24. Displacement (a), Creep Strain (b), and Strain-Rate (c) Histories for Composite Solder at 85°C.....	79
Figure 25. Displacement (a), Creep Strain (b), and Strain-Rate (c) Histories for Composite Solder at 85°C.....	81
Figure 26a. Non-Composite Fracture Surface, $T = 25^{\circ}\text{C}$, $\tau = 21.7 \text{ MPa}$. (Sample 038)...	84
Figure 26b. Non-Composite Fracture Surface, $T = 25^{\circ}\text{C}$, $\tau = 23.5 \text{ MPa}$. (Sample 040). .	84
Figure 26c. Composite Fracture Surface, $T = 25^{\circ}\text{C}$, $\tau = 32.2 \text{ MPa}$. (Sample 052).....	85
Figure 26d. Composite Fracture Surface, $T = 125^{\circ}\text{C}$, $\tau = 9.1 \text{ MPa}$. (Sample 036).....	85
Figure 27. Formation of Circular Areas Under High Stress Conditions:	
(a) Formation of Circular Areas.	88
(b) 'Pop' Out Upon Further Deformation.	88
(c) Collapse of Circular Area.	88
Figure 28. Solder Joint Micrographs Before (a) and After (b) Further Deformation.	89
Figure 29. Onset of Local Tertiary Creep vs. Global Secondary Creep-Rate.....	93

Figure 30. Strain Homogeneity Ratio vs. Global Secondary Creep-Rate.....	93
Figure 31. Homogeneity of Deformation vs. Average Percent Porosity.....	94
Figure 32. Displacement (a), Localized Creep Strain (b), and Strain-Rate (c) Histories for Composite Solder at 25°C.....	106
Figure 33. Displacement (a), Localized Creep Strain (b), and Strain-Rate (c) Histories for Composite Solder at 25°C.....	107
Figure 34. Displacement (a), Localized Creep Strain (b), and Strain-Rate (c) Histories for Composite Solder at 25°C.....	108
Figure 35. Displacement (a), Localized Creep Strain (b), and Strain-Rate (c) Histories for Non-Composite Solder at 25°C.....	109
Figure 36. Displacement (a), Localized Creep Strain (b), and Strain-Rate (c) Histories for Non-Composite Solder at 25°C.....	110
Figure 37. Displacement (a), Localized Creep Strain (b), and Strain-Rate (c) Histories for Non-Composite Solder at 25°C.....	111
Figure 38. Displacement (a), Localized Creep Strain (b), and Strain-Rate (c) Histories for Non-Composite Solder at 25°C.....	112
Figure 39. Displacement (a), Localized Creep Strain (b), and Strain-Rate (c) Histories for Non-Composite Solder at 25°C.....	113
Figure 40. Displacement (a), Localized Creep Strain (b), and Strain-Rate (c) Histories for Composite Solder at 85°C.....	114
Figure 41. Displacement (a), Localized Creep Strain (b), and Strain-Rate (c) Histories for Composite Solder at 85°C.....	115
Figure 42. Displacement (a), Localized Creep Strain (b), and Strain-Rate (c) Histories for Non-Composite Solder at 85°C.....	116
Figure 43. Displacement (a), Localized Creep Strain (b), and Strain-Rate (c) Histories for Non-Composite Solder at 85°C.....	117
Figure 44. Displacement (a), Localized Creep Strain (b), and Strain-Rate (c) Histories for Non-Composite Solder at 85°C.....	118
Figure 45. Displacement (a), Localized Creep Strain (b), and Strain-Rate (c) Histories for Composite Solder at 125°C.....	119

Figure 46. Displacement (a), Localized Creep Strain (b), and Strain-Rate (c) Histories for Composite Solder at 125°C.....	120
Figure 47. Displacement (a), Localized Creep Strain (b), and Strain-Rate (c) Histories for Composite Solder at 125°C.....	121
Figure 48. Displacement (a), Localized Creep Strain (b), and Strain-Rate (c) Histories for Composite Solder at 125°C.....	122
Figure 49. Displacement (a), Localized Creep Strain (b), and Strain-Rate (c) Histories for Non-Composite Solder at 125°C.....	123
Figure 50. Displacement (a), Localized Creep Strain (b), and Strain-Rate (c) Histories for Non-Composite Solder at 125°C.....	124
Figure 51. Global Secondary Strain Rate for 25°C, 31.1 MPa, Composite Solder.....	126
Figure 52. Global Secondary Strain Rate for 25°C, 28.9 MPa, Composite Solder.....	126
Figure 53. Global Secondary Strain Rate for 25°C, 25.8 MPa, Composite Solder.....	127
Figure 54. Global Secondary Strain Rate for 25°C, 21.9 MPa, Non-Composite Solder	127
Figure 55. Global Secondary Strain Rate for 25°C, 19.9 MPa, Non-Composite Solder	128
Figure 56. Global Secondary Strain Rate for 25°C, 19.8 MPa, Non-Composite Solder	128
Figure 57. Global Secondary Strain Rate for 25°C, 10.5 MPa, Non-Composite Solder	129
Figure 58. Global Secondary Strain Rate for 25°C, 11 MPa, Non-Composite Solder ...	129
Figure 59. Global Secondary Strain Rate for 85°C, 10.8 MPa, Composite Solder.....	130
Figure 60. Global Secondary Strain Rate for 85°C, 10.4 MPa, Composite Solder.....	130
Figure 61. Global Secondary Strain Rate for 85°C, 12.3 MPa, Non-Composite Solder	131
Figure 62. Global Secondary Strain Rate for 85°C, 17.3 MPa, Non-Composite Solder	131
Figure 63. Global Secondary Strain Rate for 85°C, 16.3 MPa, Non-Composite Solder	132
Figure 64. Global Secondary Strain Rate for 125°C, 9.4 MPa, Composite Solder.....	132
Figure 65. Global Secondary Strain Rate for 125°C, 9.9 MPa, Composite Solder.....	133

Figure 66. Global Secondary Strain Rate for 125°C, 11 MPa, Composite Solder.....	133
Figure 67. Global Secondary Strain Rate for 125°C, 8.1 MPa, Composite Solder.....	134
Figure 68. Global Secondary Strain Rate for 125°C, 9.7 MPa, Non-Composite Solder	134
Figure 69. Global Secondary Strain Rate for 125°C, 31.1 MPa, Composite Solder.....	135
Figure 70. Fracture Surfaces and Profile for 25°C, 31.1 MPa, Composite Solder.....	137
Figure 71. Fracture Surfaces and Profile for 25°C, 28.9 MPa, Composite Solder.....	138
Figure 72. Fracture Surfaces and Profile for 25°C, 21.9 MPa, Non-Composite Solder. .	139
Figure 73. Fracture Surfaces and Profile for 25°C, 19.9 MPa, Non-Composite Solder. .	140
Figure 74. Fracture Surfaces and Profile for 25°C, 19.8 MPa, Non-Composite Solder. .	141
Figure 75. Fracture Surfaces and Profile for 25°C, 10.5 MPa, Non-Composite Solder. .	142
Figure 76. Fracture Surfaces and Profile for 85°C, 10.8 MPa, Composite Solder.....	143
Figure 77. Fracture Surfaces and Profile for 85°C, 10.4 MPa, Composite Solder.....	144
Figure 78. Fracture Surfaces and Profile for 85°C, 12.3 MPa, Non-Composite Solder. .	145
Figure 79. Fracture Surfaces and Profile for 85°C, 17.3 MPa, Non-Composite Solder. .	146
Figure 80. Fracture Surfaces and Profile for 85°C, 16.3 MPa, Non-Composite Solder. .	147
Figure 81. Fracture Surfaces and Profile for 125°C, 9.4 MPa, Composite Solder.....	148
Figure 82. Fracture Surfaces and Profile for 125°C, 9.9 MPa, Composite Solder.....	149
Figure 83. Fracture Surfaces and Profile for 125°C, 11 MPa, Composite Solder.....	150
Figure 84. Fracture Surfaces and Profile for 125°C, 8.1 MPa, Composite Solder.....	151
Figure 85. Fracture Surfaces and Profile for 125°C, 9.7 MPa, Non-Composite Solder. .	152
Figure 86. Fracture Surfaces and Profile for 125°C, 10.9 MPa, Non-Composite Solder.	153

CHAPTER 1

INTRODUCTION

As electronic components continue to develop functionally, and less expensive means of manufacturing are developed, the world becomes continually more dependent upon electronic technology. However, the use of lead bearing solders is problematic as countries strive to become more health and environmentally conscious. Outlawing lead bearing solders would drastically alter the manufacture of electronic components since eutectic Sn-Pb is the most widely utilized of all solders.

Today's electronic components are more powerful, smaller, and relatively inexpensive in respect to their functionality. Although it has been in existence for thousands of years, soldering technology still represents the vast majority of reliable electrical connections. Unfortunately, as the functionality and miniaturization of electronic components continues, the operational temperatures and stresses increase. Use of soldered components in relatively high temperature environments such as under-the-hood automotive applications also makes greater demands upon soldering technology. Issues such as high temperature creep become relevant, considering that room temperature is over half the melting point (183°C) of eutectic tin-lead solder. As a result, alternative solders which provide higher performance must be investigated.

In order to combat the detrimental effects of higher operational temperatures, solders with greater melting temperatures and creep resistance must be developed. Currently, there has been much interest in the use and development of alternative solders. However,

much of the experimentation is being performed on bulk solder specimens possessing microstructures unlike the miniature, rapidly solidified (relatively small grain size) solder joints encountered in industrial practices (See Section 2.2, page 9). There have been few investigations utilizing miniature solder joint specimens.

Investigations involving the creep characteristics of solders have dealt with creep in the classic sense, where the overall or global creep of the specimen was measured. Global creep data yields results seen in a typical or classic creep curve. Along with classic global creep, this investigation also considered creep from a localized perspective, i.e., instead of measuring the average or global creep strain, creep strains were measured at different locations across the thickness of the solder joint.

The scope of this research involves examination of creep resistance of miniature industrial-like solder joints produced from eutectic tin-silver solder with and without added intermetallics as reinforcements. Creep characteristics of these solders will be examined at room and elevated temperatures. New methods of plotting the localized creep strain-rate were explored. An attempt to determine a criterion for the onset of tertiary creep deformation is made.

CHAPTER 2

REVIEW OF RELATED LITERATURE

2.1 SOLDER OVERVIEW

2.1.1 The History of Soldering

The history of soldering dates back to over 6000 years ago [1]. Artisans from Mesopotamia first used solders in the form of gold-based, hard alloys to join together copper plates. Egypt was the next region to utilize soldering. Artifacts dating back to 3600 BC were discovered there, as well as in Greece and other Mediterranean areas, roughly 1000 years later. The most sophisticated example of early soldering comes from the Bronze Age where the Etruscans produced a gold pendent dating back to 2500 BC, in which three different types of solders were used within a 5mm proximity. This discovery was quite surprising, due to the fact that these three different solder alloys had varying melting temperatures. This is the earliest known example of a soldering process referred to as 'step joining'. Evidence of soldering in the western hemisphere dates back to only around the year 10 AD. Remnants of the La Tolita natives of South America also indicated the use of gold-based solders.

Currently, it is virtually impossible to determine whether or not these ancient civilizations were familiar with the use of soft tin-lead solders that are so prevalent today. Tin decomposes over time when exposed to tannic acid, a substance found in such organic entities as tree bark. As a result, soldering alloys which may have contained lead are indistinguishable from lead-free solders. Geographic evidence supports the notion

that the Mediterranean region was not familiar with Sn-Pb solders since tin was not readily available.

However, rich deposits of tin are found in northern Europe where soft soldering practices were developed. Historical evidence suggests that soft soldering was developed by the Celts and Gauls from northern and central Europe around 1900 BC. Their exceptional use of soft soldering techniques were recorded by the Romans. Cooking utensils and metals tools could easily be manufactured or repaired over a small wood fueled fire, due to the low melting temperature of the tin-lead alloys, which were also high enough to withstand temperatures necessary for the preparation of food or hot water.

Crude examples of soft soldering dating back to 1350 BC were discovered upon the unearthing of King Tut's tomb. Evidence also shows that by 350 BC, the Greeks were using tin-lead solders to seal pumps and other devices produced from bronze. Tin-lead solders were also readily employed by the Romans to join the lead sheets which lined the interior of aqueducts.

The application of soldering technology was greatly broadened during the Industrial revolution [1]. Due to their low cost, availability, and ease of use, tin-lead solders have prevailed through the twentieth century. With the development of portable heat sources, the use of soldering in such areas as plumbing, food container sealants, and the automobile industry vastly increased. It was not until the Second World War, when the supply of tin suddenly decreased, that alternative solders were given significant attention. Lowering the tin content as well as developing tin free solders was the major concern, but problems of higher melting temperatures and decreased fluidity were identified [2]. Today soldering is increasingly relied upon as the primary method of joining electronic

components including resistors, capacitors, and packaged integrated circuits to ceramic substrates and printed wiring boards [3].

2.1.2 Solders and Soldering

Solders can be classified as being either soft alloys or hard alloys; 350°C is the melting temperature that distinguishes the two categories. Solders melting below 350°C are considered to be soft solders and they typically contain both lead and tin. Other soft solders can be composed of such elements as bismuth, indium, and cadmium. Hard solders have melting temperatures which are greater than 350°C and they contain metals such as gold, aluminum, zinc, and silicon [1].

The process of joining two metals together via a filler metal with a lower melting temperature than the materials being joined is known as soldering [1]. The soldering process simply relies on the wetting of the substrate materials by the solder for the formation of the bond [4]. Soldering is not the only means of joining two metallic materials. Two other similar methods include brazing and welding. Brazing is a similar metallurgical joining process which occurs at a temperature greater than 425°C. Brazing also relies on the wetting of the substrate materials, but some diffusion occurs that improves the bond strength [4]. When melting of the substrate materials in the region near the bond occurs, this is known as welding. A filler material can be used, but it is not always required in this process. Diffusion of the base metals is the means for bond formation [4]. Welding is a permanent joining technique, whereas soldering and brazing processes can be reversed with the application of sufficient heat.

Often it is necessary to incorporate a flux into the soldering process. Fluxes serve a variety of purposes. They are used to clean the solder and substrate surfaces to be joined, as well as a protective coating before and during the soldering operation [5]. Fluxes were developed via the metal coatings industry where a clean surface was achieved prior to coating by immersing the substrate in an acid bath [6]. Fluxes are generally comprised of organic chemicals and organic salts. A natural resin from pine trees known as rosin can also be used. Rosin has the added benefit of not reacting until elevated temperatures are achieved [5].

The nomenclature for solders is based upon the alloy composition. The solder is described by its composition in weight percent from the most abundant to the least abundant element. For example, eutectic Sn-Pb solder (62Sn-38Pb), the standard soft solder, has a composition of 62 weight % tin with lead as the balance. Solder composition is quite a diverse matter. There are a wide variety of solders available which allows for a wide variety of specialized uses. As a result, the soldering process is not a simple matter of simply surface cleaning along with the addition of heat. There are many soldering techniques available, and the most prevalent issues concern types of solders, fluxes, base materials and their finishes, cleaning agents, and the design of the solder joint [3].

2.2 CURRENT SOLDERING ISSUES

Today, issues concerning solders and soldering are of paramount importance. Electronic components are being utilized in an ever increasing number of applications. The continual miniaturization of more powerful electronic components, makes the soldering process increasingly difficult. Along with miniaturization, higher temperatures are generated in certain applications. Also there is the continual concern of legislation or marketing pressures that could regulate or ban lead, which would dramatically affect the electronics industry in the United States.

Many lead bearing products have already been outlawed due to noted effects on health as a result of prolonged exposure. Some of these products include paint and crayons, and the use of lead bearing solders in plumbing supplies were restricted in 1986. Internal combustion engines which could operate on unleaded gasoline were produced in the early 1970's. Means of limiting human exposure to lead are continually being researched [1]. Even though solders comprise about 1% of the lead used in the U.S., there have been several attempts made by Congress, including a very recent one, to further reduce the use of lead, or tax its use severely. Lead bearing solders utilized in electronic components have yet to come under restriction in the U.S., although a number of European nations have already banned the use of lead bearing solders. This is a very relevant issue for American companies desiring to do business with European nations.

Greater emphasis on the integrity of solder joints has resulted from the heightened functionality of electronic components [3]. Since the world is relying more and more on electronic components, solder joint failures must be kept to a minimum and designed in

the most efficient manner. Many of the failures occurring in electronic systems are due to the failure of solder joints, not the components themselves [1].

In the earlier part of the twentieth century, as soldering became the most reliable means of electrical connections, the solder joint had only a single purpose which was just to maintain electrical continuity between components [1]. With today's silicon chip technology, solder joints are also expected to provide structural support as well. The continual decrease in component size along with the need for solder joints to provide both electrical and structural support results in an increasing demand for stronger and more creep resistant soldering alloys [1].

It is well known that eutectic Sn-Pb solder coarsens after aging, leading to shortened life to failure. Thus we need to find a better alloy system that not only has no lead content but also possesses higher thermal fatigue resistance [7]. Current tin-lead solders lack shear strength, resistance to creep, and resistance to thermo-mechanical fatigue [8]. Eutectic Sn-Ag solder has a melting point of 221°C (compared to 183°C for eutectic Sn-Pb) so it may be suitable for higher temperature applications such as under-the-hood electronics in automobiles [9].

In most electronic systems, differential thermal expansion induces stresses resulting in substantial thermal cycling deformation of solder joint, which leads to eventual failure [10]. Soft solders are commonly used for electrical interconnects between components in electronic equipment. The stresses induced in these low melting temperature materials resulting from thermal expansion mismatch between the joined materials eventually leads to cracking that can limit component reliability [10]. While fatigue deformation is a major concern for electronic solders, creep constitutes an important state of deformation

since stress relaxation occurs after a temperature change. In realistic thermal cycles there is sufficient time for stress relaxation processes to occur and creep induced damage may result [10]. It has been suggested that solder creep behavior may be directly associated with the joint fatigue lifetime [11].

Due to difficulties in experimental procedures, much of the data published concerning solder microstructure and mechanical properties has been based upon bulk solder rather than actual solder joints. Disagreement has existed regarding the use of bulk solder data in the design and analysis of actual solder joints. The microstructures of bulk solders differ from those of solder joints in significant ways [9]: Bulk solder does not have Cu intermetallics that form as a result of interactions between the solder and the Cu substrate. Solder joints are significantly stronger than the bulk tensile specimens [11]. These intermetallics (whether in the solder or in the solder/base metal interface) reduce the joint ductility. Secondly, large bulk specimens generally cool more slowly than joints on real printed wire boards, greatly affecting the creep properties of the solders. The creep behavior of the solder alloy may in large part determine the joint fatigue lifetime and may be the best means by which to understand the fatigue results [11]. The Sn-Ag shear-lap specimens were significantly stronger than the bulk tensile specimens [11]. Comparatively, there have been fewer investigations utilizing miniature solder joint specimens.

There is a need to develop new solders that have similar processing properties to tin-lead solders, but which are lead-free and have improved mechanical properties and microstructural stability [8]. Coarsening during aging is more difficult in eutectic Sn-Ag solder because of the thermally stable intermetallics, therefore its rate of coarsening is

much slower than that in eutectic Sn-Pb [7]. This indicates that known phenomena about Sn-Pb solders is not indicative of phenomena in other solders.

2.3 MICROSTRUCTURE TAILORING

The microstructure of a metal or alloy exposed to temperatures close to half of its melting point can become dynamic. Due to the processing history of a material, a variety of microstructures may result just for one particular composition. An investigation performed by Frost *et al.* indicated that creep behavior of solder alloys was continually influenced by microstructural changes occurring at elevated temperatures [12]. Experimental evidence has shown that Sn-Ag and Sn-Pb solder microstructures can undergo significant coarsening at temperatures similar to operational temperatures observed in under-the-hood automotive conditions [13, 14].

Eutectic Sn-Ag solder joints are characterized with a relatively fine microstructure with well dispersed Ag_3Sn intermetallics [13] which is excellent for fatigue resistance, but for creep resistance a coarse grain size is generally desired. The well dispersed Ag_3Sn intermetallics observed in eutectic Sn-Ag solder can show significant growth after only 100 hours at temperatures between 60 and 150°C. The naturally forming Cu_6Sn_5 intermetallics at the Cu substrate/solder interface have also been shown to coarsen [14]. The presence of these brittle intermetallics at the substrate/solder interface can effect solder joint reliability. Loss of mechanical strength especially under high loading conditions is associated with these interfacial intermetallics [1]. In order for Sn-Ag solders to be considered for future use under these high temperature conditions, the microstructure needs to be stabilized.

By introducing a second phase (dispersoids) into an existing microstructure, grain boundary mobility can be inhibited which would result in improved microstructural

stability. In addition to inhibiting grain growth, a second phase may also cause a more homogeneous distribution of strains [13]. Strengthening of the solder alloy against creep and fatigue deformation can also result through the addition of a second phase [15]. The composite solder used in this investigation contained a dispersed phase of Cu_6Sn_5 intermetallics on the order of 20 volume percent. Upon initial examination, the intentionally added intermetallics indicated no improvement in controlling Ag_3Sn particle coarsening, but the added Cu_6Sn_5 particles appeared to be quite stable [13]. In an investigation on Bi-Sn eutectic solder alloy [15] coarsening was suppressed and creep resistance greatly enhanced through the addition of Fe particles

A comparison of creep properties of aged and unaged composite solder as compared to that of non-composite eutectic Sn-Ag solder was performed by Choi *et al.* The composite solder demonstrated dramatic decreases in the strain-rate as compared to the non-composite solder. Strain-rates decreased by a factor of 100 for aged specimens to 1000 for the unaged specimens [10]. Microstructural observations showed no displacement of the added Cu_6Sn_5 particles for specimens with strain-rates on the order of 10^{-7} s^{-1} . Displacement was apparently limited to the Sn matrix. Under similar loading conditions, the composite solder showed a decrease in creep strain as compared to the non-composite solder. As a result, less stress relaxation may occur forcing the failure process away from the solder and instead to the components it joins [13].

2.4 CREEP OVERVIEW

Materials under stress at elevated temperatures can undergo a phenomenon known as creep. This phenomenon of continuous deformation under a constant load can occur at all temperatures above absolute zero and is also observed in non-metals [16]. This time-dependent strain includes elastic, viscous, and plastic deformation, but usually only plastic deformation is measured [16]. Creep strain is probably the most important time-dependent damage accumulation factor affecting solder joint reliability [17]. Problems usually associated with creep occur only at high homologous temperatures [18].

For design purposes, components used under stress at elevated temperatures must be capable of resistance to distortion over the life span, as well as creep failure should not occur within the required operating life [18]. Processes of creep deformation at low temperatures, less than about fifty percent of the melting temperature, are believed to be related to non-diffusion controlled mechanisms, while creep occurring above this temperature are generally associated with diffusion controlled mechanisms [16]. However, there still exists a great deal of controversy concerning mechanisms of creep deformation.

2.4.1 History of Creep

The phenomenon of time-dependent strain, or creep, was discovered hundreds of years ago. One of the earliest examples involved churches from the medieval period. Many of these churches were adorned with steep pitched roofs composed of lead. Since the roofs were at such a sharp angle, the lead would stretch under its own weight in a manner similar to liquid running down an inclined plane. This resulted in cracked roofs that

needed repair [19]. Another example of creep was discovered in domestic water supplies consisting of lead pipes. Gradual sagging of the lead pipes would occur which was not much of a concern, until this caused cracking and eventual bursting of the pipes. The sagging was more pronounced in pipes which supplied the hot water. Cold water pipes had fewer problems [19].

In terms of significant recorded work on creep, there are several important dates [16]. In 1905 Philips demonstrated that the creep of metals at low stresses was possible. Andrade also supported this theory in 1910 and again in 1914, however serious consideration was not given to the creep phenomenon until 1919 when Chevenard performed experimental work demonstrating that creep was not exclusive to just soft metals. Other significant research was accomplished by Dickenson in 1922. Major work on the theoretical aspects of creep was done by Becker (1925, 1926) and Orowan in 1934 [16].

2.4.2 Stress and Strain

Considering the general properties of a typical stress-strain curve, no plastic deformation will occur until the stress increases beyond the proportional limit of the material, where the onset of yielding occurs. However, if the material is held under a constant load below the yield stress at sufficiently high temperature conditions, plastic deformation can occur. This temperature and time-dependent deformation is known as creep and it can occur at stresses below the macroscopic yield strength by at least one order of magnitude or greater due to thermal fluctuations which aid the motion of dislocations [16].

Shear forces can also induce creep deformation [16]. Shear strain causes the displacement, dx , of a finite element in the direction of the shearing force in respect to the thickness, y_0 , of the element, where y_0 remains constant. The shear strain, γ , is given by, $\gamma_{xy} = \frac{\partial x}{\partial y}$. Strain is related to stress through Hooke's law, which can be stated in terms of normal strain, $\epsilon = \frac{\sigma}{E}$, and simple shear strain, $\gamma = \frac{\tau}{G}$. The variable E is known as the elastic or Young's modulus and G is the shear modulus. Both moduli are temperature sensitive, i.e. with increasing temperature the moduli decrease. Most creep tests assume constant load

2.4.3 Homologous Temperature

Experimental evidence has shown that creep is an extremely temperature sensitive phenomenon where local thermal agitation provides the additional energy (beyond mechanical forces) necessary to overcome barriers to creep deformation [16]. The extent to which a material will deform under constant stress depends greatly on the material's melting point. For example, a specimen of nickel ($T_{\text{melt}} = 1453^\circ\text{C}$) under stress at room temperature may not exhibit any signs of creep, whereas a specimen of eutectic tin-lead solder (60Sn-40Pb, $T_{\text{melt}} = 183^\circ\text{C}$) under similar proportional stress conditions can creep excessively. An important term when considering the phenomenon of creep is a material's homologous temperature which is defined as the ratio of the applied absolute temperature to the material's absolute melting point, $T_{\text{Homologous}} = \frac{T_{\text{applied}}}{T_{\text{melt}}}$.

The higher a material's homologous temperature, the more likely it is to undergo creep deformation. At room temperature, nickel has a homologous temperature of around

0.17, whereas 60Sn-40Pb is at a homologous temperature of 0.65, a value over half of the absolute melting point. Temperatures where creep becomes important for pure metals are above $0.4T_{\text{melt}}$. The significance of this temperature resides in the fact that atomic rearrangements of the crystal lattice are possible via diffusion. The homologous temperature is an important parameter in the profile of creep curves as well as the onset of creep deformation mechanisms [18].

2.4.4 Creep Testing

In order to characterize creep properties, it is necessary to measure changes in the gage length with time. No completely satisfactory method of accomplishing this problem has yet been designed. The most common test method employed is the application of constant load (tension, but creep tests can also be done in compression) under constant temperature. Specimens used for a typical creep test are generally cylindrical with threaded ends which thread directly into the creep machine. The gage lengths typically range from 10 to 60 *mm*. It is important to consider that when testing at severe temperatures where oxidation of the specimen can occur, the specimen needs to be enclosed in a vacuum or inert atmosphere [20].

Currently the most common method for measuring this change is by using an extensometer in direct contact with ridges machined onto the gage length of the specimen or on to enlarged specimen shoulders. The change in gage length between the ridges can then be monitored via displacement of the extensometer arms. Some of the more common displacement detecting devices which can be used with the extensometer include dial gages, linear variable differential transformers (LVDT), and differential

capacitance transducers. Another method involves monitoring the displacement of scribe lines on the surface of the specimen via a vernier telescope focused through a viewing slot in the furnace. This requires manual operation and the scribe lines often disappear or become indistinct if the specimen surface oxidizes. [20]

Creep tests can take anywhere from several minutes to several years. In general, it is desirable to avoid accelerated testing and carry out tests in real time. However, in order to ensure that successive batches of components are being manufactured under the customer guidelines, or for theoretical means such as determining how added composites affect the creep characteristics of a given material, accelerated creep tests are commonly conducted [18]. It is possible to predict the creep rupture life through a relationship developed by Monkman and Grant. They found that the rupture life is inversely proportional to the minimum or secondary creep-rate, $\dot{\epsilon}_s$. The relationship is given by, $\log t_r + C \log \dot{\epsilon}_s = K$, where C and K are constants for a given material, and t_r is the rupture life.

2.4.5 The Creep Curve

Accumulation of strain with respect to time (strain history) is the basic information resulting from deformation under constant temperature and stress. The total accumulated creep strain can be described with the equation, $\epsilon_{total} = \epsilon_o + \epsilon$, where ϵ_o represents the instantaneous strain upon loading, and ϵ is the time-dependent strain. The creep-rate, $\dot{\epsilon} = d\epsilon/dt$, can be determined by measuring the slope at any point on the creep curve. The resulting shape of the strain history profile is associated with different stages of creep.

sh

cr

st

S

b

in

in

c

P

s

s

i

i

c

s

s

s

v

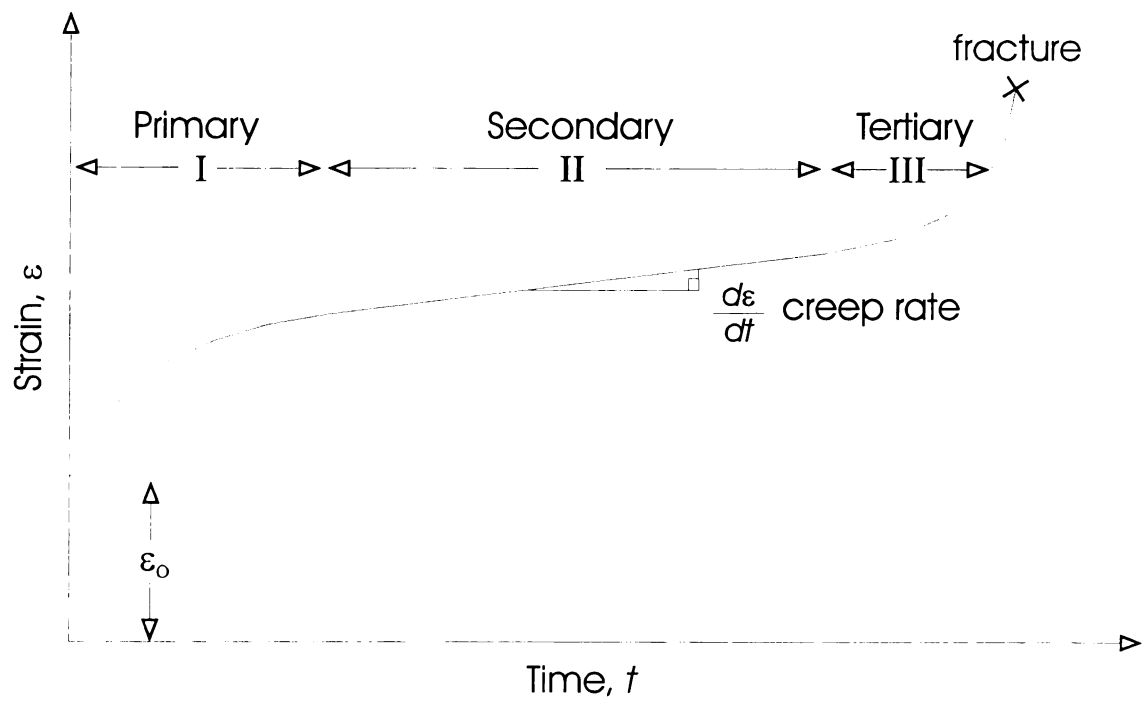
s

c

The first stage in creep, *Stage I*, is also known as primary creep which is a relatively short lived phenomenon. This transient period of creep represents a region of decreasing creep-rate. This stage of creep can be characterized by strain hardening. The second stage which can be seen from Figure 1 is known as secondary creep, steady-state creep, or *Stage II*. This stage is characterized by a nearly constant creep-rate that results from a balance between strain hardening and recovery.

The final stage of creep, *Stage III*, also known as tertiary creep occurs from a decrease in cross-section area of the specimen either because of necking or the formation of internal voids or cracks which can be associated with metallurgical changes such as coarsening of precipitate particles, recrystallization, or diffusional changes in the phases present [16]. Tertiary creep is associated with high stresses due to the decrease in cross-sectional area. Throughout the creep experiment, the load is held constant. The axial stress increases as the specimen elongates and decreases in cross-sectional area. The initial stress is usually the reported stress, not the instantaneous stress [21].

The theoretical shape of a typical creep curve is shown in Figure 1. After an almost instantaneous strain of the specimen, ϵ_0 , due to loading, there is a decrease in the rate of creep (*Stage I*) which transforms into a steady state process (*Stage II*), where there is little noticeable rate change. This creep-rate then rapidly increases (*Stage III*) until the specimen fails [21]. Individual creep tests do not always yield all of the three stages. The shapes of the creep curves resulting from individual tests can vary greatly according to temperature, test duration, and the stress value. For example, tests performed at low stresses have a tendency to yield a sigmoidal (S-shape) curves as well as curves with short or long range oscillations [16].



Adapted from Dieter, page 439.

Figure 1. The Model Shape of a Typical Creep Curve.

Temperature has a notable effect upon the shape of a creep curve. Under low homologous temperatures, the total resulting strains are quite low (<1%) and the creep curve may only enter stages of primary and secondary creep. At homologous temperatures in the range of 0.3 or less, the creep strain varies linearly with log(time) when crept in tension [16]. Failure seldom occurs for tests performed at low homologous temperatures [18]. However, as the temperature is increased to a homologous value near 0.4, the profile of the creep curve deviates from this logarithmic form [18]. In contrast, during creep tests performed at high homologous temperatures, all three stages of creep, including tertiary, will be experienced. Once tertiary creep is underway, failure is inevitable.

2.4.5.1 Secondary Creep-Rate

The minimum creep-rate is the average value of the creep-rate during *Stage II*. Generally, the creep characteristics of a material are described by values obtained from the ‘secondary’ or ‘steady state’ creep-rate, $\dot{\epsilon}_s$, resulting from normal high temperature creep tests. This eliminates the need for a wider variety of equations representing the creep properties of materials tested at high homologous temperatures [18]. The creep-rate, $\dot{\epsilon}$, can be determined by measuring the slope of the curve, $d\epsilon/dt$ in Stage II. Even though it is simple in theory, the measurement of creep resistance is a tedious task which requires extensive laboratory equipment. Typical tests can run over a wide range of times, from a few minutes to over ten years [21].

A linear relationship between the secondary creep-rate and temperature can be obtained by plotting $\ln(\dot{\epsilon}_s)$ vs. $(1/T)$. This indicates that the secondary creep-rate increases exponentially with temperature [18]. Temperature dependence of this nature

can be seen in other processes such as diffusion. Creep can be classified as an Arrhenius function [18]. This results in the proportion, $\dot{\epsilon}_s \propto \exp(-Q_c / RT)$, where Q_c is the creep activation energy and R is the universal gas constant. This leads to the general form of the empirical power law creep equation which is $\dot{\epsilon}_s = A\sigma^n \exp\left(\frac{-Q_c}{kT}\right)$ [22], where $\dot{\epsilon}_s$ is the strain-rate or creep-rate, A is a constant, σ is the stress which has a measurable exponent given as n , Q_c is the creep activation energy, k is Boltzmann's constant, and T represents temperature on the absolute scale. When this form of the equation is used to represent the creep process, values for the activation energies of pure metals in a high temperature environment, have been measured to be similar to the activation energies for lattice self diffusion [18]. This indicates that the mechanism for creep at high temperatures would be controlled by diffusion. This fact also explains the transition between low and high temperature creep behavior, since the movement of atoms occurs readily near a temperature of $0.4T_m$ [18]. Another equation developed by Dorn, which mixes metallurgical theory and the empirical power law is referred to as a semi-empirical equation. This equation is given by $\dot{\epsilon}_s = A \frac{D G b}{k T} \left(\frac{\sigma}{G}\right)^n \left(\frac{b}{d}\right)^p$ [23], where b is the Burger's vector, D is the diffusivity and is given by the equation $D = D_o \exp\left(\frac{-Q}{RT}\right)$, d is the grain size, p is the grain size exponent. The term $\frac{D}{kT}$ is referred to as the mobility.

2.4.5.2 Scattering of Data

Scatter is a quality inherent in creep data. This is due partly to assumptions made during a creep test. For purposes of convenience, temperature and stress are assumed to be constant for the duration of a creep test for proper characterization of materials [20]. These substantial assumptions are rarely the actual conditions experienced in practice. Deviations from these assumptions will result in errors in the determination of creep strain, strain-rates, and rupture lives [20]. Errors in the axiality (tension or shear) of loading as well as the skill necessary in setting up the test itself along with typical errors can arise just as in any experiment from imprecise measurement of specimen dimensions or a variety of other factors [20].

2.4.6 Creep on an Atomic Scale

In order to understand creep, it is necessary to consider a material on the atomic level. Typically, a metal contains many individual crystals which are comprised of a simple lattice structure of atoms held together via atomic bonding. If a solid is subjected to a tensile force, the crystal lattice will adjust itself to oppose the applied force and maintain equilibrium. If a sufficient force were to be imposed upon this polycrystalline material, resulting in plastic deformation, the deformation is caused mainly from the movement of dislocations. The deformation which initially occurs is elastic or reversible. Once the elastic limit has been bypassed, the stress imposed is sufficient enough to cause some of the dislocations to move across the crystals, resulting in permanent or plastic deformation. After some deformation occurs, strain will quickly cease, unless the applied

load is increased. Deformation is halted because forces are generated to prevent further deformation. This phenomenon is known as work hardening.

2.4.7 The Role of Dislocations in Deformation

As dislocations move through the material as a result of deformation caused by a stress higher than roughly 10^{-5} of the shear modulus [24], they multiply rapidly. A consequence of this rapid multiplication is dislocation crossing and tangling, which impedes the further movement of other dislocations. Unless the load is increased or extra energy is supplied in the form of heat, further deformation will not occur. In creep deformation this can be associated with *Stage I* as defined previously. The stress necessary to cause continued deformation in a material is known as the flow stress, σ_o [22]. The flow stress can be defined as a material's resistance to shape change and is a function of temperature, strain, and strain-rate [20]. The flow stress, $\sigma_o = \sigma_T + \sigma_{\perp}$, consists of a thermal component, σ_T , and an athermal component associated with the dislocations inside the material, σ_{\perp} [22].

Recovery can be understood in terms of atomic vibration. The higher the temperature, the greater the degree of vibration and the less time needed for recovery to occur. The creep-rate reaches a constant value when the rate of strain hardening and rate of recovery become equal. Since atoms have a greater chance of moving from one atomic position to another when their degree of vibration is high, the creep-rate increases with increasing temperature. Diffusion of atoms can occur due to existing vacancies in the lattice. At elevated temperatures, experimentally calculated activation energies for creep usually equal the activation energy for self-diffusion [22]. This diffusion tends to make

vacancies move into the dislocation cores so that the dislocations shift from one plane of the crystal to another. This phenomenon is referred to as dislocation climb [19].

During climb of dislocations, the dislocations can either move or annihilate other dislocations of opposite sign. Since the diffusion of vacancies either towards edge dislocations (positive climb) or away from edge dislocations (negative climb) is required for edge dislocations to climb, creep deformation resulting from climb should involve the activation energy for self diffusion [22]. In this manner, the extensive tangling of dislocations sorts itself out and many dislocations disappear in a process known as recovery [19].

A material undergoing creep deformation may not do so in a homogeneous manner. Changes in the arrangement of dislocations in crystals has been observed using transmission electron microscopy. Some regions are characterized by being relatively dislocation free, while other areas possess a high density of dislocation tangles and networks [20]. As a result of this dislocation density imbalance, the specimen's state of internal stress is not uniform since each dislocation has an associated stress field that affects the movement of nearby dislocations [20]. The difference between the applied stress and these internal stresses is the driving force for the motion of dislocations. As a result, the inhomogeneous nature of the stress field can exhibit itself in some peculiar ways [20].

2.4.8 Steady-State Creep-Rate

Confusion exists concerning nomenclature for the creep-rate obtained from Stage II of a high temperature creep test. The common misconception is to refer to the second stage of

creep as ‘steady-state creep’. The term ‘steady-state’ implies an equilibrium process with respect to dislocations and is reached when the rate of work hardening is balanced by the rate of recovery. This concept forms the basis for most dislocation creep theories [20]. During steady-state creep, there are as many dislocations being created as there are being destroyed and the lifetime of each dislocation contributes one increment of strain. During steady-state creep, the dislocation density and the arrangement of the dislocations remains essentially unchanged which results in a constant strain-rate [20]. In general, measurable secondary creep-rates are found at stress levels greater than about 10^{-5} of the shear modulus and at temperatures greater than $0.4T_{\text{melt}}$ [24]. No changes in microstructure will occur under steady-state conditions.

A constant strain-rate may occur during secondary creep, but there may be changes in the microstructure such as local recrystallization near particle interfaces, etc. The linear portion of secondary creep may be misleading. In order to demonstrate true linearity, the strain-rate needs to be plotted against strain. The minimum strain-rate, which is equivalent to the steady state or secondary creep-rate, represents a balancing condition between the hardening and softening processes in the material. If the microstructure is not in a state of equilibrium, steady-state creep is not occurring. In fact very few materials undergo true steady-state creep, such as some pure metals and simple alloys. There is little convincing experimental proof justifying the existence of a steady-state creep component [16]. Unless evidence indicates the microstructure is unchanging, creep occurring during *Stage II* is better referred to as secondary creep.

2.4.9 Secondary Creep-Rate Normalization

The way in which the creep-rate changes in respect to temperature can be shown by the relationship, $\dot{\epsilon}_s = A\sigma^n \exp(-Q_c / RT)$, which is known as ‘power-law creep’. Considering secondary creep behavior, different values of n and Q_c will be associated with different regimes of stress and temperature. It is possible to condense all of the different temperature creep data into one set through a normalization process. When secondary creep behavior can be described with the power-law, if both sides of the power law equation are multiplied by the factor, $\exp(Q_c / RT)$, the result is, $\dot{\epsilon}_s \exp(Q_c / RT) = A\sigma^n$. The left side of this modified power law equation is referred to as the ‘temperature compensated secondary creep-rate’ [18]. A similar equation can be used for shear stress deformation. This modified function allows each $\log \dot{\epsilon}_s / \log \sigma$ relationship obtained from different temperatures to be superimposed onto a single line. The stress is also normalized with respect to temperature, σ / E , where ‘E’ is the value of Young’s Modulus at the appropriate creep temperature [18].

2.5 C

The pro

involve

These

sliding

expon

2.5.1 A

Disloc

therma

mecha

roughl

disloc

disloc

They

compe

rearran

W

creep.

domin

elevate

allowin

2.5 CREEP MECHANISMS

The process of creep has considerable theoretical controversy as to the exact mechanisms involved. There exists at least four different types of creep deformation mechanisms. These include dislocation glide, dislocation creep, diffusion creep, and grain boundary sliding. A chart in Appendix A summarizes the creep mechanisms, creep and grain size exponents represented by values of n and p respectively, and activation energies, Q .

2.5.1 Dislocation Controlled Creep Mechanisms

Dislocation glide occurs when dislocations moving along slip planes overcome barriers thermally assisted mechanisms involving the diffusion of vacancies or interstitials. This mechanism occurs at relatively high stresses as compared to other creep mechanisms, roughly $10^{-4} < \frac{\sigma}{G} < 10^{-2}$. The creep-rate is established by the ease with which dislocations are impeded by obstacles including precipitates, solute atoms, and other dislocations [18]. The basis for dislocation creep was developed by Orowan and Bailey. They concluded that the steady state creep-rate represents a balance between the competing factors of the strain hardening rate and the rate of thermal recovery by the rearrangement and annihilation of dislocations.

Weertmann was responsible for the development of the earliest models of dislocation creep. The models were based on a mechanism in which dislocation climb is the dominating factor. If an obstacle inhibits the movement of a gliding dislocation at elevated temperatures, a small amount of climb may allow it to overcome the obstacle, allowing it to glide to the next set of obstacles and the process is repeated. Almost all of

the strain is produced by the glide, however, the climb step controls the rate. Since diffusion of vacancies or interstitials is necessary for dislocation climb, the rate limiting factor is atomic diffusion.

This model predicts an equation for the rate of creep where the stress exponent equals three, however, creep experiments with a range of metals show that the exponent on stress varies from 3 to 8, with a value of 5 being the average [21]. Thus for a range of medium to high stress levels at temperatures above half of the melting temperature, the steady state creep-rate is characterized by a power-law relation. When more than one mechanism is functioning, the creep behavior is controlled by the fastest mechanism. If there are mechanisms operating in sequence, the slowest mechanism will control creep deformation.

2.5.2 Diffusion-Controlled Creep Mechanisms

Diffusional creep occurs under low stress, high temperature conditions. Diffusional creep involves the flow of vacancies and interstitials through a crystal under the influence of applied stress. Diffusion creep occurs for stress levels around $\frac{\sigma}{G} < 10^{-4}$. Nabarro-Herring and Coble creep are included under this category [18]. When a polycrystalline metal creeps by the diffusion of atoms through the crystal lattice, the process is known as Nabarro-Herring creep [25]. When diffusion of atoms occurs along the grain boundaries, the process is known as Coble creep [26]. Although support for the idea of diffusional creep has been offered through experimentation and can be found throughout the literature [27], it is still a controversial topic. There is an ongoing argument concerning

the validity of Nabarro-Herring creep as well as a controversy over ‘denuded zones’ which were offered as the first immediate microstructural proof for diffusional creep [28].

2.6 CREEP-FATIGUE INTERACTIONS

Solder joints used for both mechanical and electrical contacts in electronic packaging devices normally do not fail as a result of a single high stress event [29]. Usually failure is a result of repeated or prolonged load applications that result in damage accumulation via creep-fatigue failure of the solder. The nature of the environment most solder joints are exposed to involves a variety of deleterious factors. Automotive applications provide an excellent test of the solder joint. Temperature fluctuations in the range of -40°C to 150°C are possible in automotive environments, along with mechanical vibrations in a range from 20 to 2000 Hz [30]. Fatigue can arise due to both the mechanical vibrations and fluctuations in temperature. As discussed previously, because of high homologous temperatures, fatigue behavior of solder joints is related to creep as well as the process of stress relaxation [31].

Solder joints can be considered as structural materials since they function not only as electrical interconnects, but also as mechanical bonds. In electronic devices, solder joints often constrain materials of differing coefficients of thermal expansion (CTE) that upon an increase in temperature due to internal heat dissipation from an electrical current or simply from environmental changes, will result in plastic strains [32]. Plastic strains are caused by CTE mismatch. Depending upon the size of the joint, even minute changes in temperature can have a drastic effect upon the solder and the component(s) it connects [32]. If the connected components have matched CTE's, there is still a danger of plastic strain due to differential rates of heating and cooling (temperature gradients) in localized regions [33]. When these electronic devices are repeatedly turned on and off, or

te

se

in

C

o

c

t

u

a

c

temperature cycles are created by the device itself, cyclic strains can result. Typically a sequential development [29] of local stressing, microcrack formation followed by crack initiation which may result from the accumulation of creep cavitation damage [31]. Crack propagation then ensues resulting in the failure of electrical solder joints. Evidence of creep fatigue interactions include fatigue striations (fatigue) as well as intergranular cracking and voids on some of the grain surfaces (Creep) [34].

In order to improve upon the design and characteristics of solder joints, it is necessary to gain a better understanding of the mechanical and fatigue properties of solder alloys used in electronic components [35]. Currently, for a variety of solder alloys, fatigue data are available in the literature. However before applying this to the solder at hand, consideration must be given to solder composition, microstructure, design of the specimen, testing conditions, as well as the author's definition of the fatigue. Plastic deformation occurs in many solder joint designs since the accumulated strains exceed the elastic limit of the solder [31]. If these factors are ignored, assessment of the fatigue life may be incorrect [35]. Another pertinent issue involves the duration of the actual fatigue lifetime. The actual lifetimes required for field use greatly exceed plausible time for testing. As a result, service reliability must be estimated through fatigue models [31]. In other words, reliable accelerated testing procedures must be developed.

2.6.1 Stress Relaxation

Most solders are characterized as being very compliant. When stress is applied to a solder joint, especially at elevated temperatures, the solder will yield in a manner to reduce the applied stress [36]. Stress relaxation and creep are two very closely related phenomena differing by which factor is held constant. Creep occurs when stress is held constant and the strain changes with time. However, when the strain is held constant, i.e., the material's dimensions are unchanging, and the stress decreases either by way of static, dynamic, or creep conditions, the load it supports decreases with time. This process is known as stress relaxation [35, 16]. From a microstructural standpoint, the processes are virtually the same, and the profiles of strain-rate vs. stress for both processes are identical [36]. A further term, known as creep relaxation, refers to the time-dependent changes simultaneously occurring in both strain and stress [36].

A simplified model of stress relaxation was provided in a paper by Hall. When thermal stresses arise in a soldered assembly under conditions previously described, the components which are responsible for the applied stress on the solder are usually only stressed within their elastic range. A stiffness value, k , can be associated with this assembly in the form $k = -\frac{dF}{dx}$ [36]. If the solder yields (creeps) by a distance Δx , then the force on the joint will be decreased by a value of $k\Delta x$, [36]. The equation,

$$\Delta\gamma = \frac{(\alpha_s - \alpha_c)}{H} L\Delta T - \frac{\Delta F}{kH} \quad [36],$$

combines the shear strain, shear stress, and temperature components into one relation. The variable F is the force associated with each solder joint. The coefficients of thermal expansion of the solder and the component being

so

21

to

th

w

in

te

a

[.

s

i

c

g

s

u

h

s

t

v

h

r

n

soldered are given by α_s and α_c respectively. The height of the solder is given by H , and $2L$ is the in-plane dimension of the substrate. The effect described by the equation is easy to visualize, for example, if the temperature is held constant, the force will be related to the shear strain in a linear manner with the value of the slope being $-kH$ [36]. Conditions will approach stress relaxation if the value of k is large or stiff, while low values of k imply creep processes [36]. Strain is associated with a compliant solder at high temperature conditions, as well as smaller forces since relaxation due to creep can occur almost instantly. On the other hand, stress is high with a stiff solder at low temperatures [36].

The accumulation of damage will be different for different parts of the thermal cycle since stress relaxation during the heating and cooling parts is not constant [31]. The incorporation of highly flexible leads with solder joints can greatly reduce creep strains developed as a result of cyclic loading conditions. A shearing of the solder joint will generally result when conditions do not allow for the use of flexible leads, such as in surface mounting [37]. However, an investigation by Ross *et al.* [17] indicates that the use of flexible leads can cause more damage than relief if certain criteria are not met. Findings indicated that lead stiffness must be at least 1000 times more flexible than the solder [17]. The process of stress relaxation is indicated in Figure 2.

2.6.2 Fatigue

Probably the most recognizable model for the prediction of fatigue life, N_f , is the Coffin-Manson relationship. The equation is based upon an empirical relation and can be found in a variety of forms. In order to better predict the fatigue life of solders, Coffin-Manson

type

In o

lead

stra

to t

et.

fir

gre

da

fa

in

Δ

w

f

C

a

a

R

i

type relations have been adjusted to account for temperature and frequency effects [38]. In order for this model to be utilized to predict the lifetimes of components with flexible leaded parts, the strain range must be the total plastic strain range. This must also include strain associated with creep deformation which must be determined accurately and added to the total plastic strain [17].

The form included here, $N_f = \left(\frac{\Delta \epsilon_p}{\epsilon_f} \right)^{-A} + \left(\frac{\Delta \sigma}{\sigma_o} \right)^{-B}$, was provided in a paper by Tien,

et. al. The equation can be divided into two parts, low cycle and high cycle fatigue. The

first term, $\left(\frac{\Delta \epsilon_p}{\epsilon_f} \right)^{-A}$, describes low cycle fatigue which is controlled by the rate of crack

growth [38]. The plastic strain range $\Delta \epsilon_p$ which is raised to the -A power is related to the

damage stored in each cycle. The second term, $\left(\frac{\Delta \sigma}{\sigma_o} \right)^{-B}$, is described as the high cycle

fatigue component. During high cycle fatigue, the component spends most of its life

initiating cracks and the damage stored in each cycle is best described by the stress range

$\Delta \sigma$ raised to the -B power [38]. Fatigue life in the range of up 10^4 cycles is associated

with low cycle fatigue, whereas fatigue life above 10^6 cycles is associated with high cycle

fatigue [38]. The exponents A and B are respectively the low and high cycle fatigue

Coffin-Manson variables. The fracture strain is given by ϵ_f , while σ_o is the stress

associated with high cycle fatigue [38]. Vaynman, *et al.* found this model to be

acceptable at strains above 10^{-2} , when subjected Pb-Sn solders to isothermal fatigue.

However, at strains below 10^{-2} , the relationship failed due to strong creep fatigue interactions during cycling [35].

2.6.3 Fatigue of Solder Joints

Fatigue in solder joints generally results from repeated thermal cycles caused by turning on and off electrical devices. The temperature fluctuations can induce cyclic strains as a result of thermal expansion mismatches between the solder and components, as previously mentioned, and result in the eventual failure of the component [32]. Prediction of the fatigue life of solder joints is a difficult task as a result of the time and temperature dependent characteristics of creep behavior [39]. A recent investigation into fatigue modeling has illustrated that creep is the dominating factor in the determination of fatigue life [40]. When considering fatigue life, there are a variety of relevant factors which must be considered including the range of temperature fluctuations, average temperature, dwell times, dwell temperature, rates of loading and unloading, joint geometry, solder microstructure, and the presence of alloying elements and intermetallics [39].

Fatigue damage is usually the result of dislocation pile-ups which cause stress concentrations. The complex microstructure of as-solidified eutectic solders as well as its instability at high temperatures make fatigue prediction models complicated [37]. Currently, no reliable predictive theory for thermal fatigue under creep conditions exists [37]. Recent attempts at modeling the complex interactions between creep and thermal cycling have indicated that the deformation and localized accumulations of strain produced during thermal cycling are not reversible [40]. This results from distortions occurring which change the stress distribution in the joint. Subsequent thermal cycles then have an altered impact on the state of stress and strain [30]. Experimental evidence indicates that strain is not reversible since continued thermal cycling results in

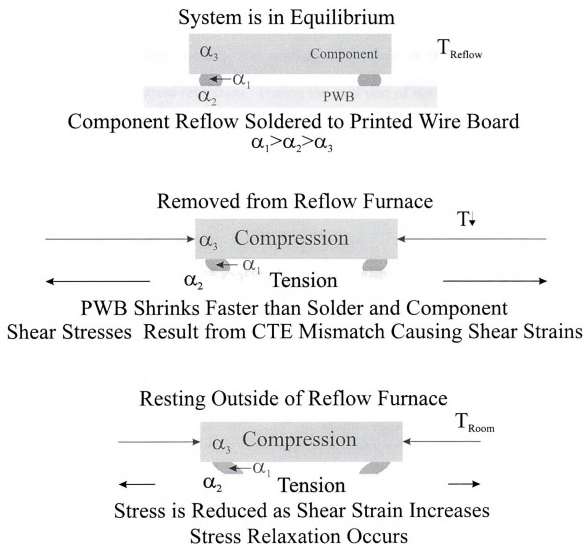


Figure 2. The Process of Stress Relaxation

pe

Fi

It

ma

co

oc

ma

de

un

permanent shape change. The process of thermo-mechanical fatigue is illustrated in Figure 3.

Inaccuracies result when accelerated thermo-mechanical fatigue tests are performed. It has been shown [41] that under accelerated thermo-mechanical fatigue testing, the majority of plastic deformation occurs during loading of the specimen, whereas, in a test conducted under realistic heating and cooling rates, most of the plastic deformation occurs as a result of stress relaxation. During the cold part of the cycle, stress relaxation may not be as significant as during the warm part of the cycle since creep has a high dependence upon temperature [34]. As a result, the effects of creep are greatly ignored under accelerated test conditions. The differences are illustrated in Figure 4.

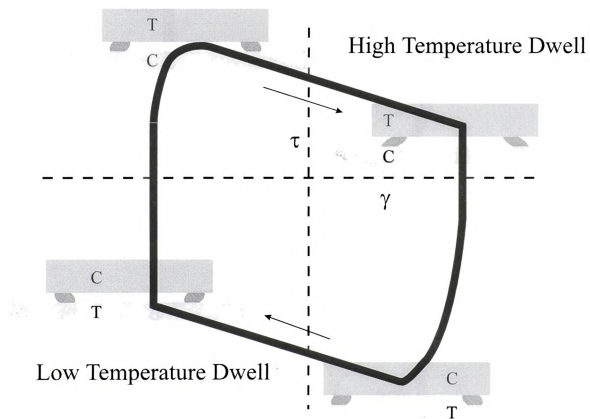


Figure 3. The Process of Thermo-Mechanical Fatigue

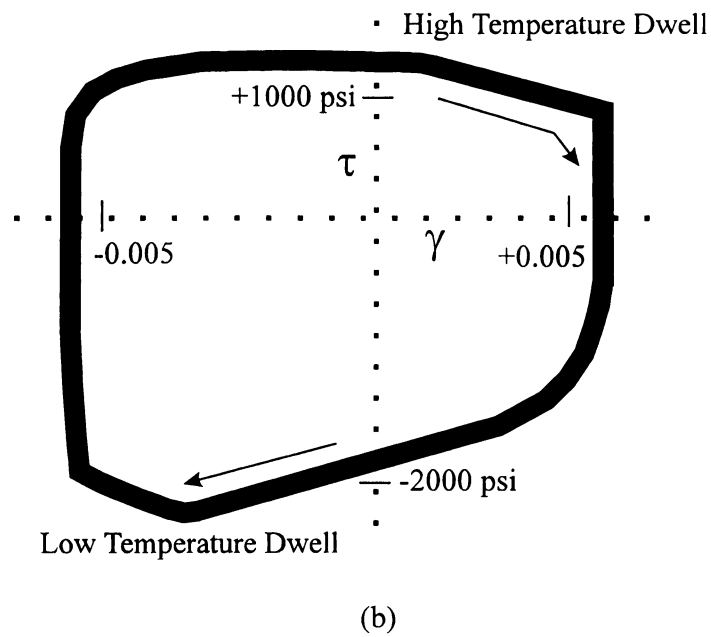
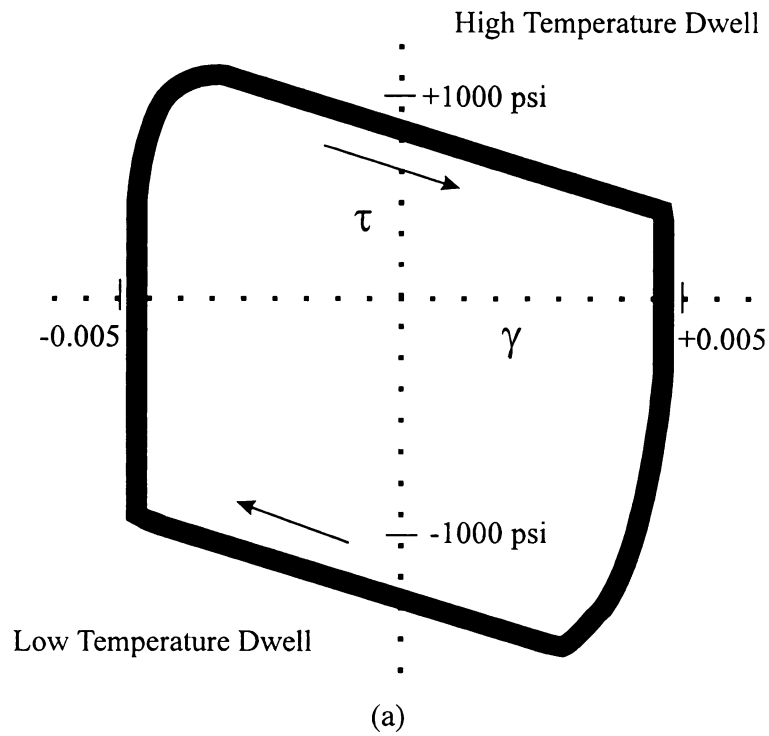


Figure 4. Differences Between Normal (a) and Accelerated (b) Thermo-Mechanical Fatigue Testing Adapted From Darveaux *et al.*

2.7 CREEP IN SOLDER JOINTS

Recently, there has been much work done concerning the creep of solder. It has also been acknowledged in a variety of papers that there is a significant difference between testing easily fabricated bulk specimens of solder and testing actual solder joints. The discrepancies are related to a smaller grain size due to faster cooling rates during fabrication as well as the lack of substrate constraint in bulk specimens which eliminates the formation of intermetallics near and at the substrate/solder boundary. Both of these effects are believed to be responsible for the significant increase in strength of solder joints compared to bulk specimens.

It has been noted [5] that solder containing silver (Ag) offer some of the highest creep resistances. This also results in reducing the strain observed during creep. Raeder, *et al.* [5] found in a study comparing Sn-Ag and Sn-Bi solder joints that at strain-rates greater than 10^{-4} s^{-1} , Sn-Bi has a higher flow stress, and at strain-rates lower than 10^{-4} s^{-1} , Sn-Ag solder has a higher flow stress. Raeder also noted significant creep differences between bulk solder and solder joint specimens.

Studies on composite solders have also been conducted within the last several years [10, 15, 41]. In all instances, the addition of a dispersed phase significantly increased the creep resistance of the solder. It has also been noted that increased porosity may result from these additions.

CHAPTER 3

EXPERIMENTAL PROCEDURE

3.1 SAMPLE PREPARATION

3.1.1 Joint Fabrication

The substrate material used in the fabrication of the solder joints consisted of copper dogbone halves, fabricated via electrical discharge machining (EDM). The substrate dimensions are shown in Figure 5a. In order to achieve a solder cross-sectional area of approximately 1 mm^2 , a solder mask was applied with a fine brush, approximately 1 mm from the narrow end of the copper substrate. The freshly masked copper substrate halves were then heated at a temperature of 150°C for one hour.

Before the solder joints could be fabricated, the Cu substrates were chemically cleaned with a solution of 50% Nitric acid and 50% water. Once the Cu substrates were cleaned and dried, a fine drop of Alpha 200-L flux was applied to the narrow end of the dogbone shaped substrate. Half of the Cu substrates were then placed, flux side up, into a specially machined aluminum fixture shown in Figure 5a. Two pieces of solder foil, approximately 1mm^2 in area and 30 microns in thickness, were sandwiched between the two Cu substrates as shown in Figure 5a. A thermocouple was connected to the aluminum fixture which was then placed directly onto a preheated hot plate. The fixture was heated to a temperature of 270°C on a hot plate and then quickly removed and placed on an aluminum chill block to simulate a cooling temperature history of industrial practice for reflowed solder joints. Once the aluminum fixture reached

0.26 mm

Figure 3

Figure 5

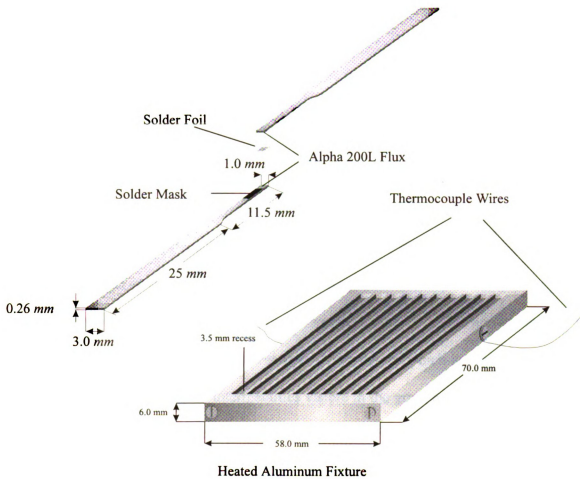


Figure 5a. Assembly of the Solder Joint.

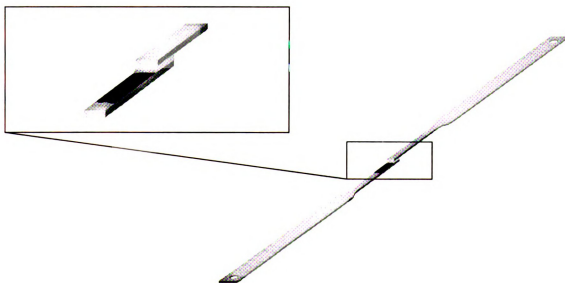


Figure 5b. Finished Solder Joint with Magnified View of Joint Area.

ambient

The inta

from 50

3.1.2 *Se*

Two typ

eutectic

which w

two diff

character

distingu

intermet

visible a

visible t

solder-s

3.1.3 *P*

During

properly

the first

used wit

to furthe

colloidal

ambient temperature, the solder joints were removed and gently inspected by hand for integrity. The intact joints as seen in Figure 5b were then polished. The solder joints ranged in thickness from 50 to 100 μm .

3.1.2 Solder Microstructures

Two types of lead-free solder were used in this investigation. Solder joints were fabricated from eutectic tin-silver solder (96.5Sn-3.5Ag) with and without 20v% 5-8 μm Cu_6Sn_5 intermetallics which were added as reinforcements. Scanning electron microscope (SEM) micrographs of the two different solder microstructures are shown in Figure 6. The non-composite solder is characterized by a colony type microstructure. The colonies which are only slightly visible, are distinguished by minute Ag_3Sn intermetallics visible in the grain boundaries. A layer of Cu_6Sn_5 intermetallics which formed at the solder-substrate interface during the soldering operation is visible at the top of the micrograph. In the composite solder, Cu_6Sn_5 intermetallics are clearly visible throughout the matrix. Naturally forming Cu_6Sn_5 intermetallics are also visible along the solder-substrate interface in the upper right corner.

3.1.3 Polishing

During the polishing procedure, the solder joints were held with a special grip designed to properly support the specimen as shown in Figure 7. Wet/dry sandpaper (240 and 600 grit) was the first medium employed in polishing the solder joints. Next, a 0.5 micron polishing solution used with a standard metallurgical polishing cloth adhered to a narrow aluminum block was used to further polish the specimen. The specimen was then finished with a 0.05 micron SiO_2 colloidal suspension in the same manner.

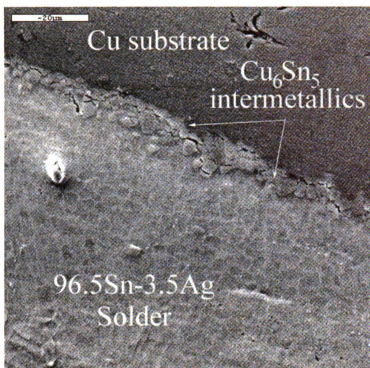


Figure 6a. Eutectic 96.5Sn-3.5Ag Non-Composite Solder Micrograph.

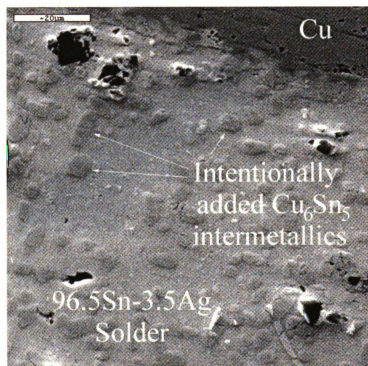


Figure 6b. Eutectic 96.5Sn-3.5Ag Composite Solder Micrograph.

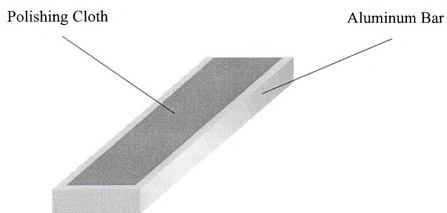
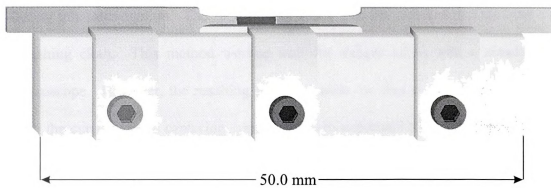


Figure 7. Specimen Grip and Polishing Bar.

In order to monitor displacement of the solder joints during creep testing, it was necessary to intentionally scratch the polished surface across both Cu substrates and the solder area. This is illustrated on page 53 with Figure 11. Several methods were used during this investigation. The first method was to rub the polished surface over a coarse polishing cloth. This method worked well for images taken with a standard optical microscope. However, the resulting scratches were too fine to be adequately monitored with the current image capturing system which incorporated a traveling microscope with a digital camera mounted on a tripod. A single-sided razor blade lightly pressed across the polished surface seemed to give the best results for this investigation. The scratch appears relatively large under a standard optical microscope, but when used in the current image capturing system, it provided sufficient results.

3.2 CREEP TESTING

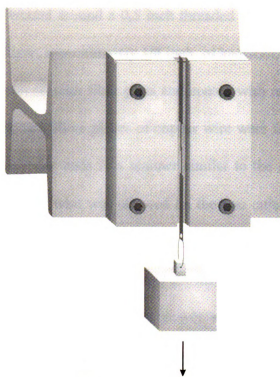
In order to subject the miniature solder joints to creep deformation at room and elevated temperatures, it was necessary to develop suitable testing equipment. The method chosen for free strain measurement required that the digital camera have an unobstructed view of the solder joint. This resulted in a variety of difficulties. Further problems were encountered when it was necessary to supply heat for elevated temperature creep tests. The devices and methods employed for this experiment underwent several stages of development until satisfactory testing methodology was achieved.

3.2.1 Miniature Creep Frame

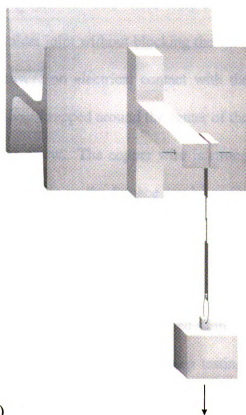
The miniature creep frame underwent significant development throughout this investigation. The first design (Figure 8a) worked relatively well, but did not allow incorporation of the miniature furnace. It was simply an aluminum machined plate connected an I-beam. It consisted of one vertical slot in front which provided clearance for the suspended solder joint and another narrow slot traversing the top which allowed for the solder joint to be suspended with a piece of piano wire. The next version depicted in Figure 8b was developed to incorporate miniature furnace.

3.2.2 Miniature Electrical Resistance Furnace

A miniature electrical resistance furnace was constructed for use with the shear-lap soldered specimens. *Nichrome*, an alloy commonly used for electrical heating elements, due to its strong oxidation and electrical resistance, was used in wire form to create heating coils. In order to achieve even spacing of the coils, the *Nichrome* wire was



(a)



(b)

Figure 8. Development of the Miniature Creep Frame.

wound around a 0.5 inch threaded bolt. The wound wire was then covered with a thin layer, approximately 1/4 inch, of kaowool, for thermal insulation. The assembly was then wound with fiber glass and coated with resin. In order to keep the fiber glass windings secure, three pieces of copper wire were fastened around the middle of the assembly and near the ends in a manner similar to the steel rings found on a wooden barrel. Excess copper wire was allowed on the two outer windings to be employed as electrical leads. The terminal ends of the *Nichrome* wire were fastened to the two outer copper wire windings. The furnace is shown in Figure 9.

A variable voltage power supply was used to provide current for the miniature furnace. The temperature was monitored with a thermocouple. *Teflon*[®] coated type K thermocouple wires were fastened to the shear-lap specimen. The wires were twisted onto the copper substrate as near as possible to the solder joint without blocking the view of the camera. Coated wires were employed to ensure no electrical contact with the *Nichrome* wire coil. A heavier piece of copper wire was wrapped around the center of the furnace and secured onto the I-beam with a machine screw. The copper wire is strong enough to support the light weight furnace and also flexible so the furnace can be easily aligned with the hanging shear-lap specimen. See Figure 10.

3.2.3 Deformation of Solder Joints

The miniature solder joint was placed in the creep frame which was equipped with an electrical resistance heater (when necessary) and designed for dead load creep testing. The microscope and fiber optic lighting system were then positioned for optimum resolution of details. The scratch must be clearly visible before testing begins, because as

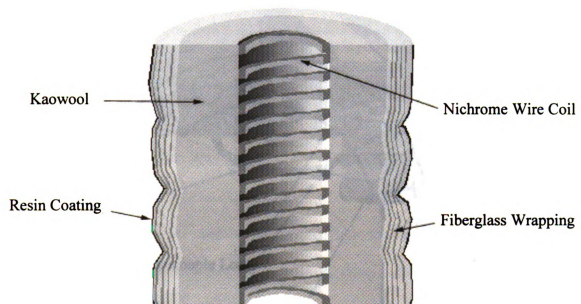


Figure 9. Miniature Electrical Resistance Furnace.

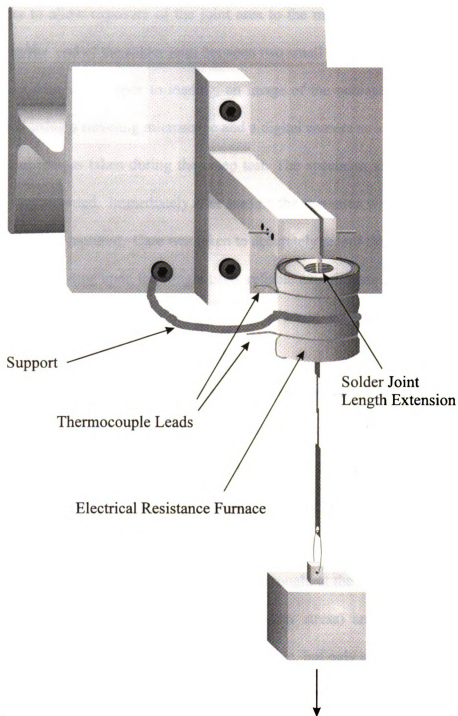


Figure 10. Creep Frame Set Up for Elevated Temperature Testing.

the creep test progresses, the scratch becomes less distinguishable (Figure 11). If the resistance furnace was used, the length of the solder joint was extended at the suspended end in order to allow exposure of the joint area to the microscope. This was done by sandwiching the end of the solder joint between two small lengths of metal and fastening the assembly with wire. Prior to loading, an image of the undisplaced scratch position was captured using a traveling microscope and a digital camera as a basis for comparison to subsequent images taken during the creep test. The specimen identification and load used were also recorded. Immediately after loading the specimen with the desired weight, another image was captured. Care was taken to accurately record the time associated with each image. Depending upon the weight used, reliable experiments lasted anywhere from 10 minutes to more than three months, so this made accurate time measurements imperative for the short duration experiments.

The frequency of image capturing depended upon the load used. Usually 10 to 30 data points are sufficient for generating an accurate creep curve. Variance in temperature as well as safety precautions during elevated temperature testing required the operator to remain present so that adjustments in temperature could be performed.

The creep tests used for this investigation were performed at 25°C, 85°C, and 125°C with temperature fluctuations less than 7 degrees throughout the duration of each elevated temperature experiment. Both longer duration (low stress) and short duration (high stress) creep tests were performed at room temperature, but only short duration tests were performed for the elevated temperature creep. The short duration or accelerated tests were conducted in a range from 30 minutes to approximately 24 hours, while the long duration creep tests usually lasted for 2 to 3 months.

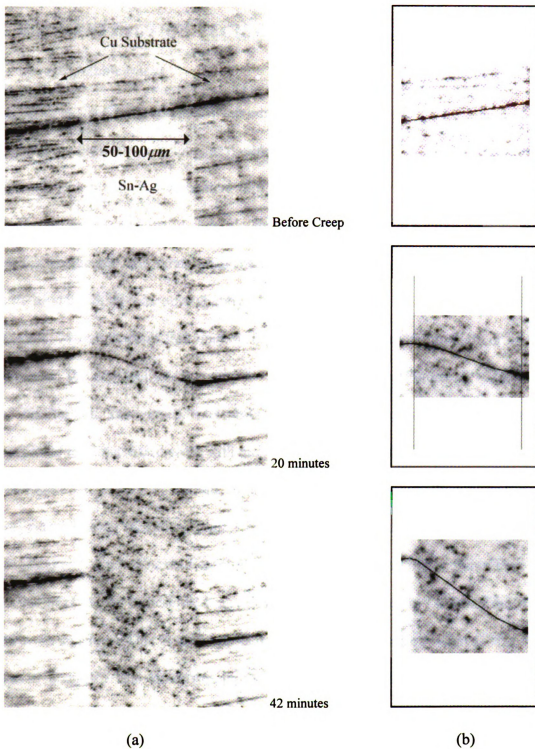


Figure 11. Displacement of Scratch Due to Creep Shown as
 (a) Raw Captured Image in Negative Format.
 (b) Enhanced Image for use in *Datathief*.

3.3 DATA EXTRACTION TECHNIQUE

3.3.1 Image Enhancement

After an image has been captured, it was edited in *Adobe Photoshop*[®]. Several tasks were performed on each photo before they were ready for analysis. Each digitally captured image was first inverted to a negative format. A white image with a black scratch was more convenient for analysis in *Datathief* than a black image with a white scratch. As the creep test progressed, the scratch became more difficult to detect as illustrated in Figure 11. A scratch which was only slightly visible in Photoshop was almost impossible to distinguish when opened in *Datathief*. It then becomes necessary to highlight or trace the scratch with the line tool in *Photoshop*[®]. This is illustrated in Figure 11. Most of the error involved in these creep tests probably occurs during this procedure, since the resolution of the scratch decreases with increasing displacement.

In Figure 11, images in the left column are examples of digitally captured scratch displacement images (negative format) from a composite solder creep tested at 125°C. Time of capture is noted next to each image. The images in the right column have been enhanced in *Datathief* as described previously. The images used in *Datathief* must be of uniform dimensions. This is accomplished by establishing a uniform canvas size for all enhanced images. This eliminates the possibility of non-uniform image distortion in *Datathief*. Both solder/substrate interfaces can be seen in the enhanced images and are highlighted in the image captured after 20 minutes.

If the full raw image is opened in *Datathief*, the area of interest is too small for accurate analysis. For these reasons each image is carefully cropped. However, as the

creep experiment progresses, the area of interest from each image increases vertically. By changing the canvas size or image border, the dimensions of the images stay the same while the surrounding 'canvas' is enlarged. Since subsequent images only grow in the vertical direction, the simplest process is to edit the final, tallest image from the creep experiment first. Sufficient borders are required on every image for the ease of data extraction. By examining the final image, appropriate dimensions can be determined and applied to all the previous images, with the first image having the largest vertical border.

3.3.2 Data Extraction

Datathief is a data digitizing shareware package available only for the Macintosh platform, which allows the user to extract data points from a digitized image by establishing an x-y coordinate system directly onto the image. Since the displacement of the scratch must be measured by extracting data from many images, it was necessary to establish the same x-y coordinate positions on each subsequent image. Since shear displacements were measured, a normalized dimensional scale based on the thickness of the joint was used as a basis for computing shear strains (Figure 12). The displacement of the scratch was modified or scaled with respect to the thickness in order to obtain a value of zero for the maximum displacement. See Appendix B for a detailed example of the data extraction process. The axes must be established in a manner so they can easily be accurately transferred to each subsequent image. The technique developed in this instance, was to use an 8.5 " by 11" transparency overlaid onto the computer monitor. Several images from the same creep test, from beginning to the end, were then opened in the *Datathief* program and analyzed for similarities in an attempt to find an identifying

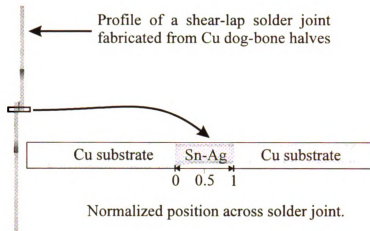


Figure 12. Normalized Position Across the Thickness of a Solder Joint.

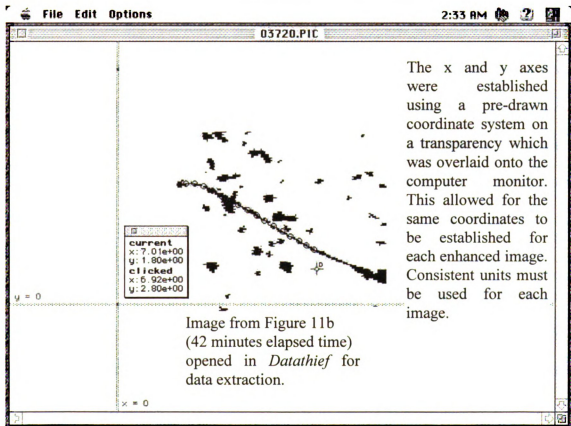


Figure 13. Screen Capture of Data Extraction Using *Datathief*.

mark visible on each image near the stationary interface which could be used as a landmark throughout the data extraction procedure. This could be anything from a scratch to a small pore, but it must be visible on each subsequent image. A marker pen was then used on the overlaid transparency to trace this landmark as well as the left and right interfaces. These highlights can then be confirmed by opening different enhanced images, as seen in Figure 11b, in *Datathief* and checking for alignment of the transparency and the image. Once this was carried out, axes could then be drawn onto the transparency with the aid of a ruler. The longer the axes, the less error was involved due to the angle of view and parallax distortion inherent in the computer monitor. Figure 13 is a screen capture of an enhanced image seen, in Figure 11b, opened in *Datathief*.

Once the axes are established, an x-y coordinate window in *Datathief* displays the current position of the cursor. The cursor was traced along the length of the enhanced scratch via the mouse. The mouse was then clicked at even increments, usually every centimeter or two on the monitor according to the pop up x-y coordinate window which indicates position on the image (Figure 13). The exact x-coordinate positions were noted and used on each subsequent image. The process was then repeated for the remaining images. Since it was impossible to determine the duration of each creep test beforehand, images were captured frequently, although well defined creep curves could be produced without extracting data from every image. Once the coordinate axes were established, about 10-20 datum points were extracted from the scratch, at the same x-coordinate positions for every image.

3.3.3 Reproducibility of Data Extraction

In order to determine how sensitive the data were to human interpretation, comparisons were made of a set of data extracted from the same set of images several months apart using the same procedure. The error between the two measurements of the same average strain increased with strain from about 1 to 10%, due to the degraded clarity of the captured image at larger strains.

3.4 DATA PROCESSING

From the extracted data, a single plot can be produced which illustrates the entire scratch displacement history on one specimen (Figure 14). This is similar to overlaying all of the captured images onto one image, but in the form of a plot. Global creep strain is defined as the average creep strain across the thickness of a specimen. Measured global strains generally result in creep curves of the classic sense as shown in Figure 1. This designation is made since a comparison between the two forms (global and localized) is necessary.

3.4.1 Global Creep Strain Measurement

The first step in calculating the global creep strain was to measure the shear displacement of one side of the specimen with respect to the other. Displacement during creep deformation occurred only at one solder/substrate interface, while the other interface remained stationary. A coordinate system was established by designating the end of the scratch at the stationary solder/substrate interface as a reference origin.

The next step was to calculate the net shear displacement. In order to account for the non-horizontal shape of the initial scratch, the difference between the data for the initial scratch position and a simplified horizontal origin was subtracted from the subsequent scratch position data derived from images captured during the creep test. The resulting global net shear displacement after 8520 seconds was plotted with position across the thickness in Figure 15, where the bolder lines represent the net shear displacement. From this figure, the global creep strain was computed by dividing the total net displacement by the thickness.

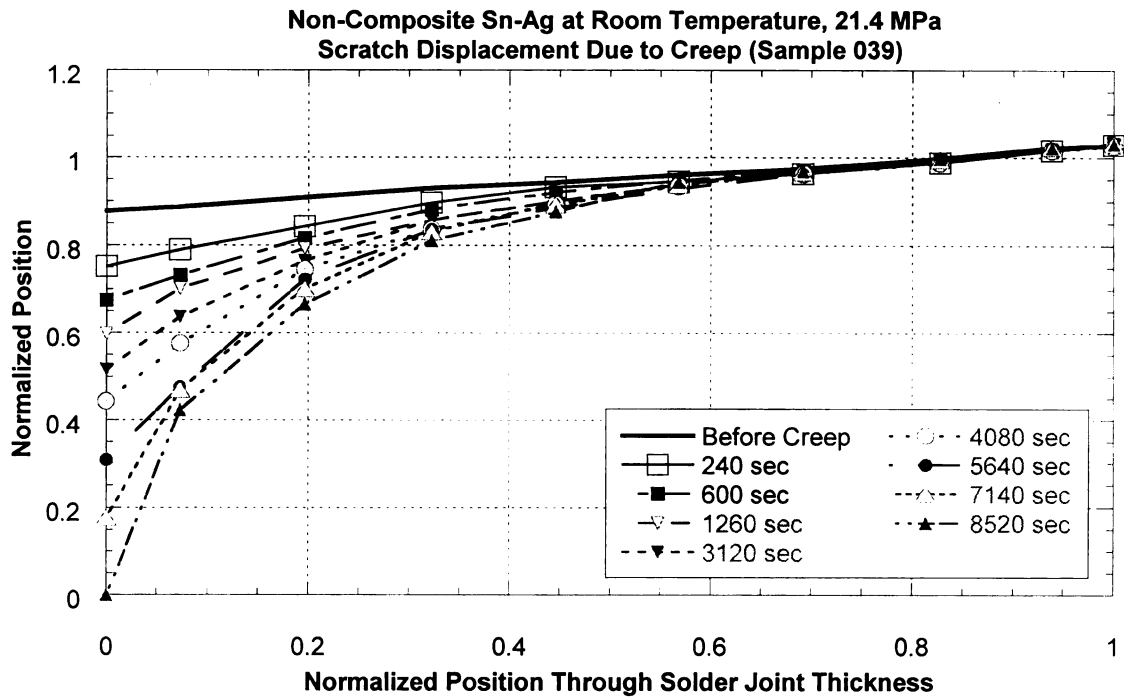


Figure 14. Scratch Displacement History.

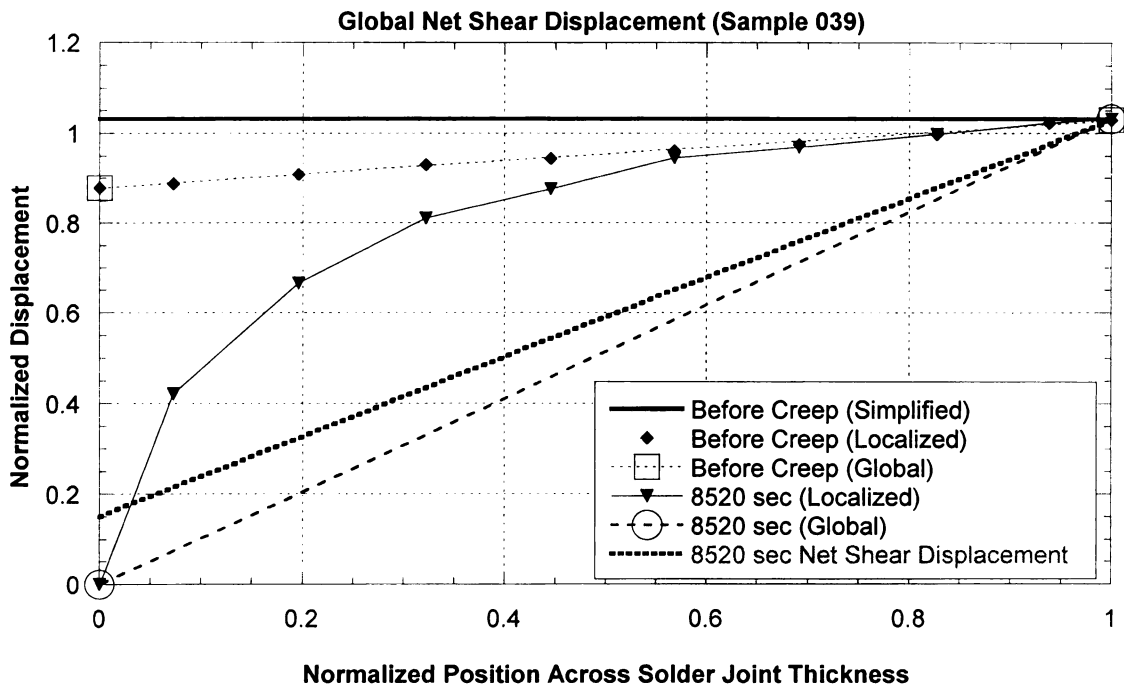


Figure 15. Difference Between Global and Localized Deformation.

3.4.2 Localized Creep Strain Measurement

The local shear strain was determined by fitting a cubic polynomial function using *Kaleidagraph*[®] software to the shape of each scratch. The same procedure for determining the net shear displacement was employed. This resulted in the localized net shear displacement shown in Figure 16. By differentiating the resulting cubic polynomials, the local slope of each scratch, which is the local shear strain, was computed. Note that in some locations reverse (negative) strains were observed, such as position 0.7. The degree of accuracy of each fitted curve was indicated by the coefficient of determination, R^2 , where a value of 1 indicates a perfect fit. The average value of R^2 for all of the curve fitting procedures in this experiment was 0.99.

A plot indicating the creep strain history for different positions across the solder joint thickness (indicated by normalized position) was then produced from this information as illustrated in Figure 16 (strain-time history at selected illustrative positions is shown, note that at position 0.7, the strain rate is negative at later times).

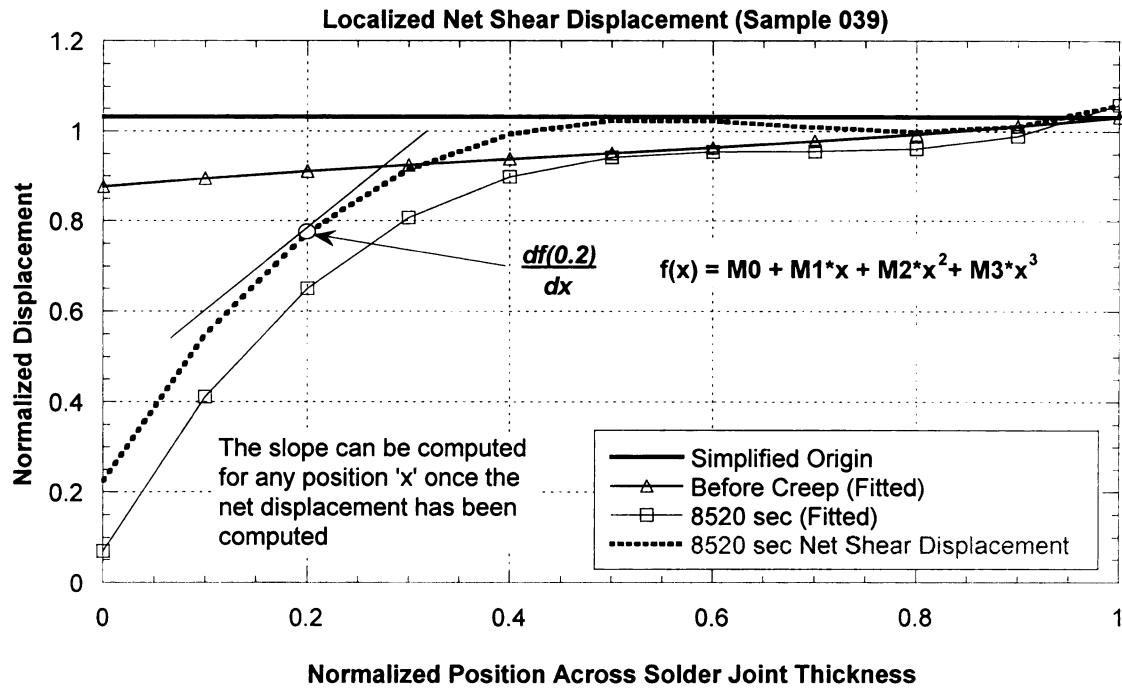


Figure 16. Cubic Polynomial Curve Fit.

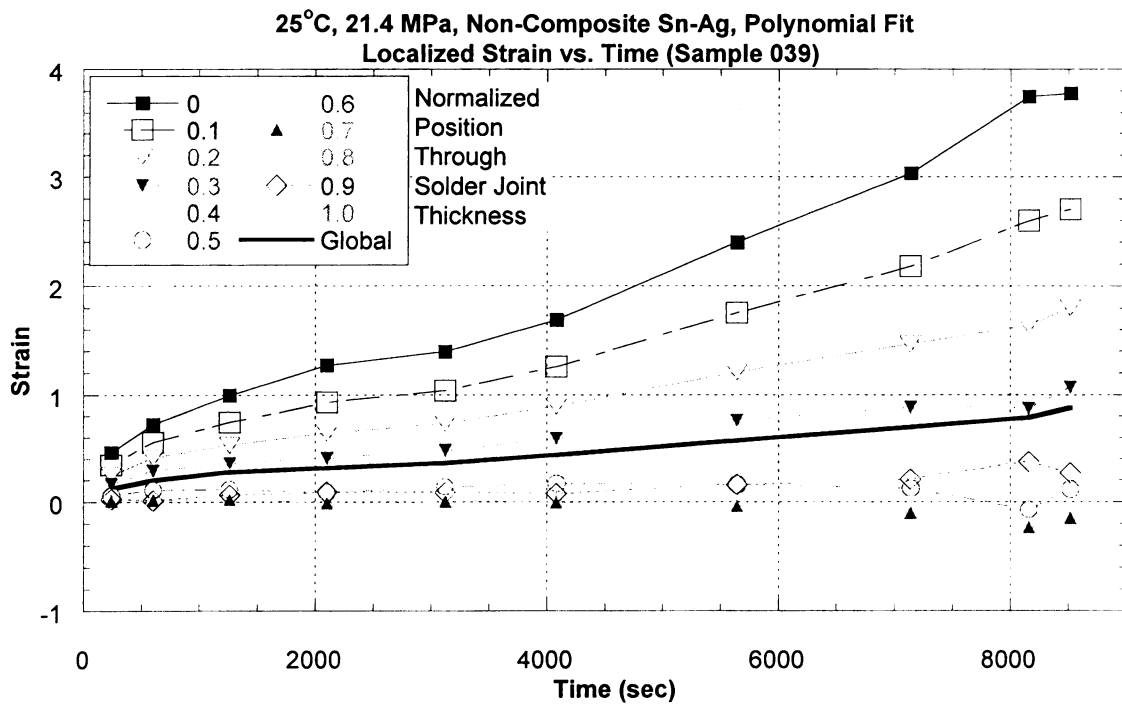


Figure 17. Localized and Global Creep Strain.

3.4.3 Strain-Rate, Position, and Time

In order to examine how the strain-rate varied with time and normalized position, three-dimensional plots were produced from the localized strain history plots. Polynomial curves of order 3-7 were used to fit the strain time curves (Figure 17) at each position. The derivative was calculated with respect to position to obtain the strain-rate, and plotted using *Deltagraph*® 3.0 software as illustrated in Figure 18. The 3-D surface is represented as a contour plot on the top of the plotting space. The shape of the 3-D surface varied from specimen to specimen. The example shown in Figure 18 illustrates the variability in the detailed strain-rate history in the measured part of the specimen.

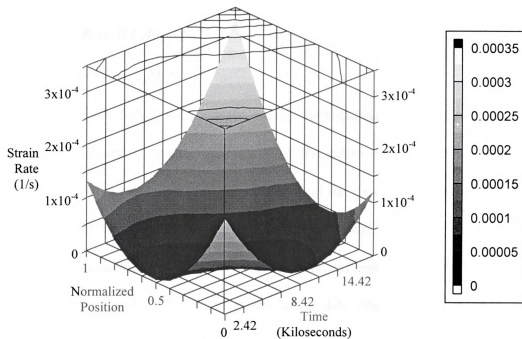


Figure 18a. Variation of Strain-Rate to Time and Normalized Position for a Composite Solder Creep Tested at 25°C.

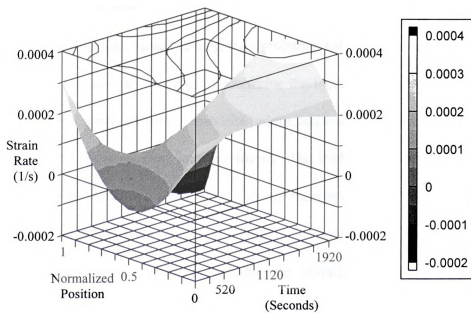


Figure 18b. Variation of Strain-Rate to Time and Normalized Position for a Non-Composite Solder Creep Tested at 85°C.

3.5 SEM OBSERVATIONS

3.5.1 Determination of Stress

After the specimen failed, the fractured halves were examined optically or with a SEM, and low magnification images were taken of the entire fracture surface, as shown in Appendix C. All specimens exhibited porosity, and the area of pores larger than $500 \mu\text{m}^2$ were subtracted from the entire surface area, using *NIH image* software, in order to determine the actual cross-sectional area of the soldered region. The true stress operating on the cross sectional area was computed using this reduced area. Due to the long moment arm effect of the two copper tabs, strain in the joint was nominally uniform in the straining direction even though porosity present throughout the solder joint could lead to asymmetry in load carrying area with respect to the center-line.

3.5.2 Initiation of Fracture

The method employed for creep testing the miniature solder joints did not allow for detection of crack initiation. In order to determine the location of fracture initiation four solder joints, two fabricated from composite solder and two from non-composite solder were subjected to high stress dead load conditions. The solder joints were prepared in the same manner as described in Section 3.1.3. Visual records of the polished surfaces were recorded prior to loading with the use of a SEM. The solder joints were strained using the miniature creep frame. Each solder joint was initially subjected to a weight low enough to avoid rupture, approximately 2.27 Kg. (5.0 lb.). The load remained on the solder joint for roughly 10 seconds and was then removed. The solder joint was then removed from the creep frame and examined under an optical microscope. If no signs of

crack initiation were visible, the process was repeated with load increments of 0.23 Kg. (0.5 lb.). This procedure resulted in differing strain-rates depending upon each specimen. The strain-rates were not measured. When significant changes in the polished solder joint were detected, examination was performed with an SEM.

3.5.3 Location of Fracture

Examination of the fractured solder joints was performed to determine the location of the fracture across the polished thickness of the solder joint. These images were compared with the fracture surfaces images in order to better characterize the mode of fracture.

CHAPTER 4

RESULTS

4.1 COMPARISON OF EXPERIMENTAL CREEP DATA TO DATA FOUND IN THE LITERATURE

In order to determine the reliability of the testing methods used in this investigation, a comparison of the creep data acquired was compared to data found in the literature. The data used for the comparison came from an investigation by Darveux *et al.* [41]. They subjected aged, realistically sized solder joints (ceramic chip carriers soldered together with eutectic Sn-Ag) to creep deformation at temperatures of 131°C, 77°C, and 27°C. Solder joints used in this study were not subjected to aging processes. The data of Darveaux *et al.* was normalized with respect to temperature in a manner described in Section 2.4.9. The normalized secondary (or minimum) creep strain-rate was plotted against normalized shear stress. Darveaux *et al.* used a 'trial and error method' to produce a best fit curve to represent the normalized creep data. Values determined by Darveaux *et al.* for $G = G_0 + G_1 T(^{\circ}C)$, where $G_0 = 2.8 \times 10^6$ psi and $G_1 = 1.0 \times 10^4$ psi/°C were assumed for this investigation. In order to simplify the comparison, a single plot comparing the data from this investigation to the data of Darveaux *et al.* was produced (Figure 19).

Another reason for this comparison was to examine the effects that the intentionally added Cu₆Sn₅ particles had upon creep behavior at room and elevated temperatures. From this comparison, it is apparent that the composite solder is more creep resistant than the

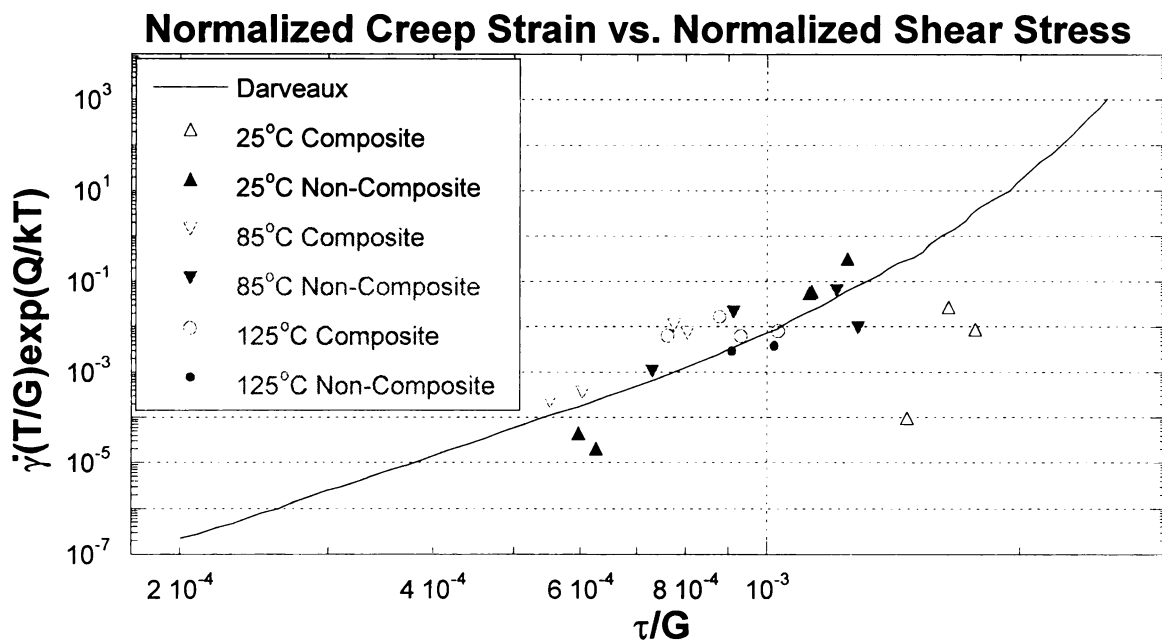


Figure 19. Comparison of Secondary Creep-Rate Data.

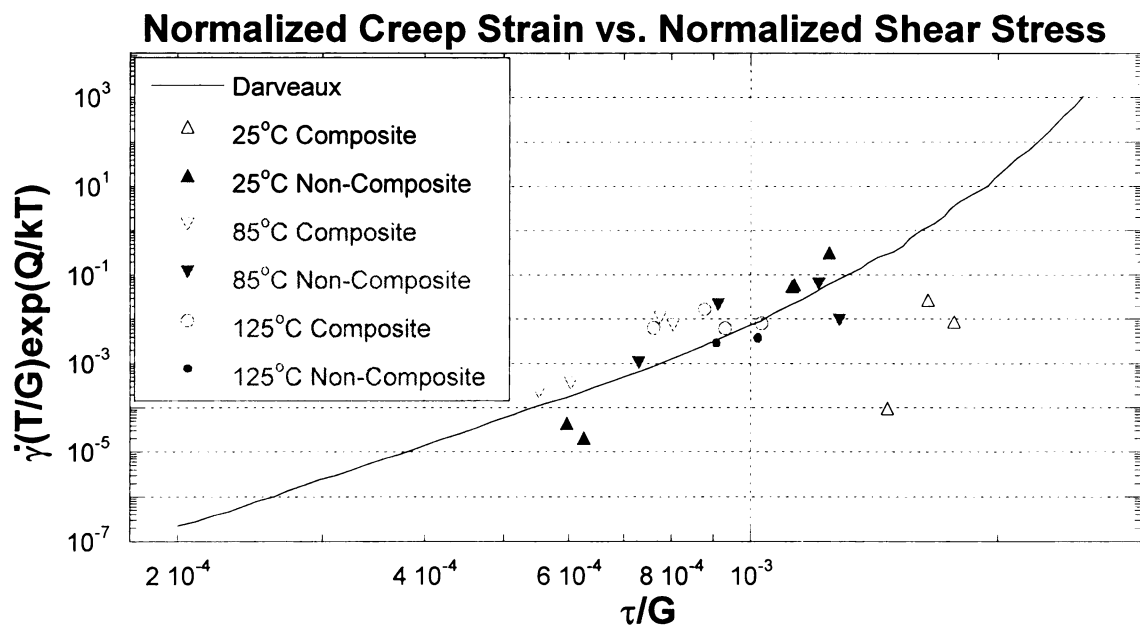


Figure 19. Comparison of Secondary Creep-Rate Data.

non-composite solder, at room temperature and 85°C, but the composite solder joints are comparable in creep resistance to the non-composite at 125°C.

4.1.1 Room Temperature Composite Data

The composite solder joints tested at room temperature exhibited superior resistance to creep as compared to the non-composite solder joints. The strain-rate of the solder joint tested at the lowest stress was near 3.5 orders of magnitude less than the trend established by Darveaux *et al.* As stress increased this difference decreased by an order of magnitude on average. A trend different from that established by Darveaux *et al.* for the non-composite data appears to be present for the composite data resulting from this experiment.

4.1.2 Room Temperature Non-Composite Data

Room temperature (25°C) creep data obtained in this study was in relative agreement with the trend established by Darveaux, *et al.* The three solder joints tested at higher stresses were all characterized by strain-rates within an order of magnitude of Darveaux's best fit curve. Two of the points were in such proximity that only one was visible. Of the two solder joints tested at lower stresses, both were characterized by strain-rates which were lower than the established trend. One solder joint had a strain-rate within an order of magnitude of the established trend, while the other specimen had a strain-rate more than an order of magnitude less than the established trend.

4.1.3 85°C Data

The two composite solder joint tested at lower stresses agreed well with the best fit curve. Both were characterized by strain-rates well within one order of magnitude of the established trend. As stress increased, the margin between the data and the best fit curve increased to around one order of magnitude. Non-composite solder joints tested under this temperature environment exhibited similar results to the composite data.

4.1.4 125°C Data

All of the composite solder data was characterized by strain-rates within one order of magnitude of the trend established by Darveaux *et al.* Two of the solder joints tested exhibited higher strain-rates than the established trend. The other two specimens were characterized by strain-rates which were equal or almost equal to the established trend. Both of the non-composite solder joints tested at this temperature had strain-rates nearly equal to the established trend and their data points fell almost directly upon the best fit curve. These samples appeared to have slightly better creep resistance than non-composite solder joints tested under lower temperature conditions. However, this apparent trend should be disregarded due to the inherent scattering of data associated with creep.

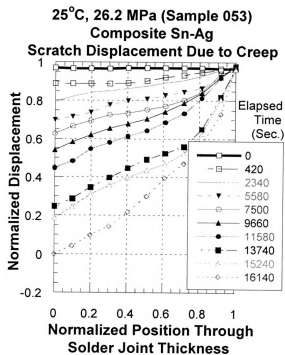
4.2 GLOBAL VS. LOCALIZED CREEP STRAIN

The global strain-time history usually exhibited classical primary, secondary and tertiary strain behavior as indicated by the heavy lines in Figure 20b. The vertical scale of a global creep curve became flattened when plotted with the localized creep curves from a single specimen since a wider range of values were present. As a result, plots of individual global creep curves are available in Appendix D. Characterization of the local strain history of all samples included in this investigation is provided in the following sections. As mentioned previously, these specimens include composite and non-composite solder joints deformed at room temperature, 85°C, and 125°C. Since there are more than 20 solder joints tested, descriptions will be limited to the most representative specimens. The associated figures include a scratch displacement history (a), a strain history (b) and strain-rate history with respect to position (c).

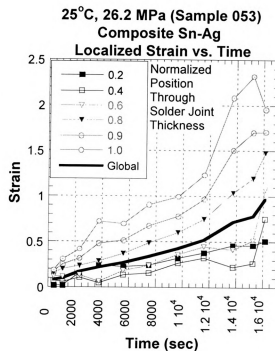
4.2.1 Room Temperature Composite Creep Data

Figure 20 illustrates creep history of a composite solder joint subjected to creep deformation under a stress of 26.2 MPa for about 4.5 hours (16.1 Ks). This specimen had highest localized strain accumulation near the interface at position 1.0. Identification of the beginning of global tertiary creep was near a shear strain of 0.5. However on a local scale, tertiary creep appeared to start at a larger shear strain of 1.2 near the interface. The secondary creep-rate was measured to be $4.2 \times 10^{-5} \text{ s}^{-1}$.

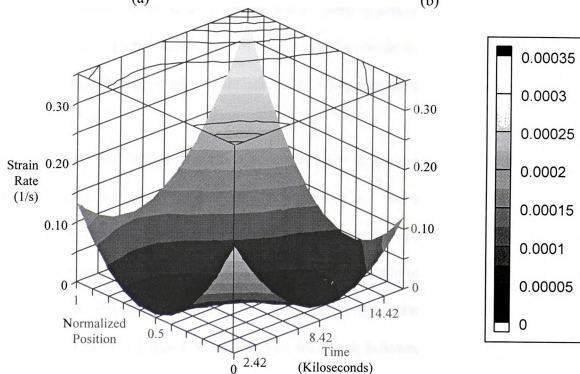
The 3-D plot indicated a sharp initial decrease in the strain-rate near the interface (positions 0 and 1.0), with a much lower initial strain-rate in the center of the specimen.



(a)



(b)



(c)

Figure 20. Displacement (a), Localized Creep Strain (b), and Strain-Rate (c) Histories for Composite Solder at 25°C.

Th

ra

th

po

4.

Fi

de

sp

ho

fo

cre

sta

be

(po

be

po

At

val

enc

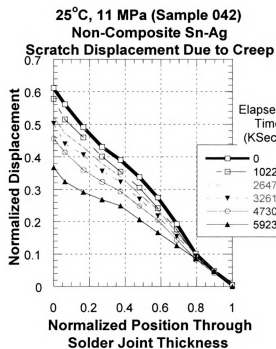
0, t

The strain-rate decreased with time in a normal way to reach a minimum strain-rate in the range of $2-8 \times 10^{-5} \text{ s}^{-1}$. The strain-rate then gradually increased to reach higher values at the two interfaces prior to rupture. The highest strain-rate ($3.3 \times 10^{-5} \text{ s}^{-1}$) was observed at position 1.0.

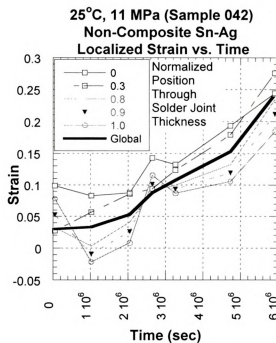
4.2.2 Room Temperature Non-Composite Creep Data

Figure 21 illustrates creep history of a non-composite solder joint subjected to creep deformation under a stress of 11 MPa for a duration near 2 months (6.0 Ms). This specimen had highest localized strain accumulation near the interface at position 0, however the specimen deformed in a homogeneous manner with the localized strains following closely to the trend of global strain. Identification of the beginning of tertiary creep is near a global shear strain of 0.15. Near the interface, tertiary creep appeared to start at a slightly higher shear strain near 0.18. The secondary creep-rate was measured to be $3.0 \times 10^{-8} \text{ s}^{-1}$.

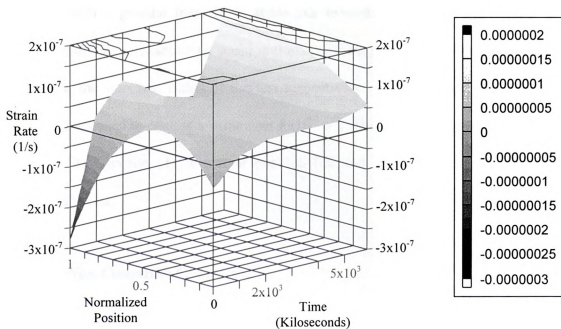
The 3-D plot indicated a sharp initial decrease in the strain-rate near the interface (positions 0) and to a much lesser extent position 1. The strain-rate initially peaked between positions 0.3 and 0.5 peaks at a value near $5.0 \times 10^{-8} \text{ s}^{-1}$. The strain-rate at position 0 remained constant throughout the test after a slight increase near the beginning. At the other interface, position 1, the strain-rate rapidly increased where it peaked at a value of $7.5 \times 10^{-8} \text{ s}^{-1}$ after 2 Msecs. It then decreased, followed by a final increase at the end of the test to a value of $2.0 \times 10^{-7} \text{ s}^{-1}$. From approximate positions in the range 0.8 to 0, the strain-rate remained relatively constant until the end of the test, where an increase



(a)



(b)



(c)

Figure 21. Displacement (a), Creep Strain (b), and Strain-Rate (c) Histories for Non-Composite Solder at 25°C.

i

P

4

F

d

h

th

te

w

pe

re

st

co

th

th

4.

Fi

de

sp

0.5

in strain was experienced across the entire solder joint with the maximum strain-rate at position 1.

4.2.3 85°C Composite Creep Data

Figure 22 illustrates creep history of a composite solder joint subjected to creep deformation under a stress of 13.2 MPa for about 1.3 hours (4.6 Ks). This specimen had highest localized strain accumulation near the interface at position 1.0. Identification of the beginning of tertiary creep was near a global shear strain of 0.5 but near the interface, tertiary creep appeared to start at a larger shear strain of 0.75. The secondary creep-rate was measured to be $9.8 \times 10^{-5} \text{ s}^{-1}$.

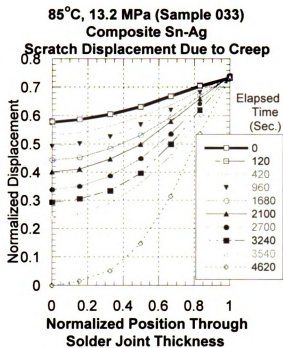
The 3-D plot indicated a slight initial decrease in the strain-rate near the interface at position 0, with a gradual increase in strain-rate towards position 1. The strain-rate remained relatively constant along position 0 except for a slight increase and decrease in strain-rate at the start and finish of the test respectively. At position 1, the strain-rate continually increased to peak at a value near $8 \times 10^{-4} \text{ s}^{-1}$. The strain-rate remained constant throughout the duration of the test at position 0.2 and increased towards position 1 throughout the test.

4.2.4 85°C Non-Composite Creep Data

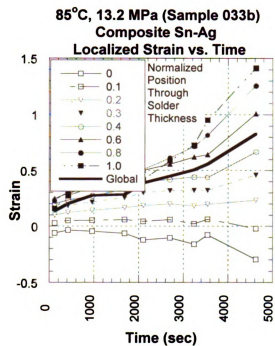
Figure 23 illustrates creep history of a non-composite solder joint subjected to creep deformation under a stress of 19.6 MPa for about 34 minutes (2.0 Ks). Unlike the prior specimen, the largest strains were observed in the center of the specimen near position 0.5. Identification of the beginning of tertiary creep is near a global shear strain of 0.24

Str
R
(P

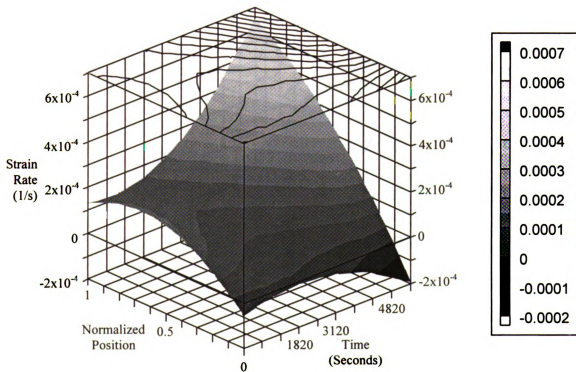
Str
R
(P



(a)



(b)



(c)

Figure 22. Displacement (a), Creep Strain (b), and Strain-Rate (c) Histories for Composite Solder at 85°C.

[illegible]

I

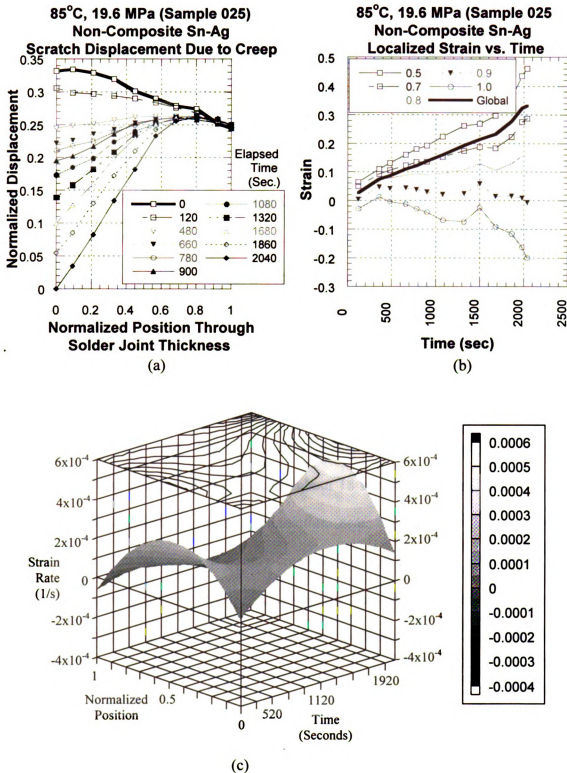


Figure 23. Displacement (a), Creep Strain (b), and Strain-Rate (c) Histories for Non-Composite Solder at 85°C.

br

Th

po

sp

str

an

an

10

of

4.2

Fig

def

ach

Ide

spe

the

cree

posi

decr

-2x1

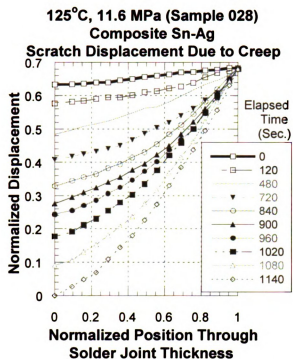
but near the center, tertiary creep appears to start at a slightly larger shear strain of 0.3. The secondary creep-rate was measured to be $1.2 \times 10^{-4} \text{ s}^{-1}$.

The 3-D plot indicated a slight initial decrease in the strain-rate near the interface at positions 1 and a higher initial strain-rate in the center of the specimen. Unlike the prior specimen, the strain-rate remained the highest at the center of the joint. At position 1 the strain decreased until specimen fracture. Then strain-rate near position 0 increases until an elapsed time of 1400 seconds where it attained a maximum strain near $2.5 \times 10^{-4} \text{ s}^{-1}$ and began a decrease in strain-rate until the end of the test. The highest strain-rate ($5.0 \times 10^{-4} \text{ s}^{-1}$) developed in the center of the specimen between positions 0.3 and 0.5 at the end of the test.

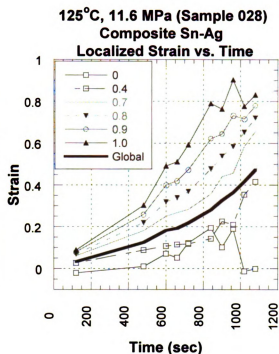
4.2.5 125°C Composite Creep Data

Figure 24 illustrates creep history of a composite solder joint subjected to creep deformation under a stress of 11.6 MPa for about 18 minutes (1.1 Ks). This specimen achieved highest localized strain accumulation near the interface at position 1.0. Identification of the beginning of tertiary creep for this specimen was not obvious. The specimen behaved in a tertiary manner after a global shear strain value near 0.1, but near the interface, tertiary creep appeared to start at a larger shear strain of 0.3. The secondary creep-rate was measured to be $5.8 \times 10^{-4} \text{ s}^{-1}$.

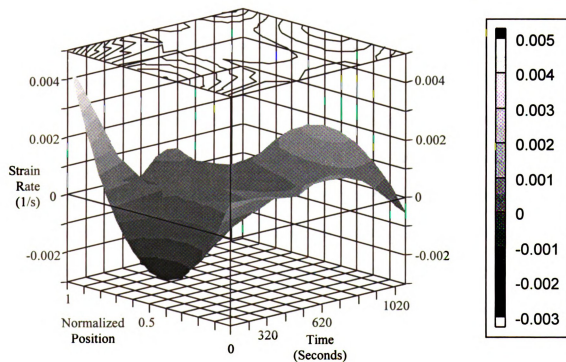
The 3-D plot indicated a sharp initial increase in the strain-rate near the interfaces positions 0 and 1.0, with a much greater increase near position 1 ($5 \times 10^{-3} \text{ s}^{-1}$). A sharp decrease in initial strain-rate initially existed at the center of the specimen with a value of $-2 \times 10^{-3} \text{ s}^{-1}$. Near position 0, the strain-rate remained relatively constant until a decrease



(a)



(b)



(c)

Figure 24. Displacement (a), Creep Strain (b), and Strain-Rate (c) Histories for Composite Solder at 85°C.

be

th

te

jo

r

a

4

I

C

2

I

I

S

S

S

1

S

S

C

I

before rupture. The secondary creep rate, the peak rate of creep, varied third of the test duration, remained constant for another third, and then increased again to terminate in a manner completely opposite of the initial strain-rate. The entire solder joint behaved in an opposite manner as it did at the beginning of the creep test achieving a maximum strain-rate of $1.5 \times 10^{-3} \text{ s}^{-1}$. The strain-rate near position 1, sharply decreased and then behaves erratically until a continual decrease half way through the test.

4.2.6 125°C Non-Composite Creep Data

Figure 25 illustrates creep history of a composite solder joint subjected to creep deformation under a stress of 12.7 MPa for about 50 minutes (3.1 Ks). This specimen achieved highest localized strain accumulation near the interface at position 0. Identification of the beginning of tertiary creep was near a global shear strain of 0.6, but near the interface, tertiary creep appeared to start at a larger shear strain of 0.9. The secondary creep-rate was measured to be $1.3 \times 10^{-4} \text{ s}^{-1}$.

The 3-D plot indicated a relatively constant strain-rate across the thickness of the solder joint with a slight decrease at position 0. The strain-rate remained constant throughout most of the test except at position 0 where the strain-rate appears to follow a sinusoidal pattern until rupture. After an elapsed time near 2600 seconds, the strain-rate sharply increased in a uniform manner, except near position 1, with the maximum value of $2.2 \times 10^{-3} \text{ s}^{-1}$ at the center of the solder joint. The strain-rate near position 1 remained relatively unchanged throughout the duration of the test.

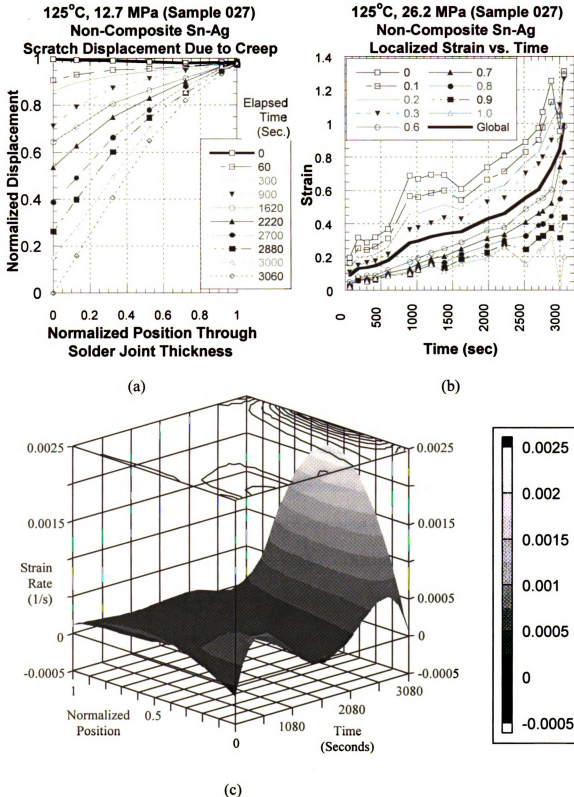


Figure 25. Displacement (a), Creep Strain (b), and Strain-Rate (c) Histories for Composite Solder at 85°C.

4

I

r

t

h

r

n

l

C

l

v

o

v

d

y

4.3 POSITION OF MAXIMUM LOCALIZED CREEP STRAIN

It is evident through determining the localized creep strain, that strains of much higher magnitudes than the global strain are present at different positions across the thickness of the solder joints. The room temperature non-composite solder joints creep tested at higher stresses all exhibited maximum localized creep strains along the interface. The non-composite solder deformed at lower stresses yielded higher localized strains near the middle of specimen.

Non-composite solder tested at 85°C resulted in two samples exhibiting maximum localized creep strain at the interface, and the other sample very near the interface. Composite specimens tested at 85°C yielded mixed results with half achieving maximum localized strains at the interfaces, and half near the middle of the solder joint.

Non-composite solder tested at 125°C all exhibited maximum localized creep strain values along the interface. The composite specimens again yielded mixed results. Two of the samples behaved in an extremely homogeneous manner with the localized creep values very similar to the global creep values. One of the two remaining samples demonstrated maximum localized strain values at the interface, while the other sample yielded maximum localized creep strain values near the middle of the specimen.

Mic

outl

con

was

test

(pla

on

roo

sur

ho

ele

so

so

sp

4.4 FRACTURE SURFACES

Micrographs of the fracture surfaces were taken using an SEM. An attempt to correlate outlying positions on the Dorn plot by analyzing the fracture surface was made but conclusive evidence was not found. However, a temperature/composition related trend was apparent. Fracture surfaces (Figure 26a) from non-composite solder joints creep tested at room temperature and low stresses, appear to be relatively smooth and flat (planar) with one or two big steps. With increasing stress, the fracture topography took on a rougher appearance with many levels of fracture surface elevation (Figure 26b). The room temperature composite samples (Figure 26c) at higher stresses possessed smooth surfaces which appeared to be stippled rather than smeared, suggesting that a more homogeneous failure process occurred. Fractures surfaces of all specimens tested at elevated temperatures (Figure 26d), were similar to the room temperature non-composite solder at lower stresses. The fracture occurs mostly on one plane, but the surface was somewhat rougher, and more pronounced smearing was present than the non-composite specimens crept at 25°C.

Fi

Fig

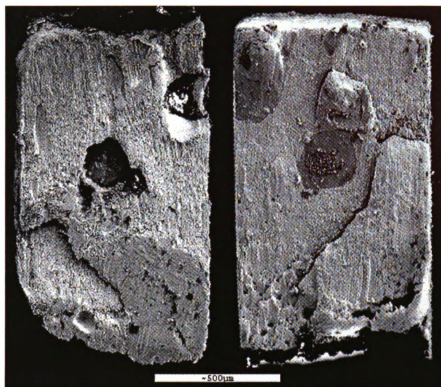


Figure 26a. Non-Composite Fracture Surface, $T = 25^{\circ}\text{C}$, $\tau = 21.7 \text{ MPa}$. (Sample 038)



Figure 26b. Non-Composite Fracture Surface, $T = 25^{\circ}\text{C}$, $\tau = 23.5 \text{ MPa}$. (Sample 040).

Fi

Fig

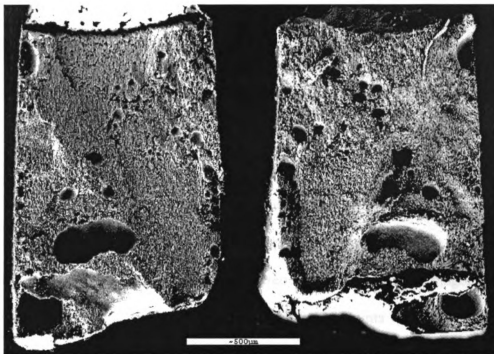


Figure 26c. Composite Fracture Surface, $T = 25^{\circ}\text{C}$, $\tau = 32.2 \text{ MPa}$. (Sample 052).

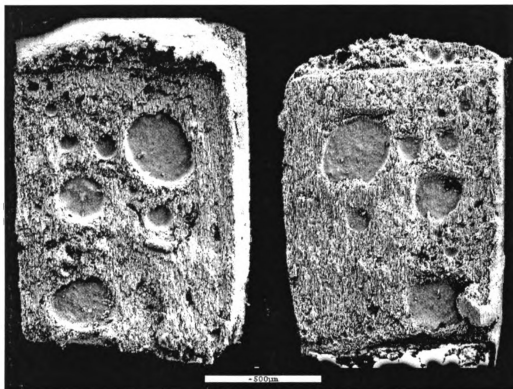


Figure 26d. Composite Fracture Surface, $T = 125^{\circ}\text{C}$, $\tau = 9.1 \text{ MPa}$. (Sample 036).

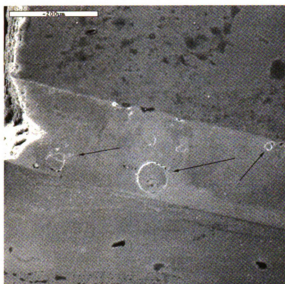
4.5 RESULTS OF LOCATION OF FRACTURE EXAMINATION

The solder joints subjected to creep deformation in this investigation underwent fracture in a consistent manner. In general, two types of fracture occurred during this investigation, fracture through the middle of the specimen and fracture near one of the interfaces. Fracture appears to be dependent upon strain-rate and the amount of porosity present in the solder joint. If a large pore was present in the solder joint, approximately 20% of the fracture surface area, fracture occurred through the center or diagonally across the thickness from one interface to the other. Solder joints which lacked porosity fractured along or near one of the interfaces when subjected to high strain-rates (10^{-4} s^{-1}). However, when subjected to low strain-rates (10^{-8} s^{-1}) fracture occurred through the middle of the solder joint for the specimens examined. No correlation between composite and non-composite solder was noticed, besides the fact that the composite solder generally possessed a greater amount of porosity. Results for the different testing conditions are indicated in Appendix E along with SEM micrographs of the fracture and fracture surfaces.

4.6 RESULTS OF CRACK INITIATION TESTS

The results of this investigation were similar to the results in Section 4.5. In general, fracture initiated along or near the interface. Three of the four solder joints tested indicated an initiation at the interface. The fourth solder joint, fabricated from composite solder, demonstrated crack initiation near the center of the solder joint. Upon rupture of the specimen a large pore was present in the center of the joint, roughly 20% of the fracture surface area in size. It should be noted that all tests in this particular investigation were performed at high strain-rates, greater than 10^{-3} s^{-1} . SEM micrographs for these tests are included in Appendix E.

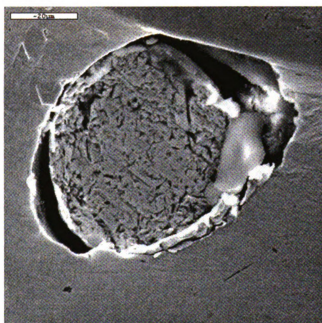
Small circular areas (Figures 27 and 28), varying in diameter from approximately 10 to 70 μm were noticed to form near an interface after some deformation. These areas were present on one solder joint prior to testing and are believed to be the results of strain during polishing. The areas appear to separate themselves from the rest of the strained matrix. Upon further deformation, the areas behave in two different manners. In some instances the areas tend to collapse into the matrix Figure 27c. The areas have also been observed to ‘pop’ out of the matrix as indicated in Figure 27b and Figure 28. Although these areas are a result of deformation, the exact cause is currently unknown to this investigator. Since they tend to form near the interfaces, they may be linked to the Cu_6Sn_5 intermetallics which naturally form there.



(a)

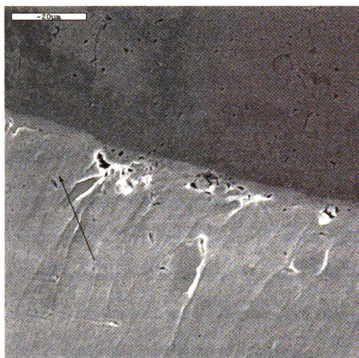


(b)

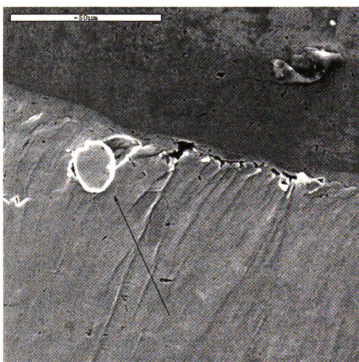


(c)

Figure 27. Formation of Circular Areas Under High Stress Conditions.
 (a) Formation of Circular Areas.
 (b) 'Pop' Out Upon Further Deformation.
 (c) Collapse of Circular Area.



(a)



(b)

Figure 28. Solder Joint Micrographs Before (a) and After (b) Further Deformation.

CHAPTER 5

DISCUSSION

5.1 CREEP BEHAVIOR

A summary of all creep tests is provided in Appendix F. The creep behavior of the solder joints is best summarized in the Dorn plot in Figure 19, which shows the normalized shear strain-rate vs. the normalized shear stress. The solid line describes the non-composite Sn-Ag data of Darveaux *et al.* and it is apparent that most of the present data are in agreement with the trend established by this best fit curve.

The addition of the Cu_6Sn_5 particles as matrix reinforcements significantly improved creep behavior at room temperature conditions. The room temperature composite data were as much as 1000 times more creep resistant than the non-composite solder. At 85°C , the composite data were in close agreement with the Darveaux data, but the non-composite crept at least 10 times faster than the composite. At 125°C , the creep resistance of the non-composite and composite solders were similar. In addition to increased strength the composite solder appeared to deform in a more homogeneous manner

5.2 HOMOGENEITY OF DEFORMATION

Determination of homogeneity of deformation can be examined using visual and analytical methods. Observations of the creep strain-time history plots conveyed a good sense of whether or not the sample deformed in a homogeneous manner. Local tertiary creep generally commenced only in a limited part of the specimens where the strains are highest. Analytically, by taking the ratio of the onset of global tertiary creep to the onset of localized tertiary creep, a value resulted representing the homogeneity of deformation. The closer the value was to 1, the more homogeneously it deformed, since a ratio of 1 implies that the onset of local and global tertiary creep occurred at the same strain, which in turn implies that local and global strain-time histories are the same.

Figure 29 shows how the onset of local tertiary creep varied with secondary strain-rate. Room temperature creep of the non-composite solder at higher stresses tolerated high local shear strains near a value of 3 before tertiary creep commenced, as compared to the composite solder, where the beginning of tertiary creep occurred at local shear strains in the range of 0.2-1.2. At lower stresses, the non-composite specimen exhibited local tertiary creep at a strain very close to the global tertiary creep strain. Since the composite specimens generally exhibited a local strain for the beginning of tertiary creep close to the global strain at the beginning of tertiary creep, this indicates that the strain evolved more homogeneously in the composite solder. It may also be an indication that strain evolves with lower stress in the non-composite solder, as indicated by the lines that suggest these trends on the various strain history plots. At elevated temperatures, localized tertiary creep began at strains between 0.2 – 1.5 for all specimens.

Figure 30 illustrates how the strain homogeneity ratio varies with strain-rate. A trend which suggests that homogeneity of deformation decreases with increasing creep-rate is indicated for the room temperature non-composite data. For room temperature and 125°C deformation, the composite solder exhibited higher levels of homogeneity than the non-composite solder. At 85°C, the trend is not as easily identified. The most homogeneous deformation occurred in the composite at 125°C, but the onset of local tertiary creep was at a lower strain than most other specimens as shown in Figure 30. The large amounts of strain tolerated by the non-composite samples under a high rate of deformation (1×10^{-4} or greater) is indicative of the inaccuracies involved in accelerated testing. The toleration of such a large amount of strain before the onset of tertiary creep is unrealistic.

A possible relationship between porosity and tertiary creep was also investigated. A plot was produced which compared homogeneity of deformation to the average percent porosity present in each fractured soldered half (Figure 31). The plot suggests no dependency upon porosity. Therefore, porosity was not a major variable on damage in this study.

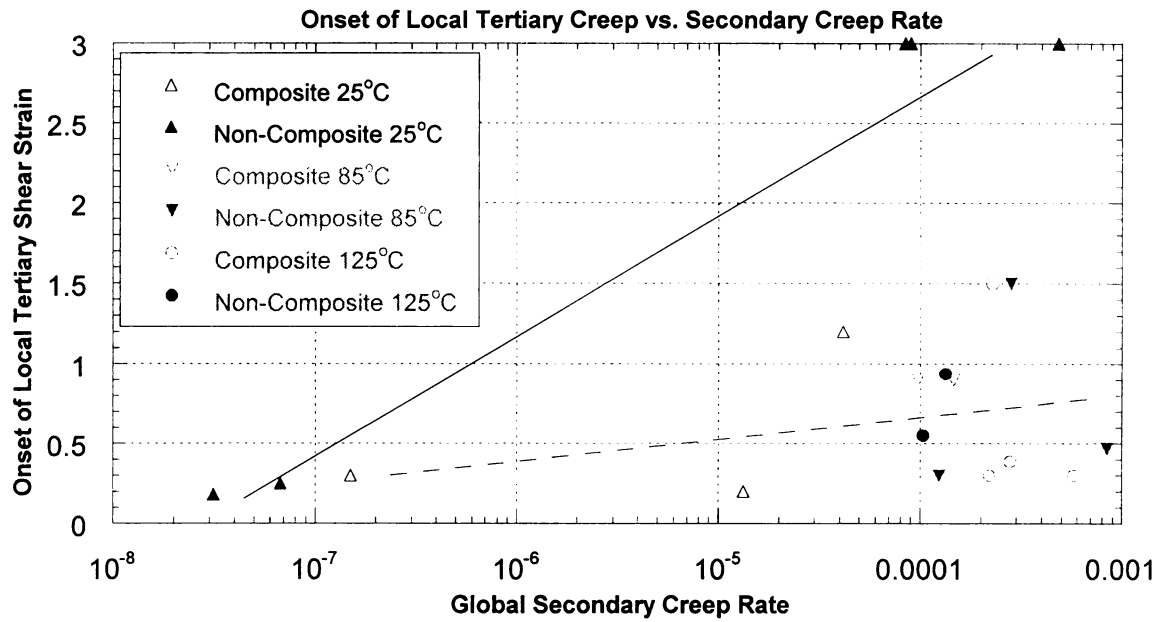


Figure 29. Onset of Local Tertiary Creep vs. Global Secondary Creep-Rate.

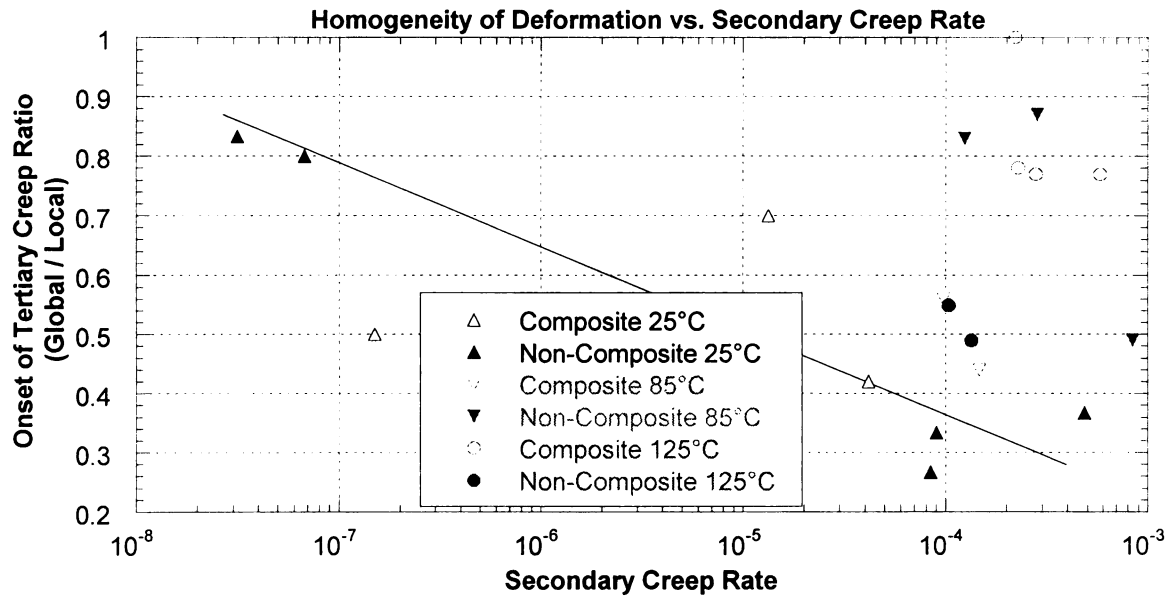


Figure 30. Strain Homogeneity Ratio vs. Global Secondary Creep-Rate.

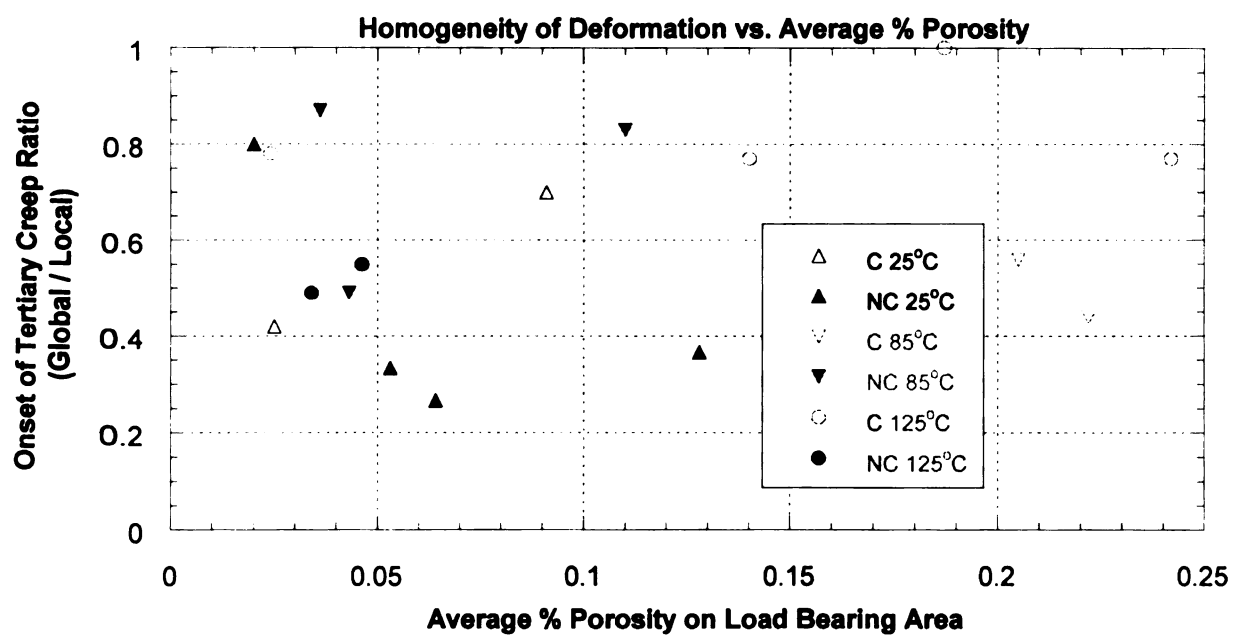


Figure 31. Homogeneity of Deformation vs. Average Percent Porosity.

5.3 ANALYSIS OF FRACTURE

The solder joints subjected to higher strain-rates (10^{-4} s^{-1}) all exhibited fracture along the interface, unless porosity was present in the amount of at least 20% of the fracture surface area. It has been observed that Cu_6Sn_5 intermetallic particles naturally form at the Cu substrate-solder interface (Figure 6). The presence of these unavoidable intermetallics would have an embrittling effect on the microstructure as compared to the compliant solder matrix. As a result, the solder joint is weaker at the interface and will tend to fracture there unless significant porosity is present throughout the solder matrix or a much lower strain-rate is experienced. This manner of solder joint fracture was consistent with expected results mentioned in Section 2.3.

CHAPTER 6

CONCLUSIONS

A criteria for damage based on the onset of tertiary creep was examined in shear creep deformation of miniature solder specimens made from eutectic Sn-Ag solder with and without 20v% 5-8 μm Cu_6Sn_5 reinforcements. The strain-time history was measured both globally and locally and the range of local strain variation was quantified. The composite solder exhibited a more uniform deformation, but tertiary creep commenced at a lower creep strain than non-composite solders at room temperature. The local shear strain where the onset of tertiary creep was observed increased with strain-rate for both solder types, and the fracture surface features became more rough. At elevated temperatures, tertiary creep commenced at a similar strain for composite and non-composite specimens, and the fracture surfaces were similar. The composite material was more creep resistant at lower temperatures, but it is not yet clear whether this benefit outweighs the fact that less strain is tolerated locally before tertiary creep commences. Porosity appeared to have no effect upon homogeneity of deformation.

APPENDICES

.

APPENDIX A

CREEP MECHANISMS

Stress Regime	n	T	p	Q	Mechanism
Low	1	High	2	Q_L	Naborro-Herring
	1	Low	3	Q_{GB}	Coble
	1	High	0	Q_L	Harper-Dorn
Intermediate	5	High	0	Q_L	Dislocation Climb (M-Type)
	7	Low	0	Q_{\perp}	Dislocation Climb (M-Type)
	3	High	0	Q_I	Dislocation Viscous Glide (A-Type)
	5	Low	0	Q_{\perp}	Dislocation Viscous Glide (A-Type)
High	*	H/L	0	Q_{\perp} or Q_L	Power Law Breakdown

Adapted from Darveaux *et al.*, page 539, and Yang *et al.*, page 1137.

Definitions

Q_L	Lattice Self Diffusion
Q_{GB}	Grain Boundary Diffusion
Q_{\perp}	Dislocation Pipe Diffusion
Q_I	Inter-Diffusion of Solute Atoms

Table 1. Creep Mechanisms

APPENDIX B

DATA REDUCTION

Table 2 represents extracted data from an enhanced scratch displacement image which was digitally captured via a traveling microscope. The data extraction was performed via the *Datathief* shareware program. The first column, 'x position', represents the thickness of the solder joint, from one interface to the other, as it appeared on the computer monitor under the *Datathief* program. Except for the first and last values, the data are extracted at equal intervals. The units are centimeters, *i.e.*, the thickness of the solder joint as it appeared on the computer monitor is represented by a value of $(15.78\text{ cm} - 5.11\text{ cm} = 10.67\text{ cm})$. The actual thickness of the solder joints ranged from 50 to 100 μm .

The remaining columns represent the position of the scratch line prior to loading of the solder joint and during the creep experiment. For example, the column labeled '2940 sec' represents data extracted from the image captured 2940 seconds into the creep experiment. On each captured image, the data was extracted at the same x position established in the first column. It can be seen that as time progressed, the position of the scratch remained relatively constant for the first row of data, labeled '5.11', but changed drastically in the last row, labeled '15.78'.

x position	Before Creep	1080 sec	1920 sec	2940 sec	4020 sec	5700 sec
5.11	8.81	8.77	8.64	8.64	8.72	8.61
5.98	8.87	8.80	8.33	8.01	7.77	7.86
6.99	8.98	8.71	7.81	7.14	6.81	6.56
7.99	9.12	8.57	7.26	6.37	5.69	4.94
9.00	9.26	8.37	6.72	5.53	4.59	3.12
10.04	9.40	8.13	6.11	4.66	3.40	0.84
11.04	9.55	7.90	5.56	3.94	2.27	-1.16
12.05	9.69	7.64	5.10	3.19	1.29	-2.72
12.99	9.83	7.38	4.64	2.41	0.22	-4.48
13.99	9.94	7.12	4.27	1.84	-0.50	-5.63
14.97	10.11	6.92	3.84	1.32	-1.17	-6.73
15.78	10.19	6.74	3.55	0.89	-1.51	-7.28

Table 2. Scratch Displacement Data.

In order to simplify the data reduction process, the data representing the thickness of the solder joint was normalized. The thickness of the solder joint was normalized by subtracting the origin, 5.11, from each value in the first column and then dividing each of those values by the established solder joint thickness (15.78 - 5.11). This resulted in a normalized solder joint thickness ranging from 0 to 1.

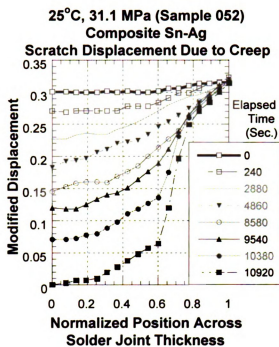
The scratch displacement data was modified or scaled according to the thickness of the solder joint. For simplicity, the maximum displacement of the scratch, represented here by a value of -7.28, was shifted to a value of 0 and then scaled to the solder joint thickness. This was done by adding a value of 7.28 to every scratch position value, *i.e.*, every number in every column with exception of the first column. Each modified value was then divided by the solder joint thickness (15.78 - 5.11). The results are seen in Table 3.

x position	Before Creep	1080 sec	1920 sec	2940 sec	4020 sec	5700 sec
0.000	1.507	1.504	1.492	1.492	1.499	1.489
0.082	1.512	1.506	1.462	1.432	1.409	1.418
0.176	1.523	1.498	1.413	1.351	1.320	1.296
0.271	1.536	1.484	1.362	1.278	1.214	1.145
0.365	1.550	1.465	1.311	1.200	1.112	0.974
0.462	1.563	1.444	1.254	1.119	1.000	0.760
0.556	1.576	1.422	1.203	1.051	0.895	0.574
0.651	1.589	1.398	1.160	0.981	0.803	0.427
0.739	1.602	1.373	1.117	0.908	0.703	0.262
0.832	1.613	1.349	1.082	0.854	0.635	0.154
0.924	1.629	1.330	1.041	0.805	0.573	0.051
1.000	1.636	1.313	1.014	0.765	0.540	0.000

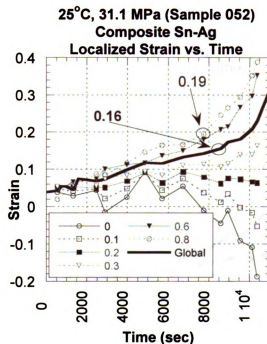
Table 3. Normalized Position and Modified Scratch Displacement Data.

APPENDIX C

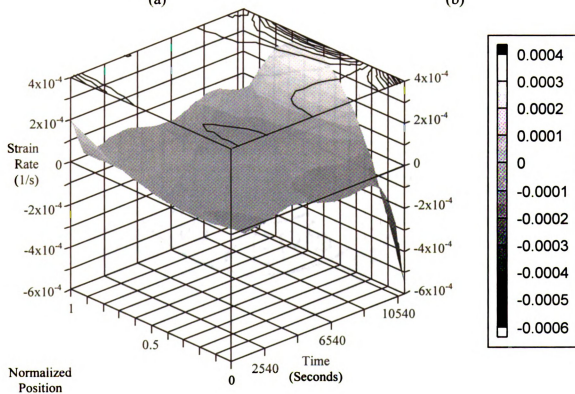
DISPLACEMENT, STRAIN, AND STRAIN-RATE HISTORIES



(a)

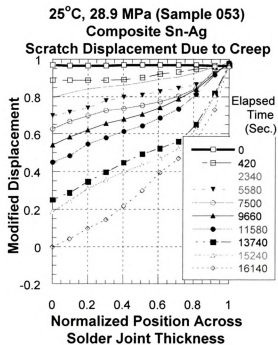


(b)

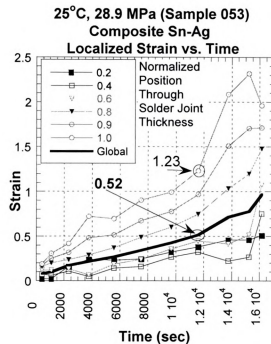


(c)

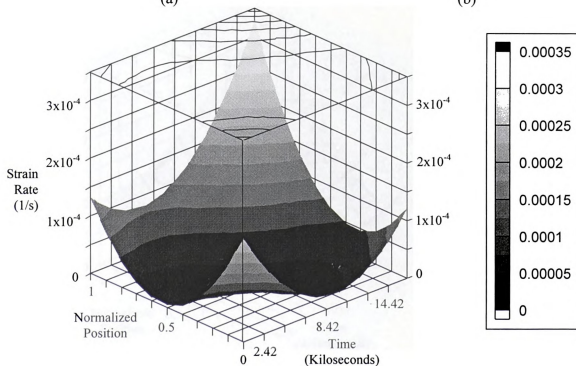
Figure 32. Displacement (a), Localized Creep Strain (b), and Strain-Rate (c) Histories for Composite Solder at 25°C.



(a)

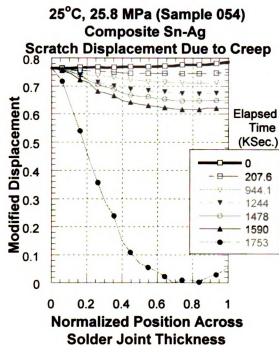


(b)

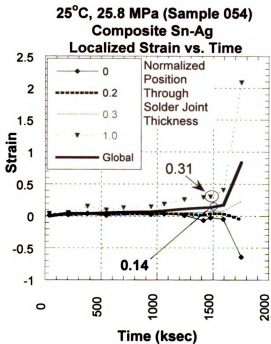


(c)

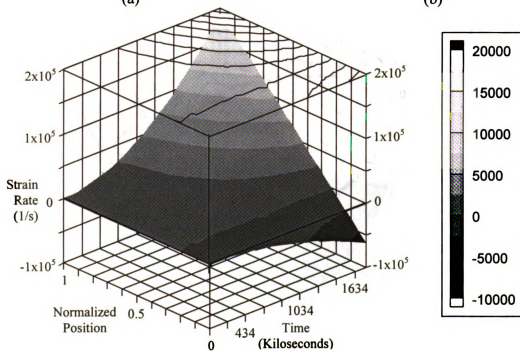
Figure 33. Displacement (a), Localized Creep Strain (b), and Strain-Rate (c) Histories for Composite Solder at 25°C.



(a)

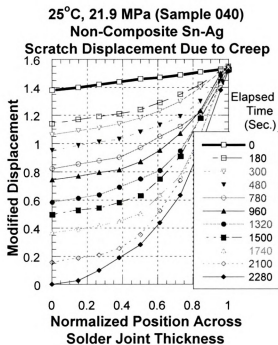


(b)

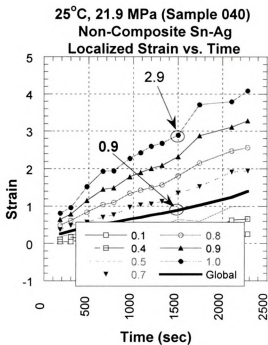


(c)

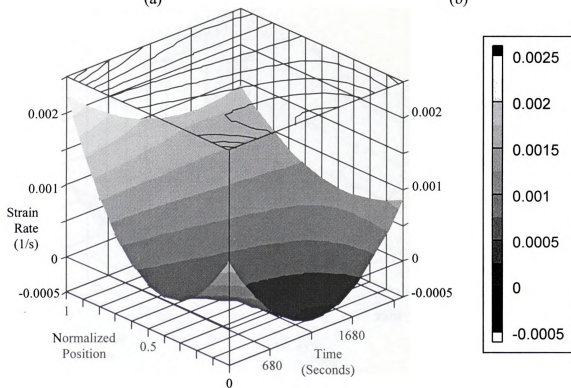
Figure 34. Displacement (a), Localized Creep Strain (b), and Strain-Rate (c) Histories for Composite Solder at 25°C.



(a)



(b)



(c)

Figure 35. Displacement (a), Localized Creep Strain (b), and Strain-Rate (c) Histories for Non-Composite Solder at 25°C.

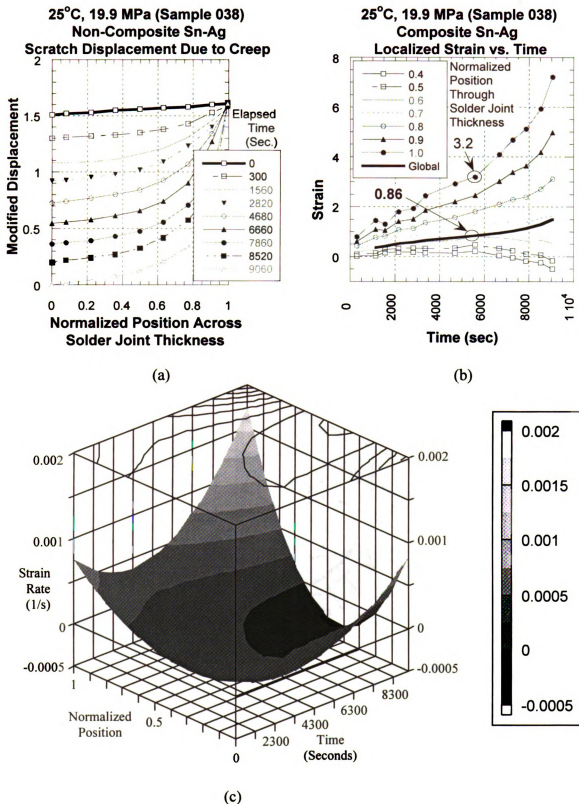
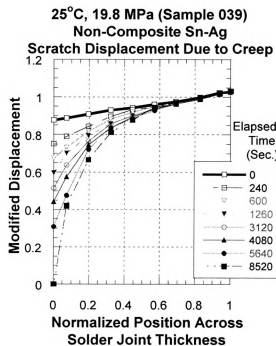
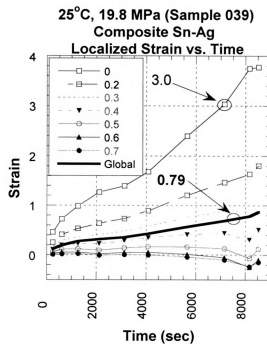


Figure 36. Displacement (a), Localized Creep Strain (b), and Strain-Rate (c) Histories for Non-Composite Solder at 25°C.



(a)



(b)

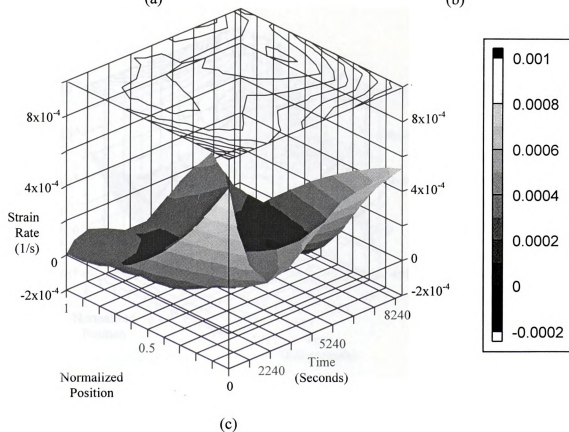
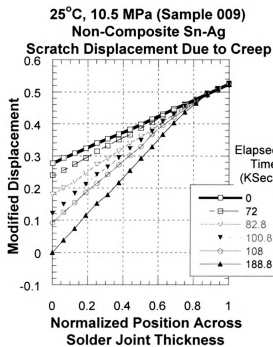
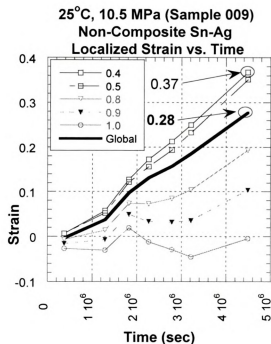


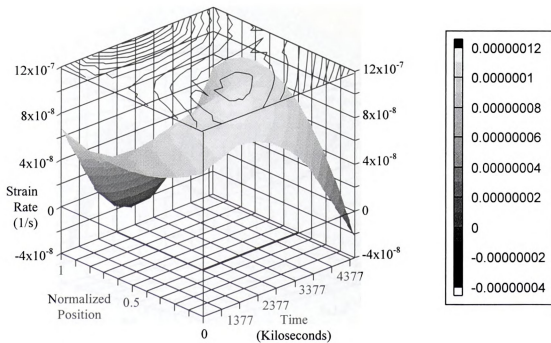
Figure 37. Displacement (a), Localized Creep Strain (b), and Strain-Rate (c) Histories for Non-Composite Solder at 25°C.



(a)

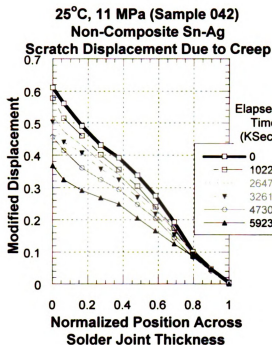


(b)

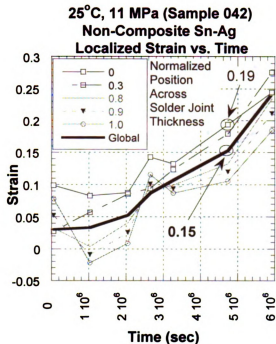


(c)

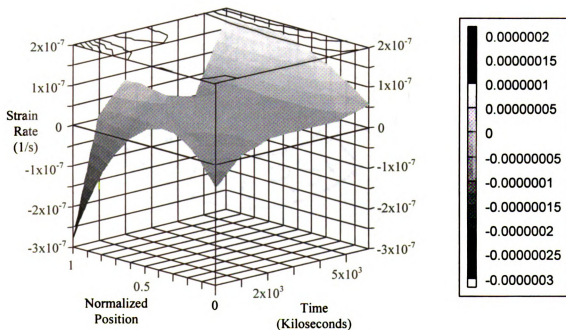
Figure 38. Displacement (a), Localized Creep Strain (b), and Strain-Rate (c) Histories for Non-Composite Solder at 25°C.



(a)



(b)



(c)

Figure 39. Displacement (a), Localized Creep Strain (b), and Strain-Rate (c) Histories for Non-Composite Solder at 25°C.

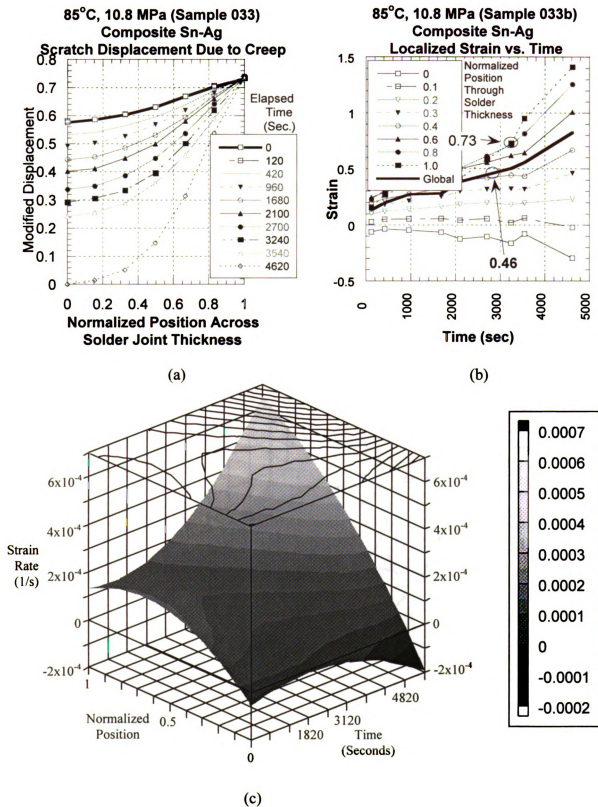
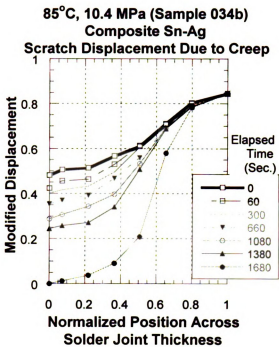
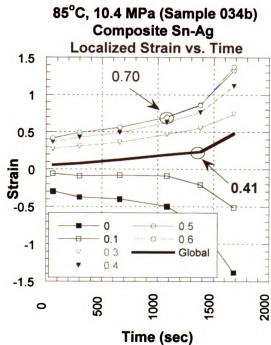


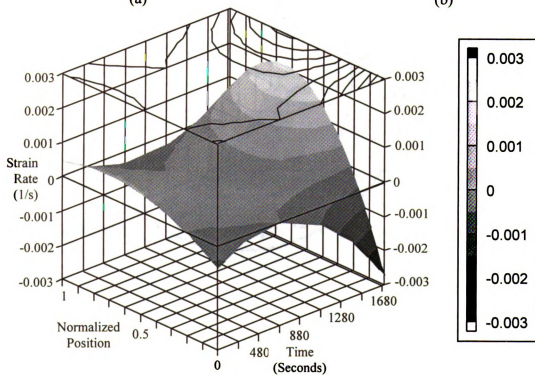
Figure 40. Displacement (a), Localized Creep Strain (b), and Strain-Rate (c) Histories for Composite Solder at 85°C.



(a)

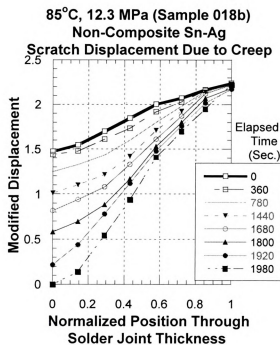


(b)

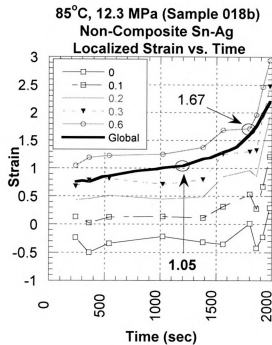


(c)

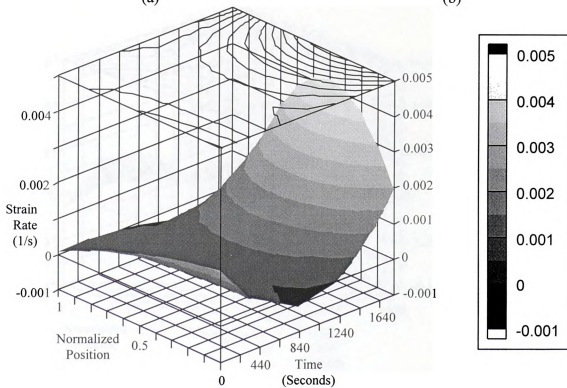
Figure 41. Displacement (a), Localized Creep Strain (b), and Strain-Rate (c) Histories for Composite Solder at 85°C.



(a)

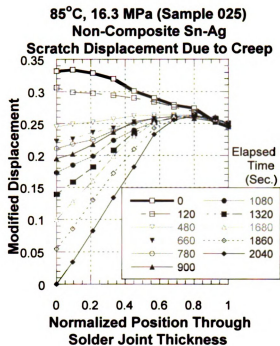


(b)

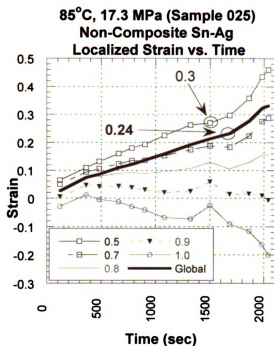


(c)

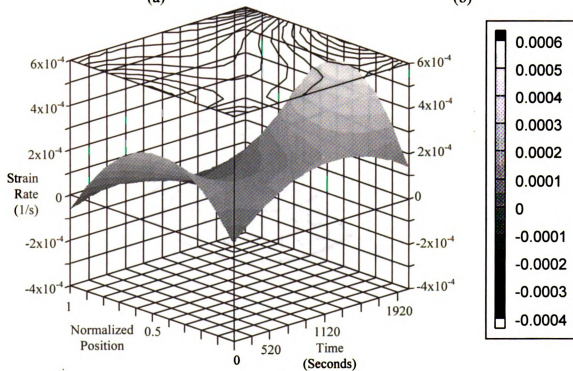
Figure 42. Displacement (a), Localized Creep Strain (b), and Strain-Rate (c) Histories for Non-Composite Solder at 85°C.



(a)



(b)



(c)

Figure 43. Displacement (a), Localized Creep Strain (b), and Strain-Rate (c) Histories for Non-Composite Solder at 85°C.

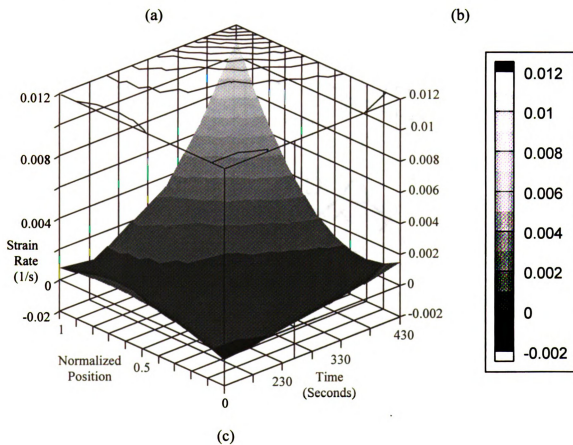
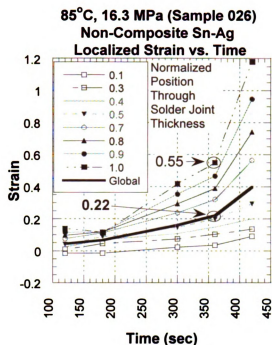
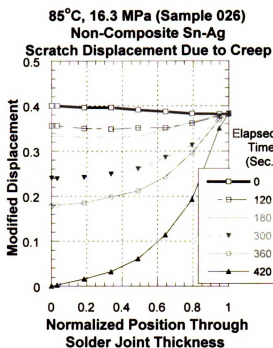
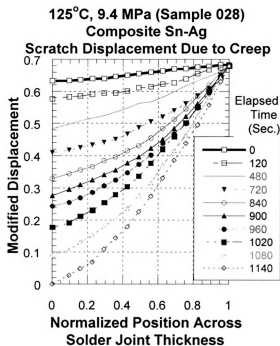
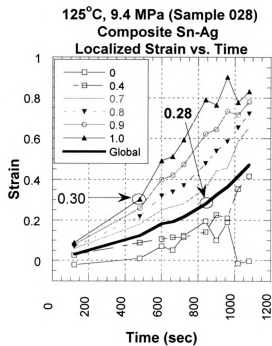


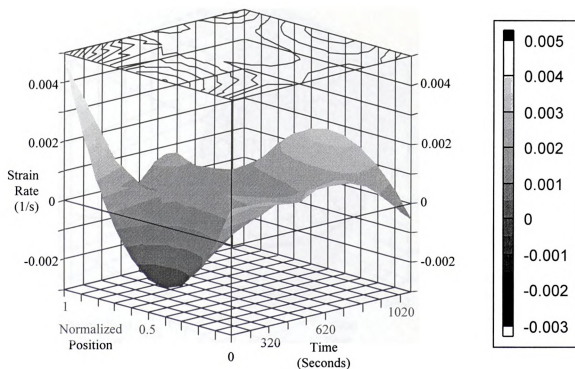
Figure 44. Displacement (a), Localized Creep Strain (b), and Strain-Rate (c) Histories for Non-Composite Solder at 85°C.



(a)

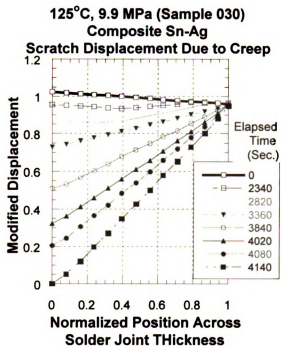


(b)

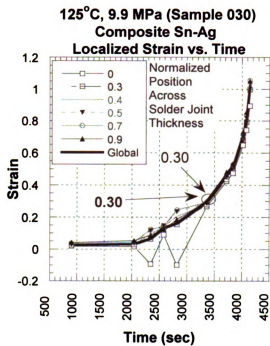


(c)

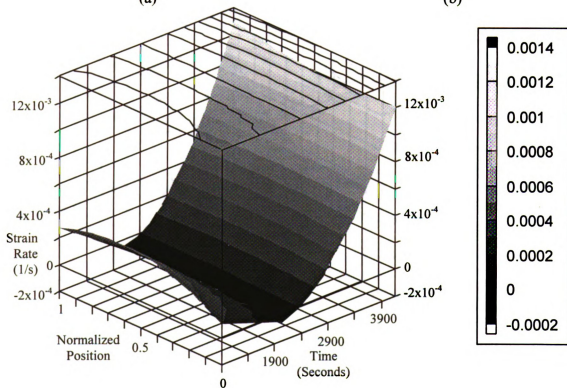
Figure 45. Displacement (a), Localized Creep Strain (b), and Strain-Rate (c) Histories for Composite Solder at 125°C.



(a)

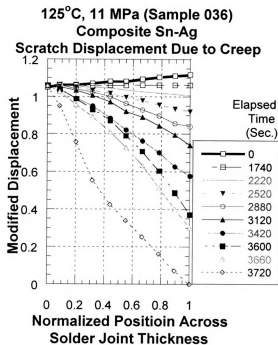


(b)

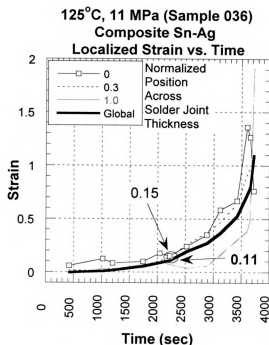


(c)

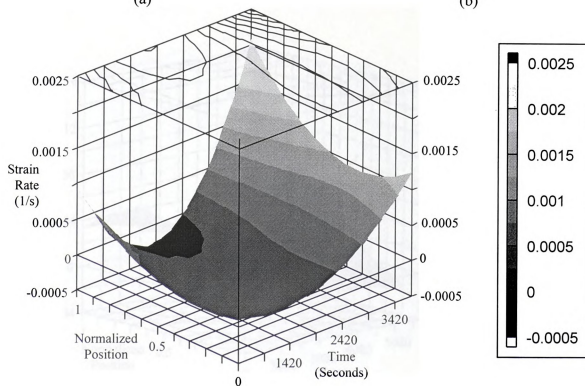
Figure 46. Displacement (a), Localized Creep Strain (b), and Strain-Rate (c) Histories for Composite Solder at 125°C.



(a)

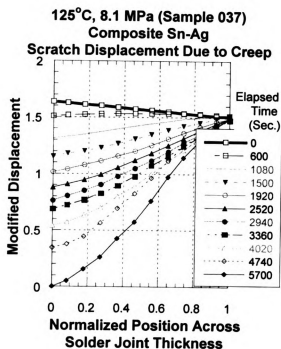


(b)

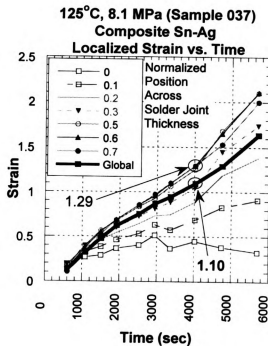


(c)

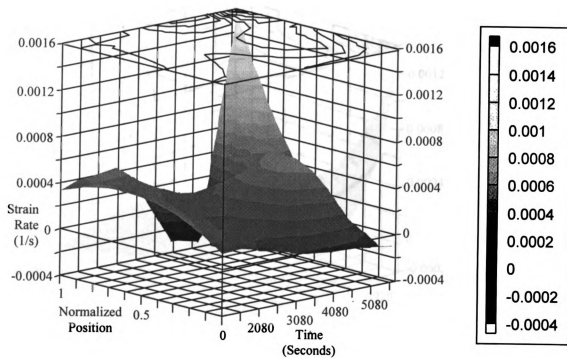
Figure 47. Displacement (a), Localized Creep Strain (b), and Strain-Rate (c) Histories for Composite Solder at 125°C.



(a)

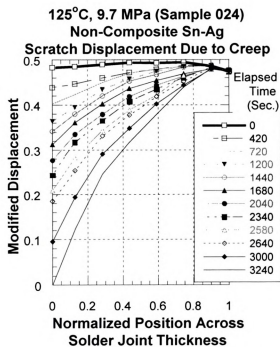


(b)

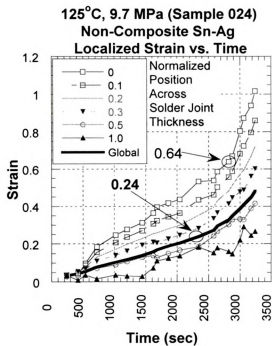


(c)

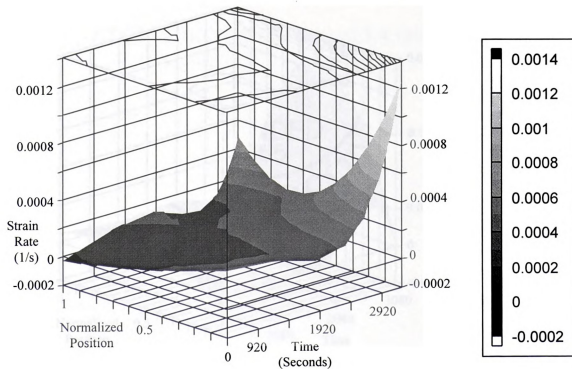
Figure 48. Displacement (a), Localized Creep Strain (b), and Strain-Rate (c) Histories for Composite Solder at 125°C.



(a)

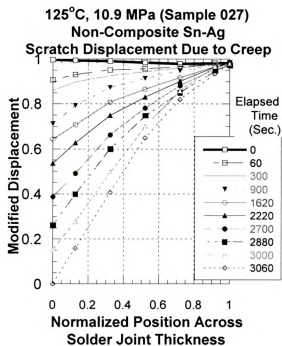


(b)

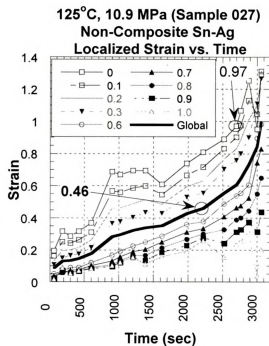


(c)

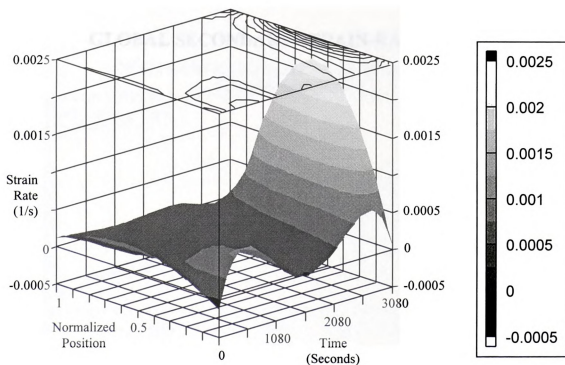
Figure 49. Displacement (a), Localized Creep Strain (b), and Strain-Rate (c) Histories for Non-Composite Solder at 125°C.



(a)



(b)



(c)

Figure 50. Displacement (a), Localized Creep Strain (b), and Strain-Rate (c) Histories for Non-Composite Solder at 125°C.

APPENDIX D

GLOBAL SECONDARY STRAIN-RATE DATA

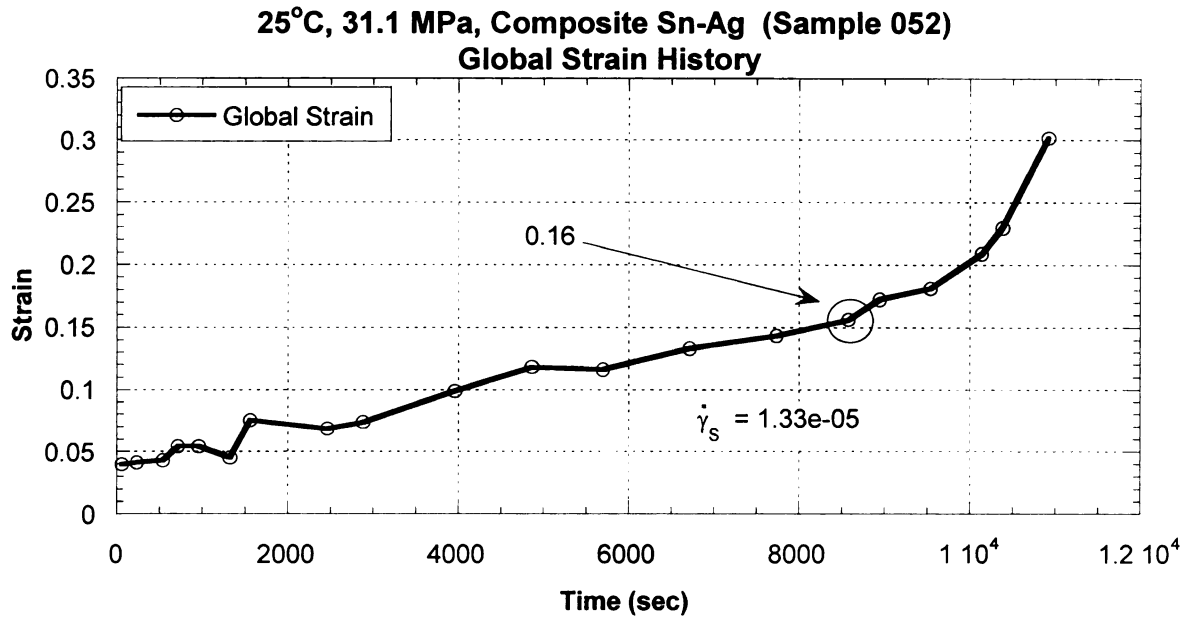


Figure 51. Global Secondary Strain Rate for 25°C, 31.1 MPa, Composite Solder

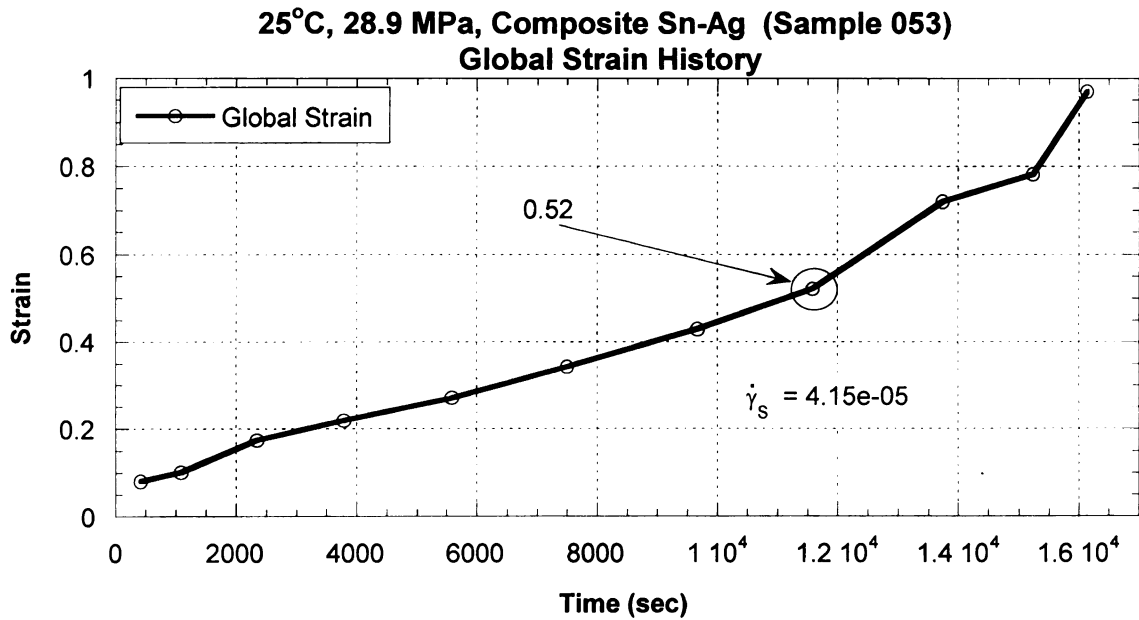


Figure 52. Global Secondary Strain Rate for 25°C, 28.9 MPa, Composite Solder

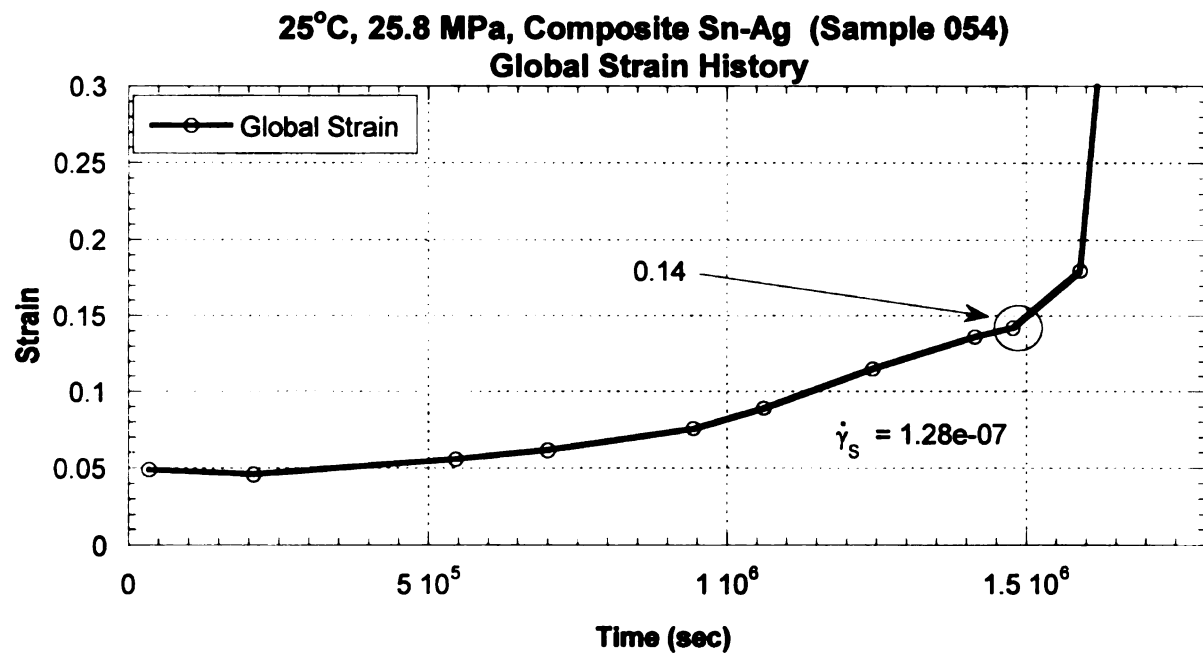


Figure 53. Global Secondary Strain Rate for 25°C, 25.8 MPa, Composite Solder

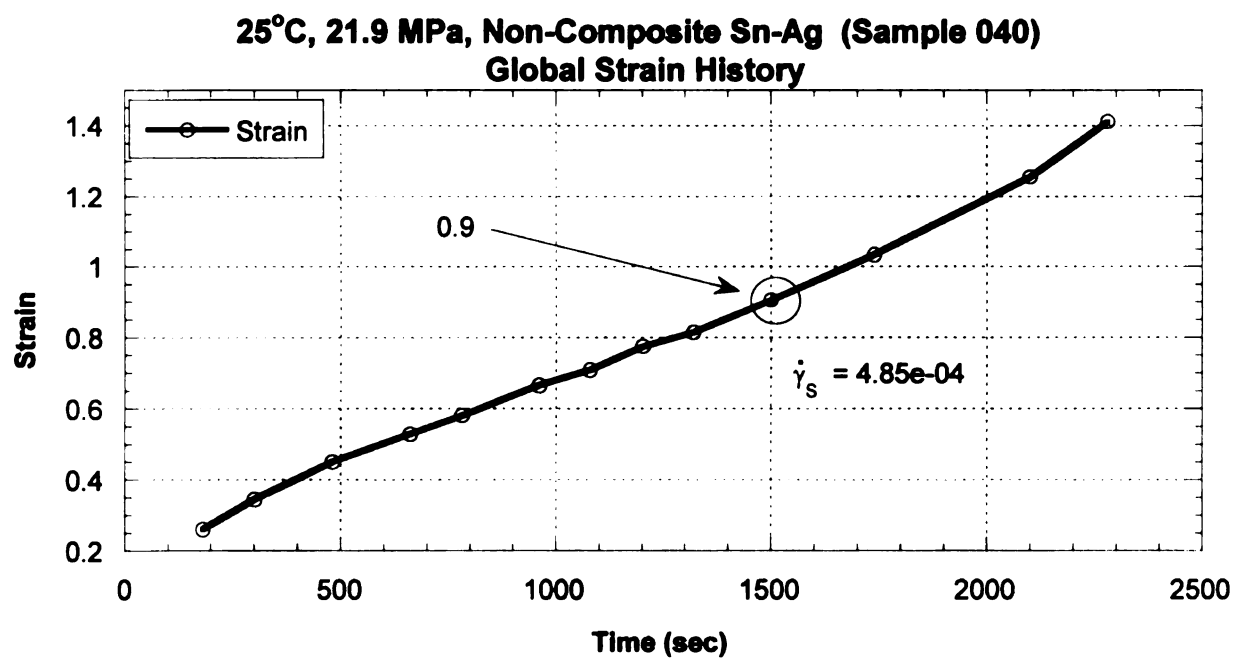


Figure 54. Global Secondary Strain Rate for 25°C, 21.9 MPa, Non-Composite Solder

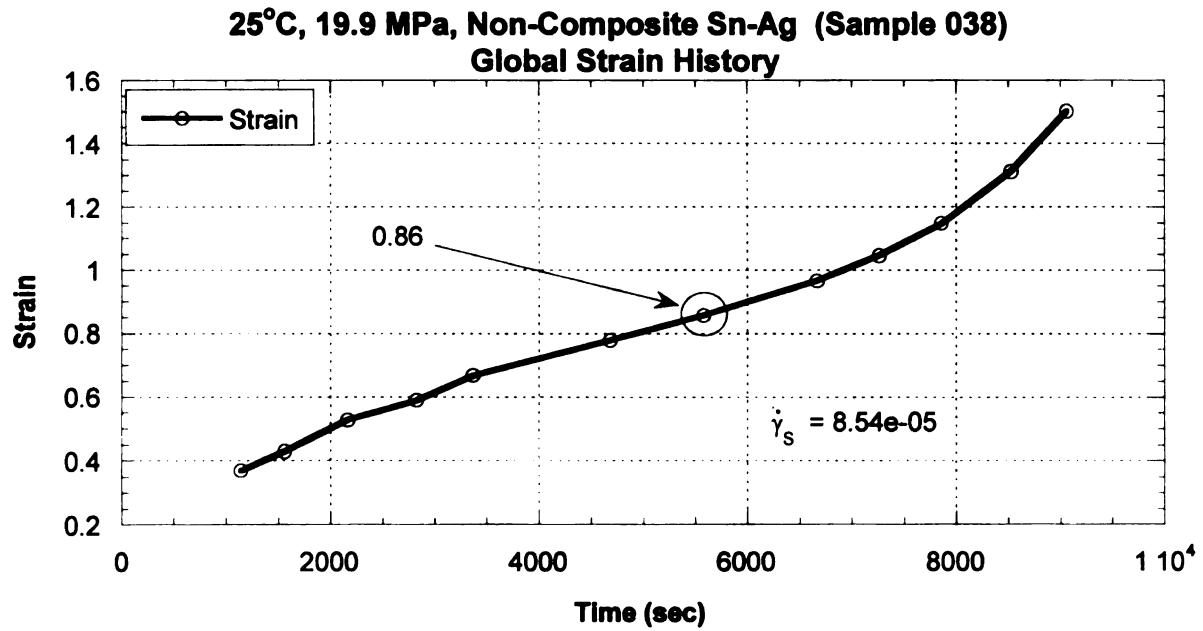


Figure 55. Global Secondary Strain Rate for 25°C, 19.9 MPa, Non-Composite Solder

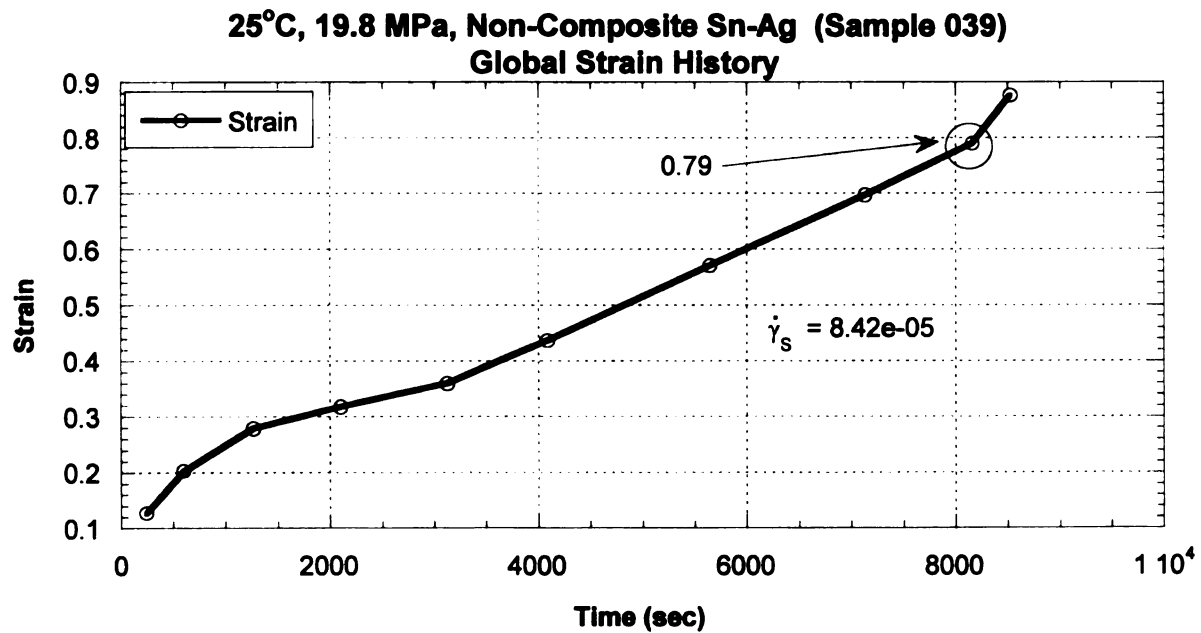


Figure 56. Global Secondary Strain Rate for 25°C, 19.8 MPa, Non-Composite Solder

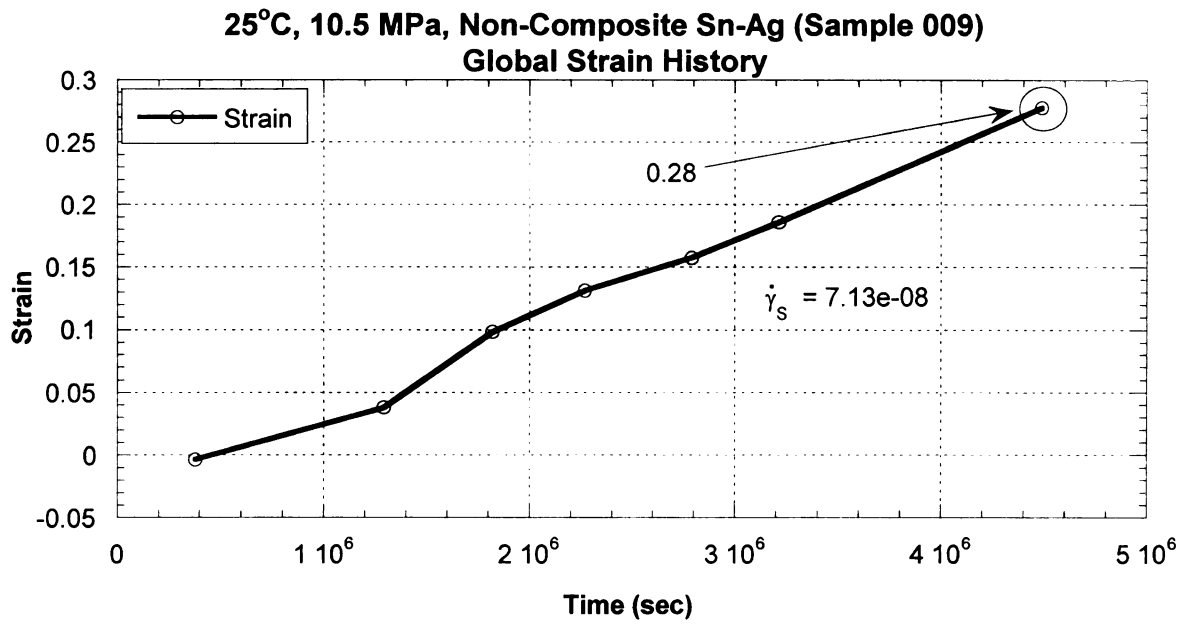


Figure 57. Global Secondary Strain Rate for 25°C, 10.5 MPa, Non-Composite Solder

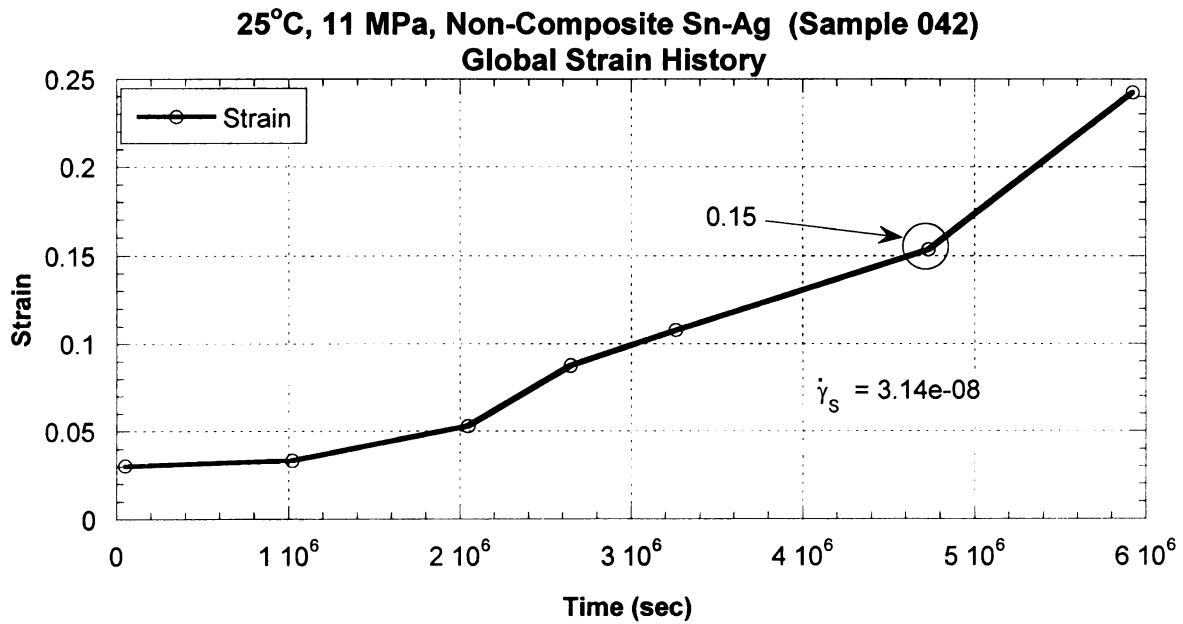


Figure 58. Global Secondary Strain Rate for 25°C, 11 MPa, Non-Composite Solder

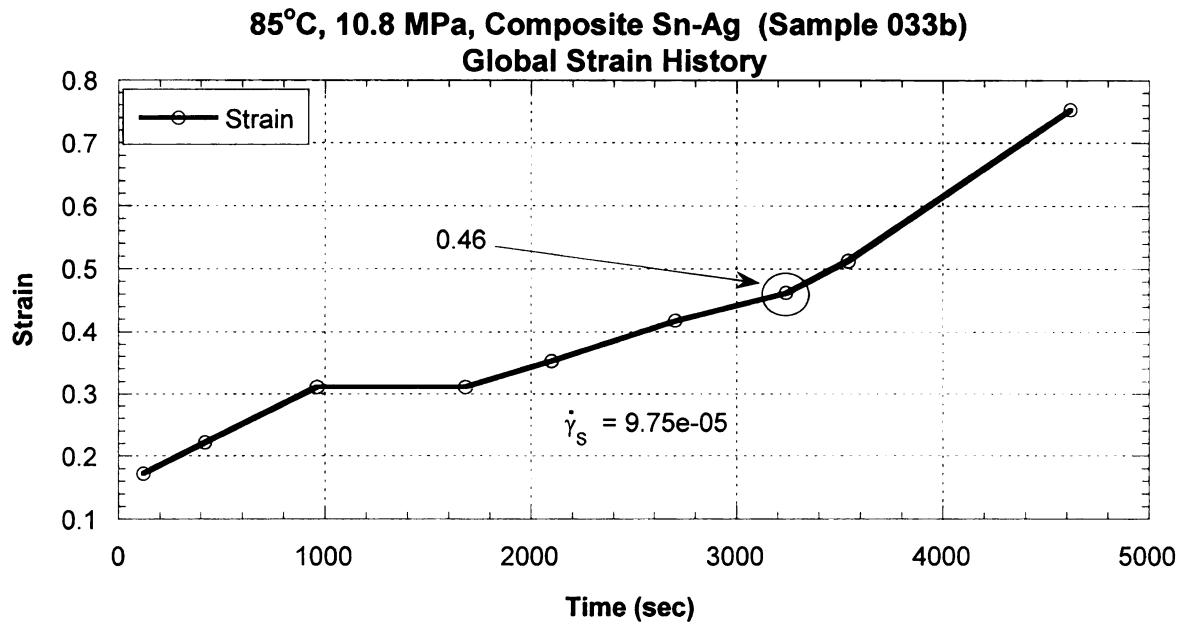


Figure 59. Global Secondary Strain Rate for 85°C, 10.8 MPa, Composite Solder

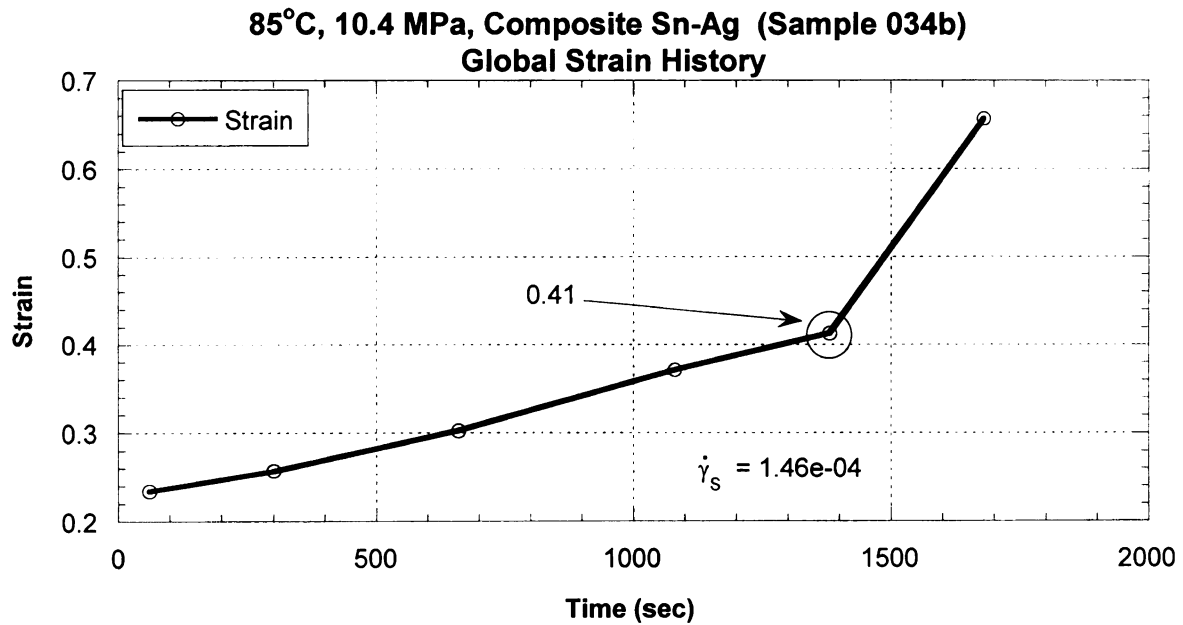


Figure 60. Global Secondary Strain Rate for 85°C, 10.4 MPa, Composite Solder

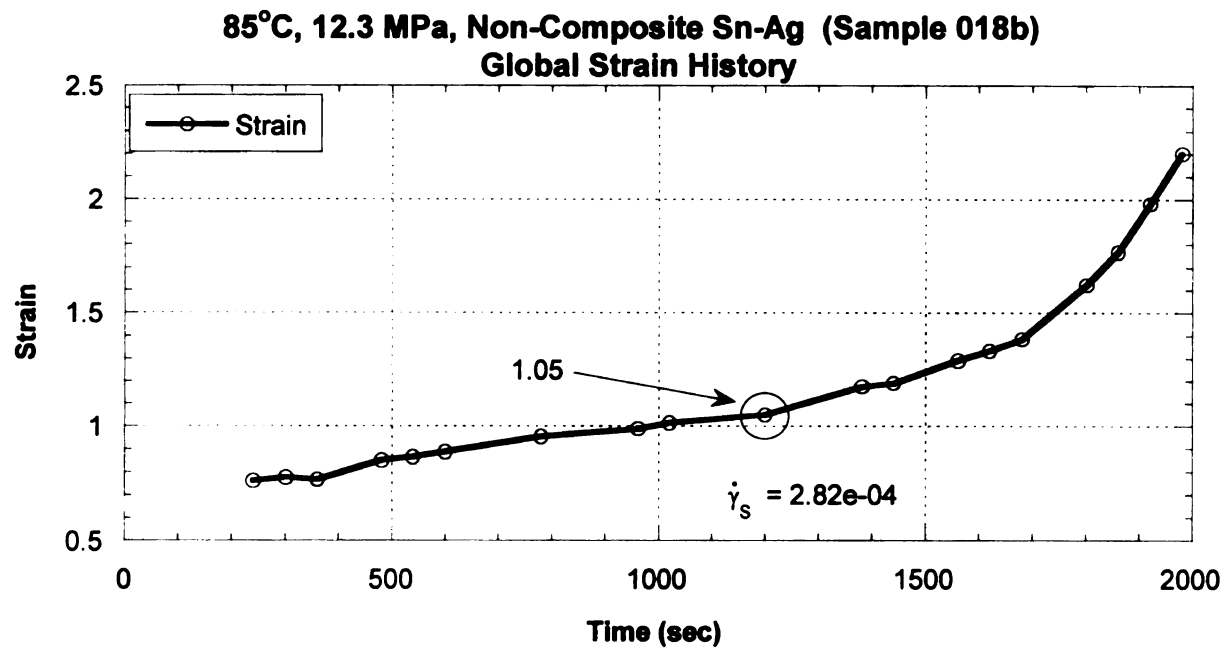


Figure 61. Global Secondary Strain Rate for 85°C, 12.3 MPa, Non-Composite Solder

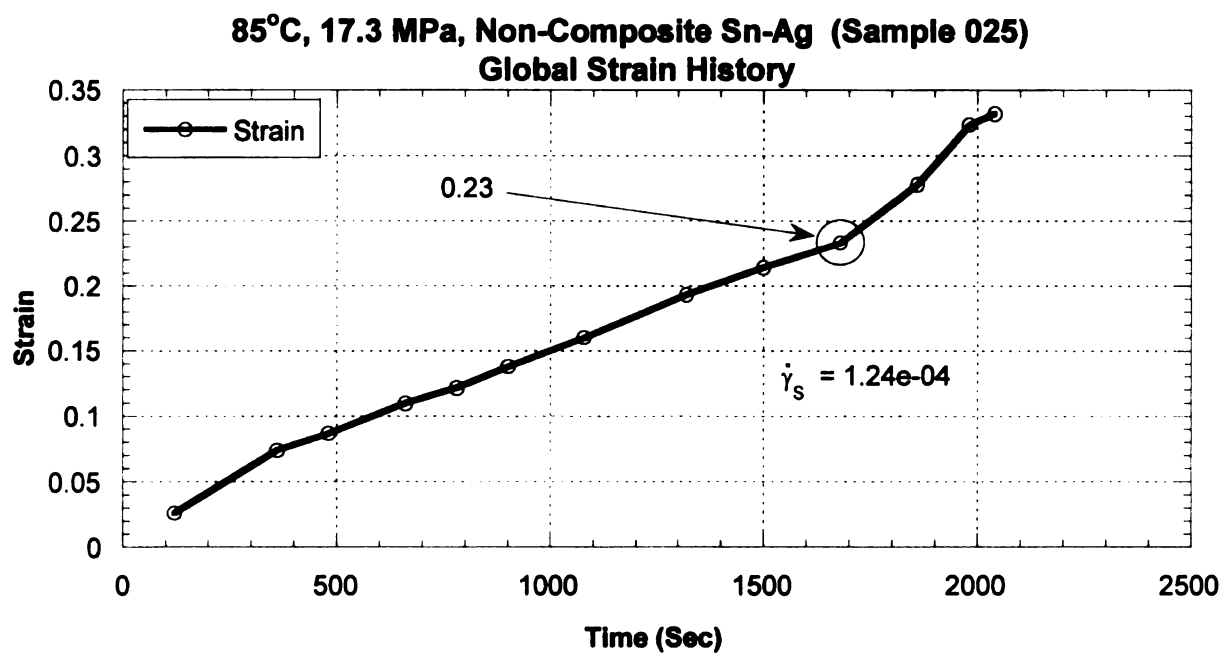


Figure 62. Global Secondary Strain Rate for 85°C, 17.3 MPa, Non-Composite Solder

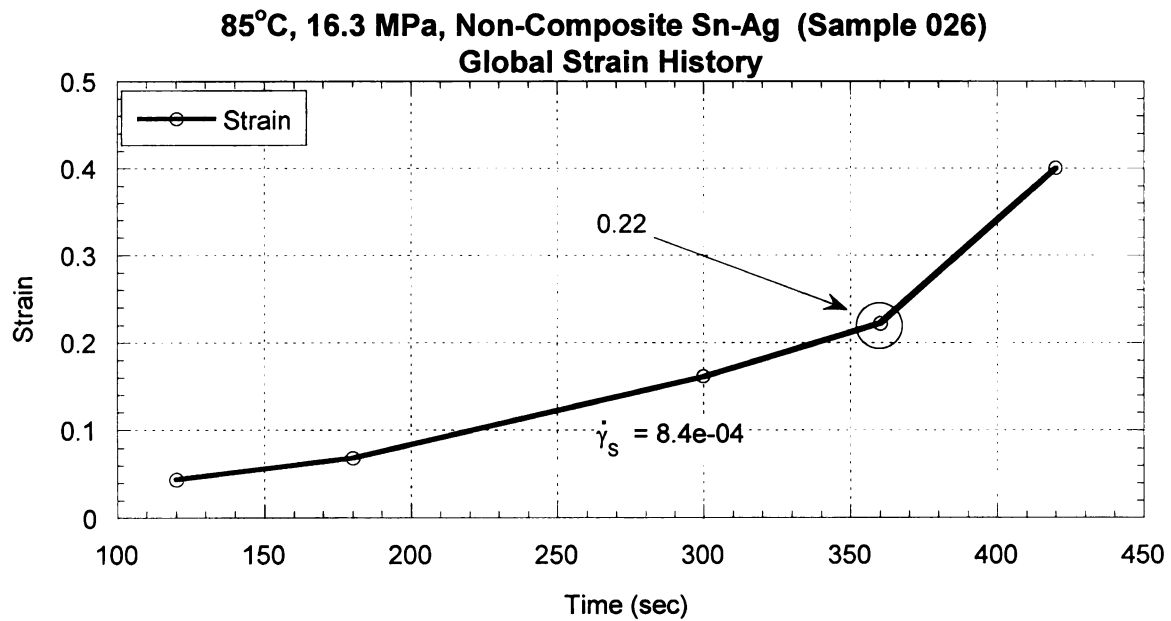


Figure 63. Global Secondary Strain Rate for 85°C, 16.3 MPa, Non-Composite Solder

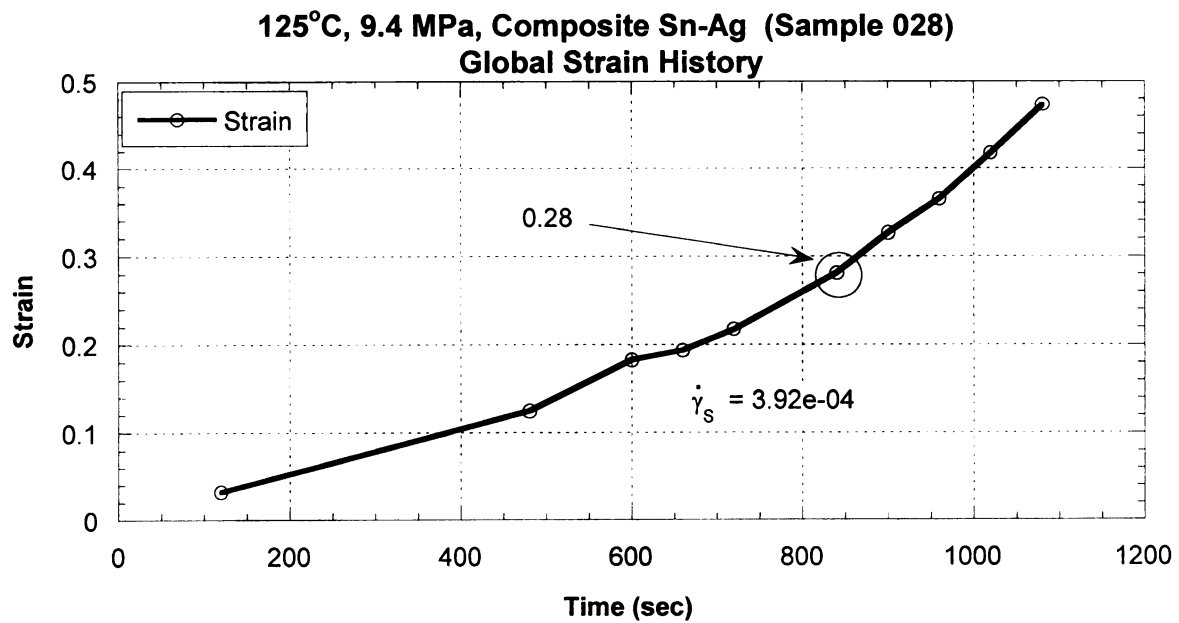


Figure 64. Global Secondary Strain Rate for 125°C, 9.4 MPa, Composite Solder

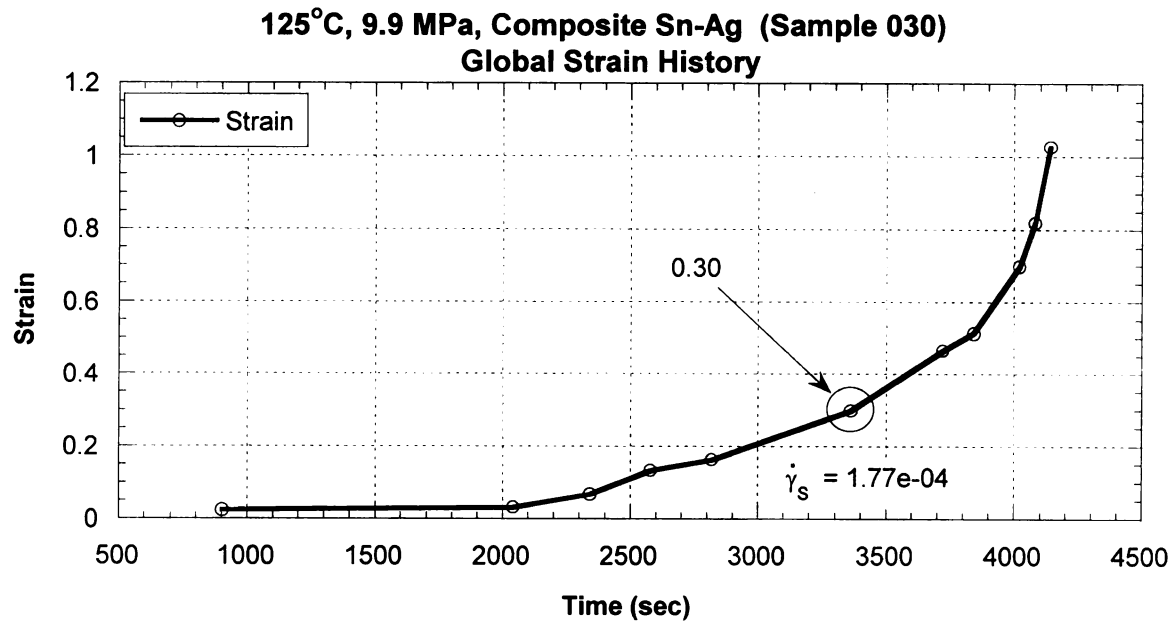


Figure 65. Global Secondary Strain Rate for 125°C, 9.9 MPa, Composite Solder

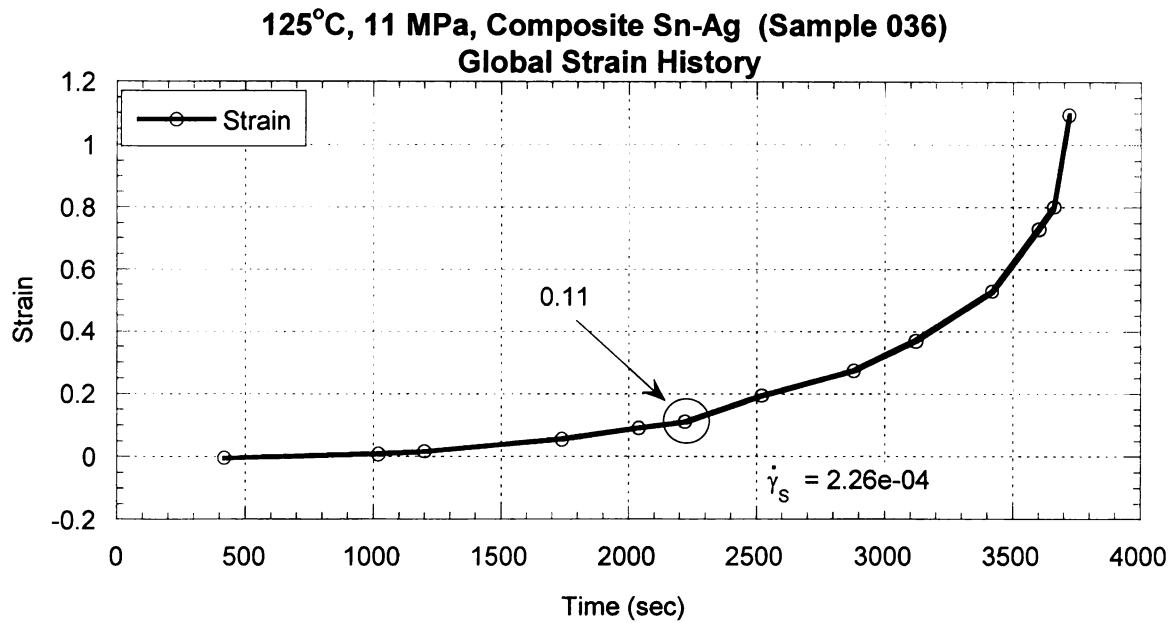


Figure 66. Global Secondary Strain Rate for 125°C, 11 MPa, Composite Solder

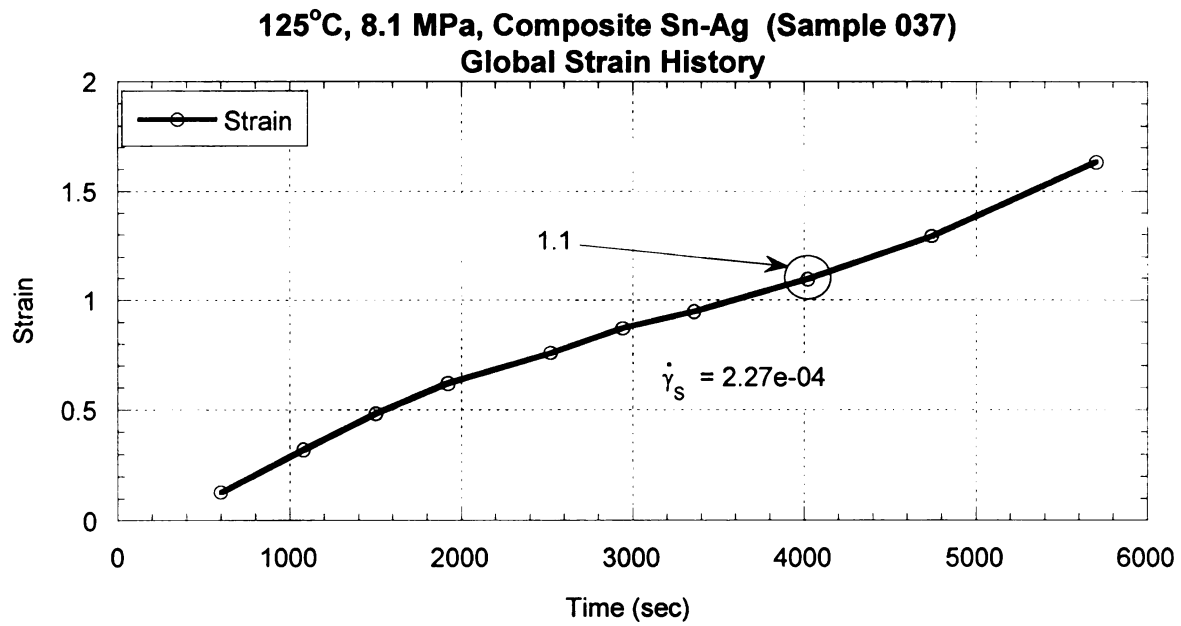


Figure 67. Global Secondary Strain Rate for 125°C, 8.1 MPa, Composite Solder

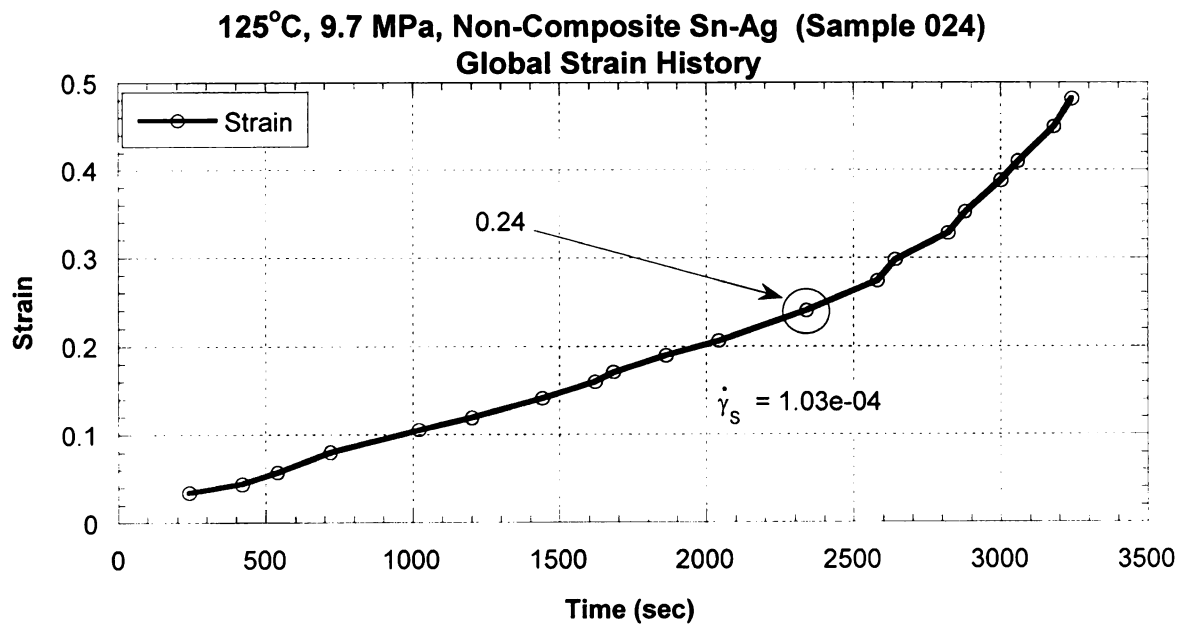


Figure 68. Global Secondary Strain Rate for 125°C, 9.7 MPa, Non-Composite Solder

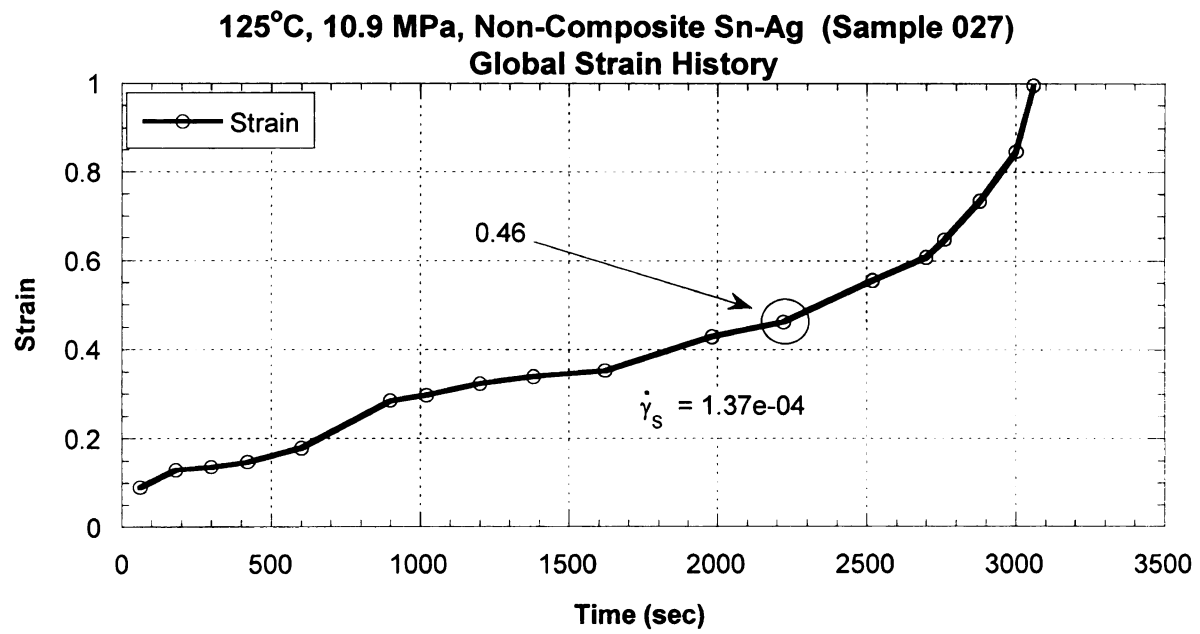
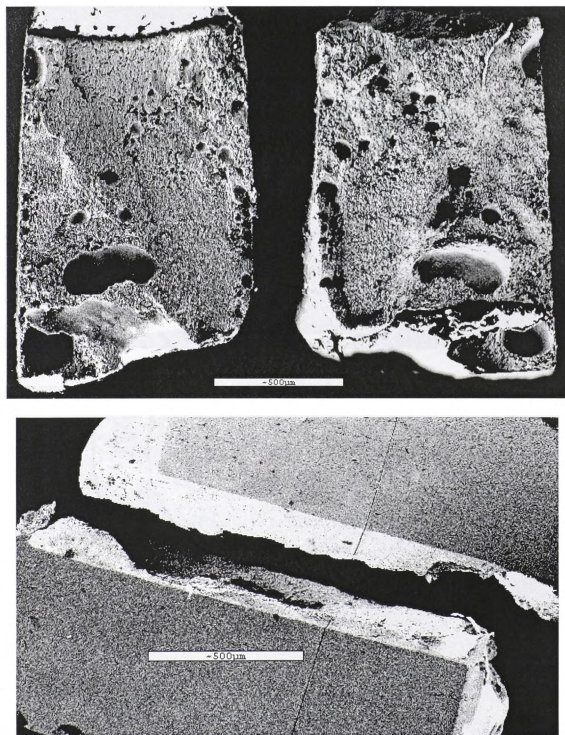


Figure 69. Global Secondary Strain Rate for 125°C, 31.1 MPa, Composite Solder

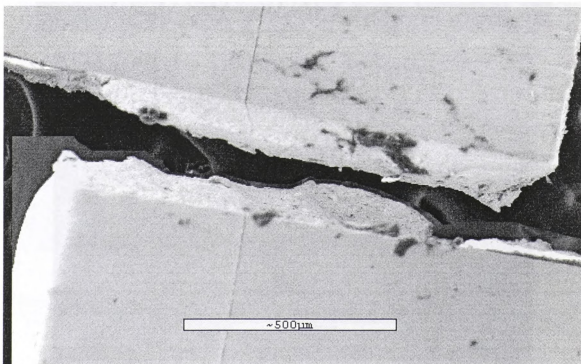
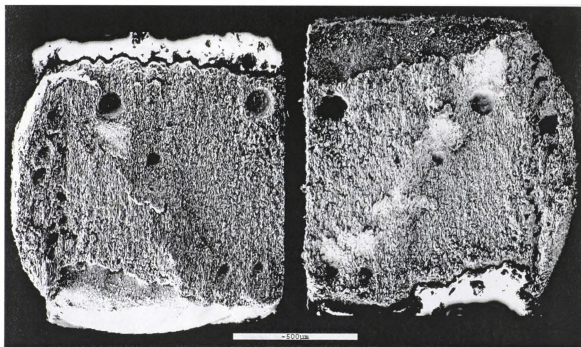
APPENDIX E

FRACTURE SURFACES AND PROFILES



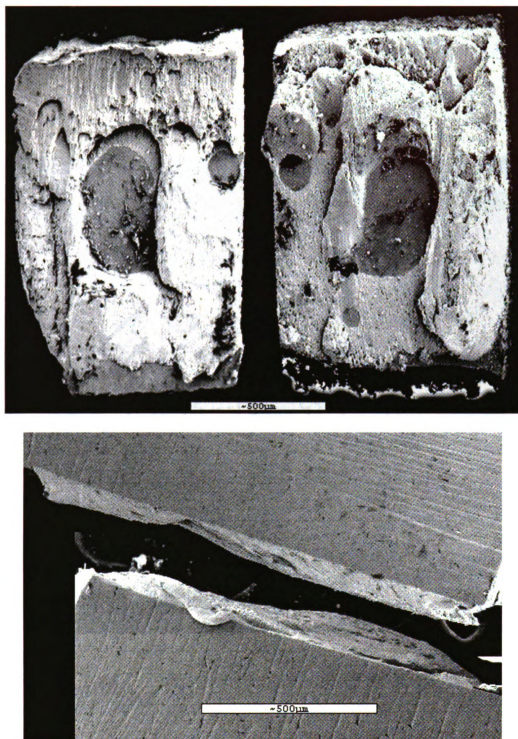
Sample	Type	°C	Stress (MPa)	$\dot{\gamma}_s$ (s ⁻¹)	OGTC	OLTTC	$\frac{\text{OGTC}}{\text{OLTTC}}$	% Porosity
052	Composite	25	31.1	1.33E-05	0.16	0.19	0.84	0.09

Figure 70. Fracture Surfaces and Profile for 25°C, 31.1 MPa, Composite Solder.



Sample	Type	°C	Stress (MPa)	$\dot{\gamma}_s$ (s ⁻¹)	OGTC	OLTc	OGTC OLTc	% Porosity
053	Composite	25	28.9	4.15E-05	0.52	1.2	0.43	0.025

Figure 71. Fracture Surfaces and Profile for 25°C, 28.9 MPa, Composite Solder.



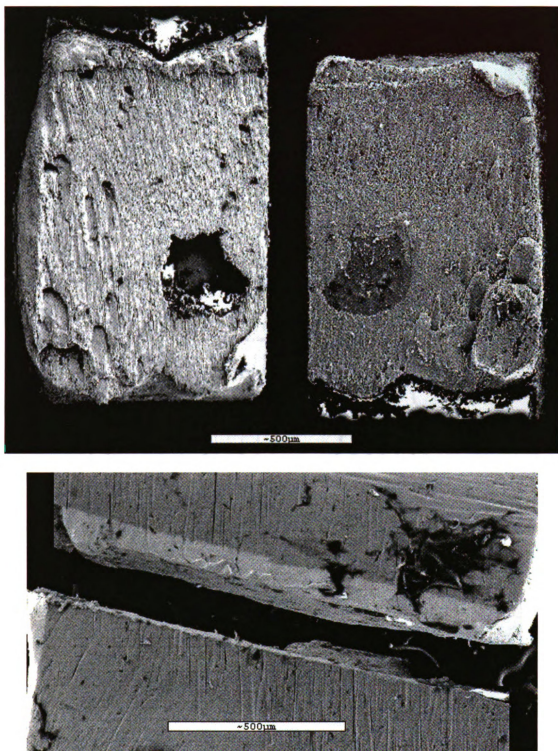
Sample	Type	°C	Stress (MPa)	$\dot{\gamma}_s$ (s^{-1})	OGTC	OLTC	OGTC OLTC	% Porosity
040	Non-Composite	25	21.9	4.85E-04	0.9	3	0.3	0.13

Figure 72. Fracture Surfaces and Profile for 25°C, 21.9 MPa, Non-Composite Solder.



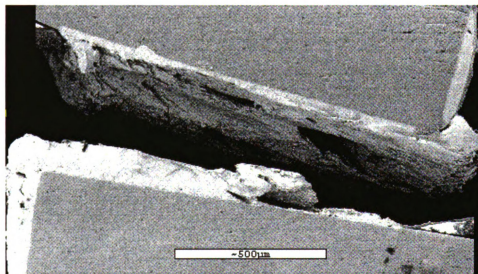
Sample	Type	°C	Stress (MPa)	$\dot{\gamma}_s$ (s ⁻¹)	OGTC	OLTC	$\frac{OGTC}{OLTC}$	% Porosity
038	Non-Composite	25	19.9	8.54E-05	0.86	0.4	0.22	0.053

Figure 73. Fracture Surfaces and Profile for 25°C, 19.9 MPa, Non-Composite Solder.



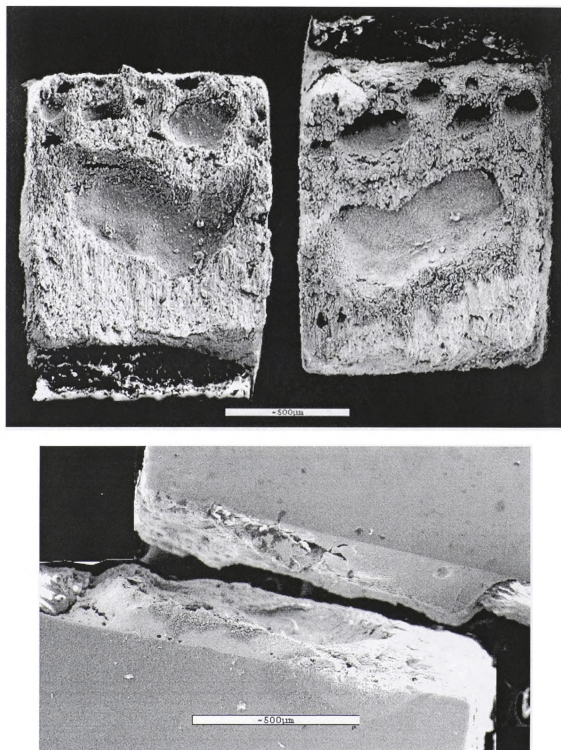
Sample	Type	°C	Stress (MPa)	$\dot{\gamma}_s$ (s ⁻¹)	OGTC	OLT	$\frac{OGTC}{OLT}$	% Porosity
039	Non-Composite	25	19.8	8.42E-05	0.79	3	0.26	0.064

Figure 74. Fracture Surfaces and Profile for 25°C, 19.8 MPa, Non-Composite Solder.



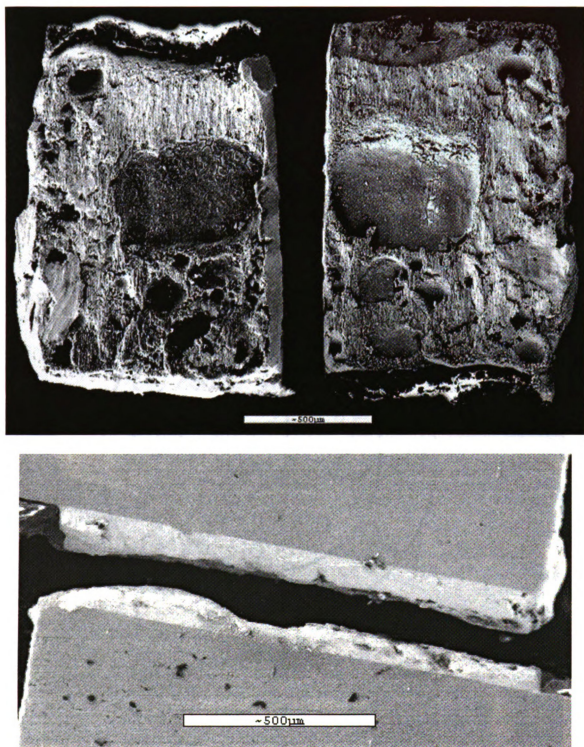
Sample	Type	°C	Stress (MPa)	$\dot{\gamma}_s$ (s^{-1})	OGTC	OLTc	OGTC OLTc	% Porosity
009	Non-Composite	25	10.5	7.13E-08	0.2	0.25	0.8	0.02

Figure 75. Fracture Surfaces and Profile for 25°C, 10.5 MPa, Non-Composite Solder.



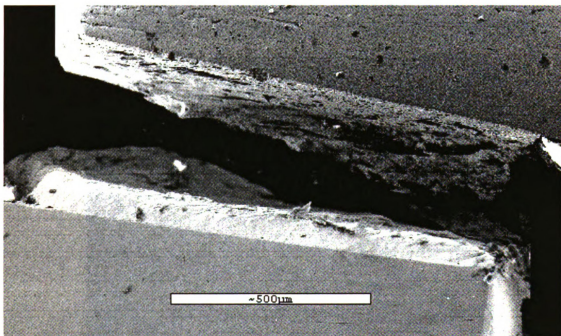
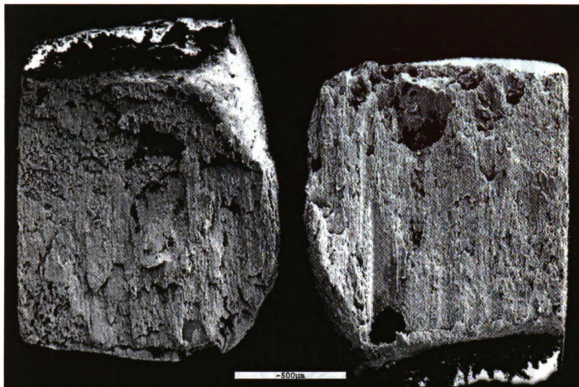
Sample	Type	°C	Stress (MPa)	$\dot{\gamma}_s$ (s^{-1})	OGTC	OLTC	$\frac{OGTC}{OLTC}$	% Porosity
033	Composite	85	10.8	9.75E-05	0.5	0.9	0.56	0.21

Figure 76. Fracture Surfaces and Profile for 85°C, 10.8 MPa, Composite Solder.



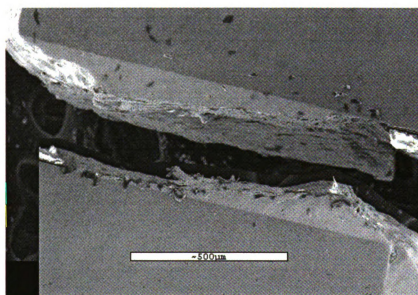
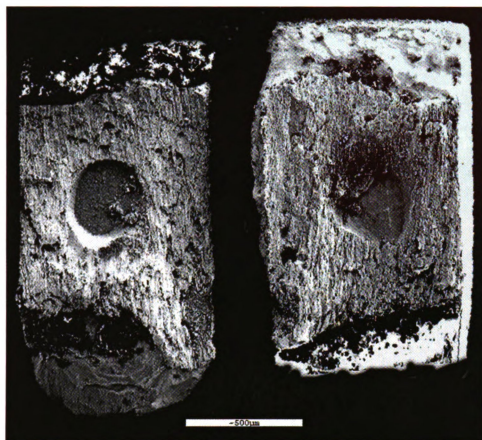
Sample	Type	°C	Stress (MPa)	$\dot{\gamma}_s$ (s ⁻¹)	OGTC	OLTC	$\frac{\text{OGTC}}{\text{OLTC}}$	% Porosity
034	Composite	85	10.4	1.46E-04	0.4	0.7	0.57	0.22

Figure 77. Fracture Surfaces and Profile for 85°C, 10.4 MPa, Composite Solder.



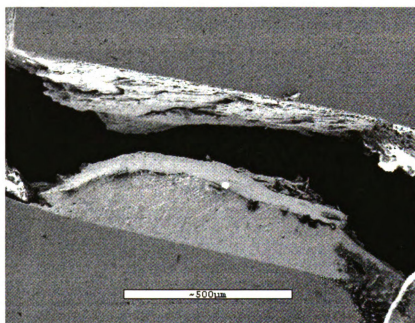
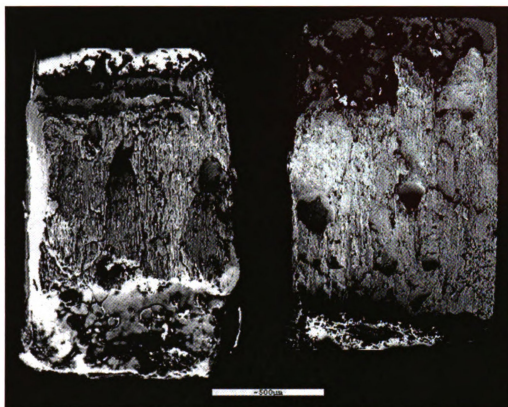
Sample	Type	°C	Stress (MPa)	$\dot{\gamma}_s$ (s ⁻¹)	OGTC	OLTC	$\frac{OGTC}{OLTC}$	% Porosity
018	Non-Composite	85	12.3	2.82E-04	1.3	1.67	0.78	0.036

Figure 78. Fracture Surfaces and Profile for 85°C, 12.3 MPa, Non-Composite Solder.



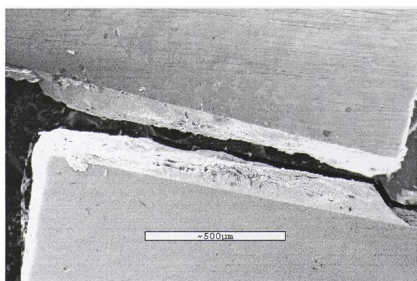
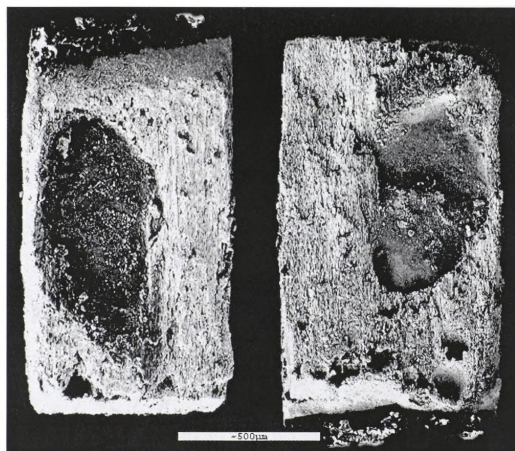
Sample	Type	°C	Stress (MPa)	$\dot{\gamma}$ (s^{-1})	OGTC	OLTTC	OGTC OLTTC	% Porosity
025	Non-Composite	85	17.3	1.24E-04	0.24	0.3	0.8	0.11

Figure 79. Fracture Surfaces and Profile for 85°C, 17.3 MPa, Non-Composite Solder.



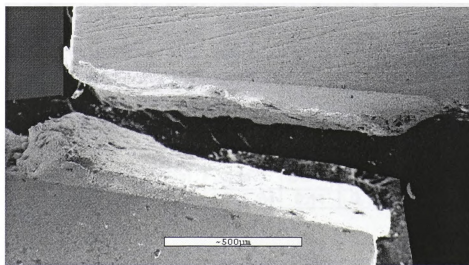
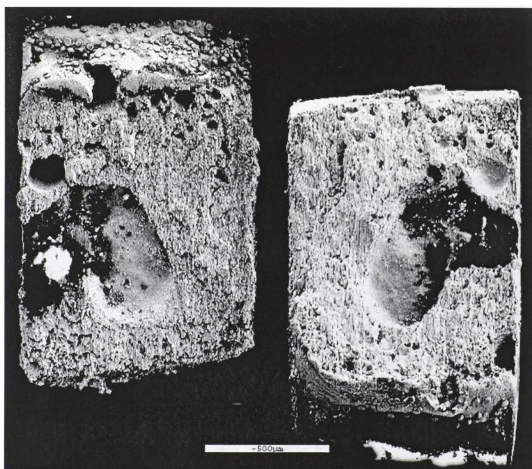
Sample	Type	°C	Stress (MPa)	$\dot{\gamma}_s$ (s ⁻¹)	OGTC	OLTCT	OGTC OLTCT	% Porosity
026	Non-Composite	85	16.3	8.4E-04	0.22	0.5	0.4	0.043

Figure 80. Fracture Surfaces and Profile for 85°C, 16.3 MPa, Non-Composite Solder.



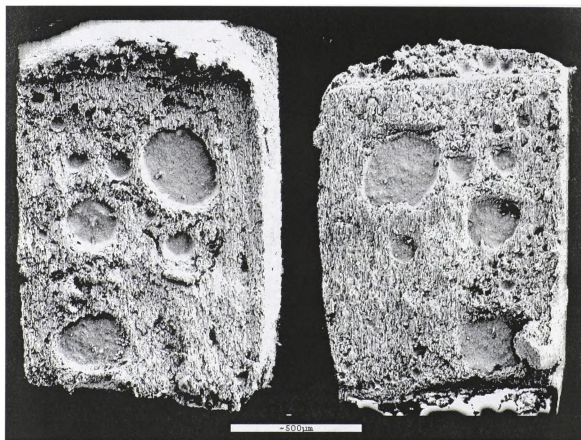
Sample	Type	°C	Stress (MPa)	$\dot{\gamma}_s$ (s^{-1})	OGTC	OLTC	$\frac{OGTC}{OLTC}$	% Porosity
028	Composite	125	9.4	3.92E-04	0.28	0.3	0.93	0.24

Figure 81. Fracture Surfaces and Profile for 125°C, 9.4 MPa, Composite Solder.



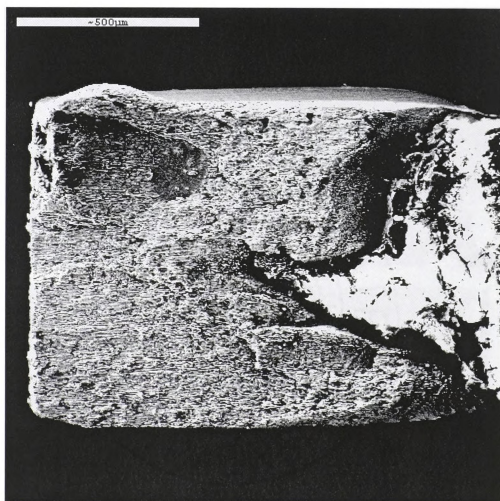
Sample	Type	°C	Stress (MPa)	$\dot{\gamma}_c$ (s^{-1})	OGTC	OLTC	$\frac{OGTC}{OLTC}$	% Porosity
030	Composite	125	9.9	1.77E-04	0.3	0.3	1	0.19

Figure 82. Fracture Surfaces and Profile for 125°C, 9.9 MPa, Composite Solder.



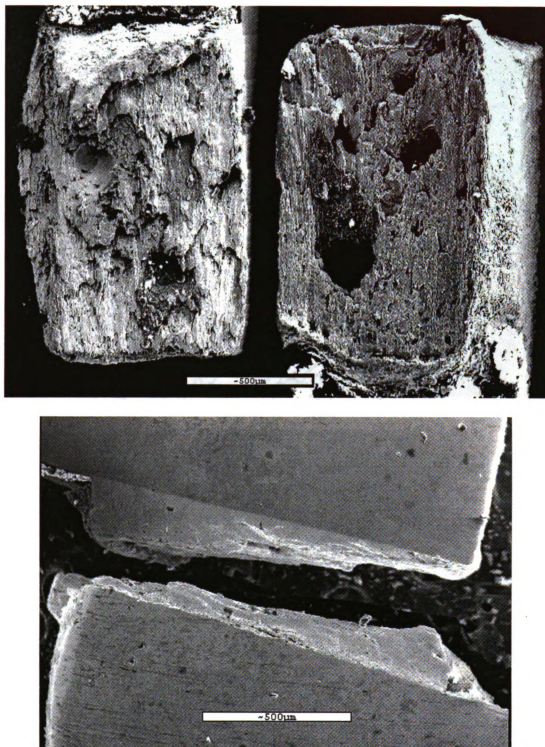
Sample	Type	°C	Stress (MPa)	$\dot{\gamma}_s$ (s^{-1})	OGTC	OLTC	$\frac{OGTC}{OLTC}$	% Porosity
036	Composite	125	11	2.26E-04	0.11	0.15	0.73	0.14

Figure 83. Fracture Surfaces and Profile for 125°C, 11 MPa, Composite Solder.



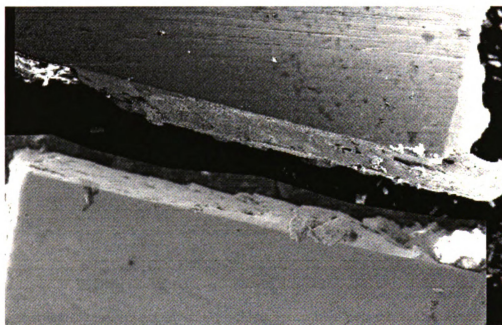
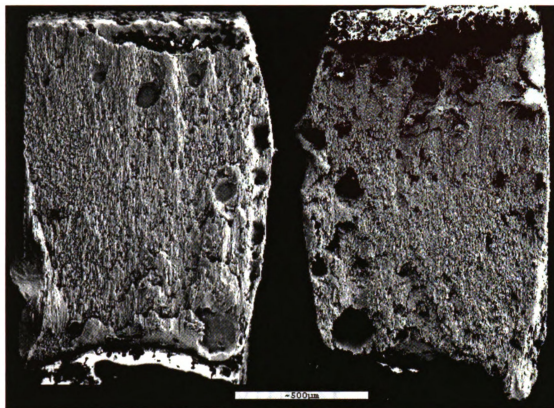
Sample	Type	°C	Stress (MPa)	$\dot{\gamma}_s$ (s ⁻¹)	OGTC	OLTC	$\frac{OGTC}{OLTC}$	% Porosity
037	Composite	125	8.1	2.27E-04	1.1	1.29	0.85	0.024

Figure 84. Fracture Surfaces and Profile for 125°C, 8.1 MPa, Composite Solder.



Sample	Type	°C	Stress (MPa)	$\dot{\gamma}_s$ (s^{-1})	OGTC	OLTCT	<u>OGTC</u> OLTCT	% Porosity
024	Non-Composite	125	9.7	1.0E-04	0.24	0.64	0.38	0.046

Figure 85. Fracture Surfaces and Profile for 125°C, 9.7 MPa, Non-Composite Solder.



Sample	Type	°C	Stress (MPa)	$\dot{\gamma}_s$ (s^{-1})	OGTC	OLTTC	OGTC OLTTC	% Porosity
027	Non-Composite	125	10.9	1.37E-04	0.46	0.97	0.47	0.034

Figure 86. Fracture Surfaces and Profile for 125°C, 10.9 MPa, Non-Composite Solder.

APPENDIX F

SOLDER JOINT CREEP DATA

Sample	Type	°C	Stress (MPa)	Secondary Creep-Rate	OGTC	OLTC	<u>OGTC</u> OLTC	% Porosity of Fracture Surface
052	C	25	31.1	1.33E-05	0.16	0.19	0.84	0.091
053	C	25	28.9	4.15E-05	0.52	1.2	0.43	0.025
054	C	25	25.8	1.28E-07	0.14	0.3	0.47	NA
040	NC	25	21.9	4.85E-04	0.9	3	0.30	0.128
038	NC	25	19.9	8.54E-05	0.86	4	0.22	0.053
039	NC	25	19.8	8.42E-05	0.79	3	0.26	0.064
009	NC	25	10.5	7.13E-08	0.2	0.25	0.80	0.02
042	NC	25	11	3.14E-08	0.15	0.19	0.79	NA
033a	C	85	7.4	3.05E-06	NA	NA	NA	0.205
033b (+ 0.5 lb.)	C	85	10.8	9.75E-05	0.5	0.9	0.56	0.205
034a	C	85	8.1	4.71E-06	NA	NA	NA	0.222
034b (+ 0.7 lb.)	C	85	10.4	1.46E-04	0.4	0.7	0.57	0.222
018a	NC	85	9.8	1.39E-05	NA	NA	NA	0.036
018b (+0.75 lb.)	NC	85	12.3	2.82E-04	1.3	1.67	0.78	0.036
025	NC	85	17.3	1.24E-04	0.24	0.3	0.80	0.11
026	NC	85	16.3	8.40E-04	0.22	0.55	0.40	0.043
028	C	125	9.4	3.92 E-04	0.28	0.3	0.93	0.242
030	C	125	9.9	1.77E-04	0.3	0.3	1.00	0.187
036	C	125	11	2.26E-04	0.11	0.15	0.73	0.14
037	C	125	8.1	2.27E-04	1.1	1.29	0.85	0.024
024	NC	125	9.7	1.03E-04	0.24	0.64	0.38	0.046
027	NC	125	10.9	1.37E-04	0.46	0.97	0.47	0.034

Definitions

+ () lb.	Increase in load upon establishing a secondary creep-rate
C	Composite Solder
NC	Non-Composite Solder
OGTC	Onset of Global Tertiary Creep
OLTC	Onset of Local Tertiary Creep
% Porosity of Fracture Surface	Average percent of the two fractured load bearing cross-sectional areas characterized by voids and porosity.

Table 4. Solder Joint Creep Data.

REFERENCES

REFERENCES

- [1] Vianco, Paul T. and Darrel R. Frear, "Issues in the Replacement of Lead Bearing Solders," *JOM*, 1993, Vol. 45, No. 7, pp. 14-19.
- [2] Samans, Carl H., *Engineering Metals and Their Alloys*, The MacMillan Co., New York, © 1949, pp. 858 - 864.
- [3] Vianco, Paul T., "Soldering in Electronic Applications," *ASM Handbook*, 1990, Vol. 6, pp. 985-1000.
- [4] Manko, Howard H., *Solders and Soldering - Materials, Design, Production, and Analysis for Reliable Bonding*, 3rd Ed., McGraw-Hill, Inc., New York, © 1992, p. 1.
- [5] Hwang, J.S., and R.M. Vargas, "Solder Joint Reliability - Can Solder Creep?" *Soldering & Surface Mount Technology*, No. 5, June 1990, p. 38.
- [6] MacKay, Colin, "Flux Reactions and Solderability", *Solder Joint Reliability - Theory and Applications*, ed. John H. Lau, Van Nostrand Reinhold, New York, ©1991, pp. 1-2.
- [7] Yang, Hong, Phillip Deane, Paul Magill, and K. Linga Murty, "Creep Deformation of 96.5Sn-3.5Ag Solder Joints in a Flip Chip Package", *1996 Electronic Components and Technology Conference*, ©1996 IEEE, p. 1136.
- [8] Miller, Chad M., Iver E. Anderson, and Jack F. Smith, "A Viable Tin-Lead Solder Substitute: Sn-Ag-Cu", *Journal of Electronic Materials*, Vol. 23, No. ?, 1994, p. 595.
- [9] Yang, Wenge, Lawrence E. Felton, and Robert W. Messler, Jr., "The Effect of Soldering Process Variables on the Microstructure and Mechanical Properties of Eutectic Sn-Ag/Cu Solder Joints", *Journal of Electronic Materials*, Vol. 24, No. 10, 1995, pp. 1465-1471.
- [10] Choi, S.L., A.W. Gibson, J.L. McDougall, T.R. Bieler, K.N. Subramanian, "Mechanical Properties of Sn-Ag Composite Solder Joints Containing Copper-Based Intermetallics", *Design and Reliability of Solders and Solder Interconnections*. R.K. Mahidhara, D.R. Frear, S.M.L. Sastry, K.L. Murty, P.K. Liaw, W.L. Winterbottom, eds. TMS, Warrendale, PA 1997, p. 241.

- [11] Raeder, C.H., G.D. Schmeelk, D. Mitlin, T. Barbieri, W. Yang, L.F. Felton, R.W. Messler, D.B. Knorr, and D. Lee, "Isothermal Creep of Eutectic SnBi and SnAg Solder and Solder Joints", *1994 IEEE/CPMT International Electronics Manufacturing Technology Symposium*, pp. 1, 5.
- [12] Frost, Harold J., Robert T. Howard, Patrick R. Lavery, and Scott D. Lutender, "Creep and Tensile Behavior of Lead-Rich Lead-Tin Solder Alloys", *IEEE Transactions on Components, Hybrids, and Manufacturing Technology*, Vol. 11, No. 4, December 1988, p. 379.
- [13] Gibson, A.W., S.L. Choi, K.N. Subramanian, T.R. Bieler, "Issues Regarding Microstructural Coarsening Due to Aging of Eutectic Tin-Silver Solder", *Reliability of Solders and Solder Joints*, TMS Conference Orlando 1997.
- [14] Yang, Wenge, and Robert Messler, Jr., "Microstructural Evolution of Eutectic Sn-Ag Solder Joints", *Journal of Electronic Materials*, Vol. 23, No. 8, 1994, pp. 765-772.
- [15] McCormack, M., S. Jin, and G.W. Kammlott, "Supression of Microstructural Coarsening and Creep Deformation in a Lead-Free Solder", *Appl. Phys. Lett.*, Vol. 64, No. 5, 31 January 1994, pp. 580-582.
- [16] Garofalo, Frank, *Fundamentals of Creep and Creep-Rupture in Metals*, The MacMillian Company, New York, © 1965, pp. 1-20.
- [17] Ross, R.G., Jr., L.C. Wen, G.R. Mon, "Solder Joint Creep and Stress Relaxation Dependence on Construction and Environmental Stress Parameters", *Journal of Electronic Packaging*, Vol. 115, June, 1993, pp.165-171.
- [18] Evans, R.W. and B. Wilshire, *Introduction to Creep*, The Institute of Materials, ©1993, pp. 1-31.
- [19] Glen, John, *The Problem of the Creep of Metals*, Murex Welding Processes LTD., Waltham Cross, Hertfordshire, England, January 1968, pp. 8 - 15.
- [20] Evans, R.W. and B. Wilshire, *Creep of Metals and Alloys*, The Institute of Metals, ©1985, pp. 37-57, 70-76.
- [21] Dieter, George E., *Mechanical Metallurgy, 3rd Edition*, McGraw-Hill Publishing Company, New York, © 1986, pp. 310-314, 438 - 449.
- [22] Reed-Hill, Robert E. and Abbaschian, *Physical Metallurgy Principles, 3rd Edition*, PWS-Kent Publishing Company, Boston, © 1992, p 854.

- [23] Bird, J.E., A.K. Mukherjee, and J.F. Dorn, "Correlations Between High-Temperature Creep Behavior and Structure", *Quantitative Relations Between Properties and Microstructure, Proceedings of an International Conference*, Haifa, Isreal, July 27-Aug. 4, 1969, p. 255.
- [24] Weertman, J., "Dislocation Climb Theory of Steady-State Creep", *Creep Symposium, Transactions of the ASM* vol. 61, ©1968.
- [25] Artz, E. M.F. Ashby, R.A. Verrall, "Interface Controlled Diffusional Creep". *Acta Metall.* Vol 31, #12. 1983.
- [26] Ashby, M.F. "Boundary Defects, and Atomistic Aspects of Boundary Sliding and Diffusional Creep", *Surface Science*, 31, 1972.
- [27] Ruano, O.A., J. Wadsworth, J. Wolfenstine, O.D. Sherby, "Evidence for Nabarro Herring creep in metals: fiction or reality?", *Materials Science and Engineering A165*, 1993.
- [28] Wolfenstine, J., O.A. Ruano, J. Wadsworth, O.D. Sherby, "Refutation of the Relationship Between Denuded Zones and Diffusional Creep", *Scripta Metallurgica* vol. 29, 1993.
- [29] Ross, Ronald G., Jr., and Liang-chi Wen, "Crack Propagation in Solder Joints During Thermal-Mechanical Cycling", *Journal of Electronic Packaging*, June, 1994, Vol. 116, p. 69.
- [30] Gibson, A.W., S. Choi, T.R. Bieler, and K.N. Subramanian, "Environmental Concerns and Materials Issues in Manufactured Solder Joints", *1997 IEEE International Symposium on Electronics and the Environment*, (IEEE, Piscataway, NJ, 1997), pp. 246-51.
- [31] Frost, Harold J., "Microstructure and Mechanical Properties of Solder Alloys", *Solder Joint Reliability - Theory and Applications*, ed. John H. Lau, Van Nostrand Reinhold, New York, ©1991, pp. 266-267.
- [32] Frear, Darrel R., "Thermomechanical Fatigue in Solder Materials", *Solder Mechanics - A State of the Art Assessment*, eds. Darrel R. Frear, Wendell B. Jones, and Kenneth Kinsman, The Minerals, Metals, and Materials Society, Warrendale, PA, 1991, p. 191.
- [33] Frost, Harold J., and Robert T. Howard, "Creep Fatigue Modeling for Solder Joint Reliability Predictions Including the Microstructural Evolution of the Solder", *IEEE Transactions on Components, Hybrids, and Manufacturing Technology*, Vol. 13, No. 4, Dec. 1990, p. 727.

- [34] Attarwala, A.I., J.K. Tien, G.Y. Masada, G. Dody, "Confirmation of Creep and Fatigue Damage in Pb/Sn Solder Joints", *Journal of Electronic Packaging*, June 1992, Vol. 114, pp. 109,111.
- [35] Vaynman, Semyon, and Moris E. Fine, "Effects of Strain Range, Ramp Time, Hold Time, and Temperature on Isothermal Fatigue Life of Tin-Lead Solder Alloys", *Solder Joint Reliability - Theory and Applications*, ed. John H. Lau, Van Nostrand Reinhold, New York, ©1991, pp. 333,357.
- [36] Hall, Peter M., "Creep and Stress Relaxation in Solder Joints", *Solder Joint Reliability - Theory and Applications*, ed. John H. Lau, Van Nostrand Reinhold, New York, ©1991, pp. 313-332.
- [37] Morris, J.W., Jr., D. Tribula, T.S.E. Summers, and D. Grivas, "The Role of Microstructure in Thermal Fatigue of Pb-Sn Solder Joints", *Solder Joint Reliability - Theory and Applications*, ed. John H. Lau, Van Nostrand Reinhold, New York, ©1991, pp. 225-226, 261-262.
- [38] Tien, John K., Bryan C. Hendrix, and Abbas I. Attawala, "The Interaction of Creep and Fatigue in Lead-Tin Solders", *Solder Joint Reliability - Theory and Applications*, ed. John H. Lau, Van Nostrand Reinhold, New York, ©1991, pp. 279-305.
- [39] Dasgupta, A., C. Oyan, D. Barker, M. Pecht, "Solder Creep-Fatigue Analysis by an Energy-Partitioning Approach", *Transactions of the ASME, Journal of Electronic Packaging*, Vol. 114, June, 1992, pp. 152-160.
- [40] Pan, Tsung-Yu, "Critical Accumulated Strain Energy (Case) Failure Criterion for Thermal Cycling Fatigue of Solder Joints", *Journal of Electronic Packaging*, Vol. 116, September, 1994, pp. 163-170.
- [41] Darveaux, Robert, and Kingshuk Banerji, "Constitutive relations for Tin-Based-Solder-Joints", *1992 Preceedings of the IEEE 42nd Electronic Components & Technology Conference*, pp. 538-551.
- [42] Wasynczuk, J.A. and George K. Lucey, "Shear Creep of Cu₆Sn₅/Sn-Pb Eutectic Composites", *Proceedings of Technical Program Vol. III, National Electronic Packaging and Production Conference*, 1992, pp. 1245-1255.

MICHIGAN STATE UNIV. LIBRARIES



31293018017453